Cape Peninsula
University of Technology

Performance Analysis of a Direct-Expansion Solar-Assisted Heat Pump for Water-Heating Application in South Africa

---

Matthew William Schouw
(BTech: Mechanical Engineering)

Dissertation submitted in partial fulfilment of the requirements for the degree.

Master of Energy: Electrical Engineering

in the Faculty of Engineering & Built Environment

at the Cape Peninsula University of Technology

Supervisor: Dr A.K. Raji

Bellville

February 2021

DECLARATION

I, **Matthew William Schouw,** declare that the contents of this dissertation represent my own unaided work, and that the dissertation has not previously been submitted for academic examination towards any qualification. Furthermore, it represents my own opinions and not necessarily those of the Cape Peninsula University of Technology.

Signed  **Date** 08 September 2021

ABSTRACT

This study investigated the potential application of direct expansion solar-assisted heat pump water heating (DX-SAHPWH). The system is a confluence of heat pumps and solar thermal water heating systems. This is normally achieved by replacing the conventional evaporator of a heat pump with a solar-thermal collector, which results in several unique advantages such as higher efficiencies, extracted from two energy sources, i.e. from both solar and ambient air, and improved collector lifetime, amongst others. However, the primary shortcoming is that the system demonstrates an erratic collector-evaporator load due to diurnal and seasonal swings in meteorological conditions. Therefore, depending on the geographical location ,the DX-SAHP system performance will vary. Consequently, to discern whether it is a suitable technology for South Africa, an analysis is therefore required to evaluate the performance of the DX-SAHPWH system prior to implementation.

A theoretical model was developed based on an analytical steady-state approach, which was used to evaluate its thermal performance characteristics of the DX-SAHPWH system. It consisted of two bare/unglazed solar collectors with a combined area of 4.2 m^2, a 680 W rotary-type hermetic compressor using R22 as the refrigerant, and a 150 L cylindrical heat storage tank with an immersed helical coil condenser. The analysis was conducted for typical summer and winter days and for an annual simulation, using the meteorological data in Stellenbosch in Western Cape for the year 2018. To assess the performance, the following metrics were used: coefficient of performance; collector efficiency; solar fraction; and heating time. Moreover, a parametric analysis was conducted to evaluate the effects of the meteorological and operational parameters on the performance of the system.

The daily results indicated that the system performance is generally better on summer days than in winter days due to the higher ambient temperature, initial water temperature and solar radiation. Moreover, the specific results indicated for the summer condition, the instantaneous energy performance showed that the system is capable of producing 1700 to 4000 W of thermal energy and a compressor consumption from 550 to 750 W based on a 24-hour average. The condenser heat gain is 2000 W, collector heat gain is 1400 W and compressor power consumption is 632 W. The coefficient of performance (COP) and collector efficiency varied from 1.83 - 5.65 and 45-51 % respectively. The solar fraction and heating time ranged from 0 - 82 % and 94 to 403 minutes. In the winter condition, the results showed that the system is capable of producing 1100 to 1800 W of thermal energy and a compressor consumption from 550 to 585 W. Based on a 24-hour average, the condenser heat gain is 1320 W, collector

heat gain is 772 W, and compressor power consumption is 547 W. The COP and collector efficiency ranged from 1.07–2.80 and 45–60 % respectively. The solar fraction and heating time ranged from 0–74 % and 300 to 480 minutes. The synthesis of the daily performance further indicated that the system should ideally run during the day when solar radiation is abundant and that the COP could increase as additional ambient energy heat gains are expected.

The annual performance results indicated that minimum (min) and maximum (max) COP expected are 1.4 and 5.75 respectively, with an annual average of 2.3. The COP is higher during the periods with higher ambient temperatures, solar radiation and higher initial water temperatures which is the converse for the colder seasons. The min and max collector efficiency is 0 and 59.96 % respectively; it can be seen that the collector efficiency remains fairly constant throughout the year. The consequence is that the temperature gradient between the collector and the ambient temperatures does not vary annually. The min and max solar fraction is 0 and 86.47 % with an annual average of 34.81 %. Higher solar fractions are expected during periods that exhibit higher solar radiation values compared to other seasons. The heating time min and max are 92 and 570 minutes with an annual average of 355 minutes. It was found that periods with lower ambient temperature, initial water temperatures and solar radiation values exhibited higher heat times.

The parametric analysis aimed to investigate the effects of meteorological conditions. The results indicated that the effect of ambient temperature (for the range 0–40°C) results in a linear increase in both the COP and collector efficiency by 77 and 81 % respectively. In addition, an increase in the solar fraction and a decrease in the heating time was found to be 95 % and 25 % respectively. The effect of the solar radiation was also investigated for a range of 200–1200 W/m^2. The results indicated an increase in solar radiation, resulting in an increase in COP and a decrease in collector efficiency by 73 % and 48 % respectively. In addition, an increase was shown in the solar fraction and a decrease in the heating time by 88 % and 43 % respectively. Lastly, the wind speed was investigated for a range 1–10 m/s. As the wind speed increases, the COP and collector efficiency decreased by 15.6 % and 34 % respectively . In addition, a decrease was noted in solar fraction and heating time of 3.7 % and 37 % respectively.

This research aimed to provide an initial benchmark for the performance of a DX-SAHPWH system in South Africa. Moreover, the research undertaken was conducted as a preliminary stage and was meant to theoretical gauge the feasibility of the specific DX-SAHPWH system. The thermal performance metrics such as COP, collector efficiency, heating time and solar fraction provided a quantitative measure of how these systems will perform for the specific

geographical location. Although the analytical modelling approach is not entirely novel and complete, it does provide a guide to the theoretical analysis of the DX-SAHPWH system, which can be used for design and manufacture purposes. The parametric analysis further provides performance insight, so that one might understand how the meteorological conditions affect performance and where the system will best be implemented. Furthermore, it must be highlighted that the results presented were only for the simulated models and thus a prototype must be correctly design, manufactured and tested to obtain accurate results. Based on the results of this dissertation, the author highly recommends the implementation of the DX-SAHPWH system in South Africa.

Keywords: *Heat pump, water heating, solar-assisted heat pump, solar energy, mathematical model; simulation; direct expansion, residential, COP, South Africa*

ACKNOWLEDGEMENTS

I am thankful to God our creator, for His wonderful grace and love, for his inspiration and protection throughout the period of this dissertation. Whenever, I was cognitively challenged or unmotivated you always answered my prayers.

This dissertation is also a result of the fantastic people and colleagues' inputs and guidance.

I wish to thank the following individuals:

- Dr. Atanda Kamoru Raji, my supervisor, for always motivating me and ensuring that all my academic and administrative requirements were addressed. You are an African hero and blessing.

- Dr. Fareed Ismail and Dr. Ouassini Nemraoui, for your constant support, mentoring, guidance and enlightening academic advice and expertise. I am truly indebted and grateful to have you as academic mentors.

- Cape Peninsula University of Technology (CPUT) and The Energy Institute for their support and guidance.

- Special thanks go to Dr.Ken Barris for the editing of this dissertation.

- My research colleagues the during the period of this dissertation for their conversation, and for inspiring me to push myself further (Gilbert, Dzon, Oliver, Daniel, Kalvin and Jakobus). I wish you all success for your endeavours.

The financial assistance of the University Research Fund and CPUT Postgraduate Bursary towards this research is acknowledged. Opinions expressed in this dissertation and the conclusions arrived at are those of the author, and are not necessarily to be attributed to the bursars and funders.

DEDICATION

I dedicate this to my wife and son *Bianca* and *Kai-Adam*, thank you for all unconditional support, smiles and love through my Master's studies*. I love you to the moon and back.*

&

To my family. My mother, and sisters. (*Felicia, Thandi, Lisa and Landa*). Your continued love ,support and conversations are most valued.

TABLE OF CONTENTS

LIST OF FIGURES

LIST OF TABLES

TERMS AND CONCEPTS

CO2	Carbon dioxide
COP	Coefficient of performance
DX-SAHPWH	Direct expansion solar-assisted heat pump water heater
ERWH	Electrical resistance water heaters
kWh	Kilowatt-hour
GHG	Greenhouse gas
HPWH	Heat pump water heaters
HT	Heating Time
IRP	Integrated Resource Plan
Min	Minimum
Max	Maximum
R22	Refrigerant R22 : (Chlorodifluoromethane)
R134a	Refrigerant R34 a: Tetrafluoroethane
SAHP	Solar Assisted Heat Pump
SF	Solar fraction
SWH	Solar water heaters
TEV	Thermostatic expansion valve
VCC	Vapour compression cycle

NOMENCLATURE

A_{cl}	Area of collector-evaporator	m^2
$\mathrm{A_{st}}$	Area of storage tank	m^2
$\mathrm{C_b}$	Bond conductance	
C_{pw}	Specific heat capacity of water	
D_i	Diameter of the collector tube	m
$d_{\mathrm{st}},$	Diameter of storage tank	m
$\mathrm{f_{solar}}$	Solar fraction	-
F	Fin efficiency	-
$\mathrm{F'}$	Collector efficiency factor	-
h_c	Wind convection heat transfer coefficient	℃ / W
h_f	Internal convection heat transfer coefficient	℃ / W
h_g	Saturated vapour enthalpy	kJ/kg
h_l	Liquid enthalpy	kJ/kg
h_r	Radiation heat transfer coefficient	kJ/kg
$\mathrm{h_{st}},$	Height of tank	m
I_T	Solar irradiation	W/m^2
m_{r_com}	Mass flow rate through compressor	kg/s
Nu	Nusselt number	-
Pr	Prandtl number	-
Q_{coll}	Useful collector heat gain	W
Q_{con}	Condenser heat gain	W
$\mathrm{Q_{Load}}$	Hot water drawn off	W
Q_w	Thermal energy required to heat water	W

$Q_{cond\ (st)}$	Conduction heat transfer loss through the tank walls insulation	W
$Q_{conv\ (st)}$	Convection heat transfer loss between stationary ta water and ambient air	W
$Q_{rad\ (st)}$	Radiation heat loss from tank to ambient air	W
Ra	Raleigh number	-
T_a	Ambient temperature	°C
T_C	Condensing temperature of the refrigerant	°C
T_e	Evaporating temperature of the refrigerant	°C
T_p	Plate temperature	°C
T_{sky}	Sky temperature	K
T_{wi}	Inlet Water temperature	°C
T_{wo}	Setpoint temperature	°C
V_d	Volumetric displacement	cm^3
V_{st}	Volume of storage tank	m^3
U_{CL}	Overall heat transfer loss coefficient of collector	°C / W
W	Pitch of the collector tube	m
W_{comp}	Input compressor power	W
u_w	Wind speed	m/s

GREEK LETTERS

α	Absorptivity	-
ε	Emissivity	-
ρ	Density	kg/m^3
σ	Stefan–Boltzmann constant	–
η	Efficiency	–
λ	Thermal conductivity	W.m.K
τ	Heating time	s
δ	Thickness	m
υ	Kinematic viscosity	m^2/s
μ	Absolute viscosity	Pa.s

LIST OF RESEARCH OUTPUTS FROM THIS DISSERTATION

- Schouw, M and Raji, A.K., Modelling & simulation of a direct-expansion solar-assisted heat pump for water heating application in South Africa (November 26, 2019). AIUE Proceedings of the 17th Industrial and Commercial Use of Energy (ICUE) Conference 2019, Cape Town, ISBN 978-0-6399647-4-4, Available at SSRN: https://ssrn.com/abstract=3659004 or http://dx.doi.org/10.2139/ssrn.3659004

OTHER RESEARCH OUTPUTS DURING THE PERIOD OF THIS DISSERTATION

- Ismail, F and Gryzagoridis, J and Nemraoui, O and Schouw, M, Experimental analysis of an integrated aquaponics and standalone solar photovoltaic system (November 26, 2019). AIUE Proceedings of the 17th Industrial and Commercial Use of Energy Conference 2019, The River Club, Cape Town, ISBN 978-0-6399647-4-4, Available at SSRN: https://ssrn.com/abstract=3638163 or http://dx.doi.org/10.2139/ssrn.3638163

- Khamlich, S and Ismail, F and Schouw, M and Nemraoui, O, Photo-Thermal Conversion Efficiency of Spectrally Selective Cr 2O 3/Cr/Cr 2O 3 Multilayered Solar Absorber (November 24, 2020). AIUE Proceedings of the 18th Industrial and Commercial Use of Energy Conference 2020, Available at SSRN: https://ssrn.com/abstract=3740748 or http://dx.doi.org/10.2139/ssrn.3740748

CHAPTER 1: INTRODUCTION

1.1 Background to the problem

Currently, South Africa faces a multitude of challenges in its energy sector, such as insecure supply of electricity, accelerated growth in electricity consumption, heavy reliance on fossil-fuelled sources and high carbon emissions, increasing electrical tariffs, low energy access rates and inefficient usage of energy sources, among others. For example, Eskom, the state-owned electricity company which operates the national electricity grid, produces around 90% of South Africa's electricity but has not adequately met the energy demands for the last two decades. This is attributed to poor maintenance and management of existing power stations, clandestine and corrupt dealings of management and failure to successfully introduce new power generation infrastructure (SAMJ, 2019). To mitigate the impacts due the lack of supply, Eskom implemented planned stages of power outages dubbed 'load shedding'. This was poorly received and had vast economic implications in all sectors of the economy.

Concurrent with energy security issues, the electricity demand is expected to proliferate. As an example, the access to electricity in South Africa increased from 60,8% to 86% in the period 1994–2016 because of the Department of Energy (DoE)/Eskom household electrification programme between 1994 and 2013/14 (refer to Figure 1.1). Moreover, energy consumption per sector has been on the rise, since 1993 (refer to Figure 1.2). For instance, from the period 1993–2003, industry sector consumption has increased between 52% and 63% over the period. Residential sector consumption also increased consistently from 16% to 20% in 2013. This is attributed to higher electrification rates and increased income of households.

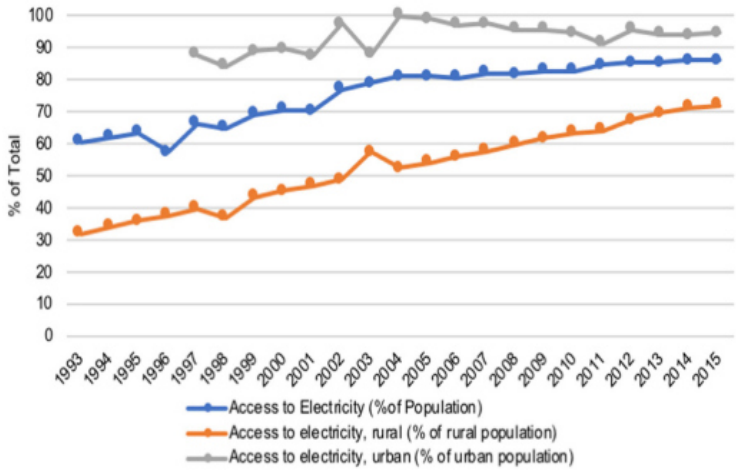

Figure 1. 1: South African access to electricity from 1993–2013 (Department of Energy, 2018a)

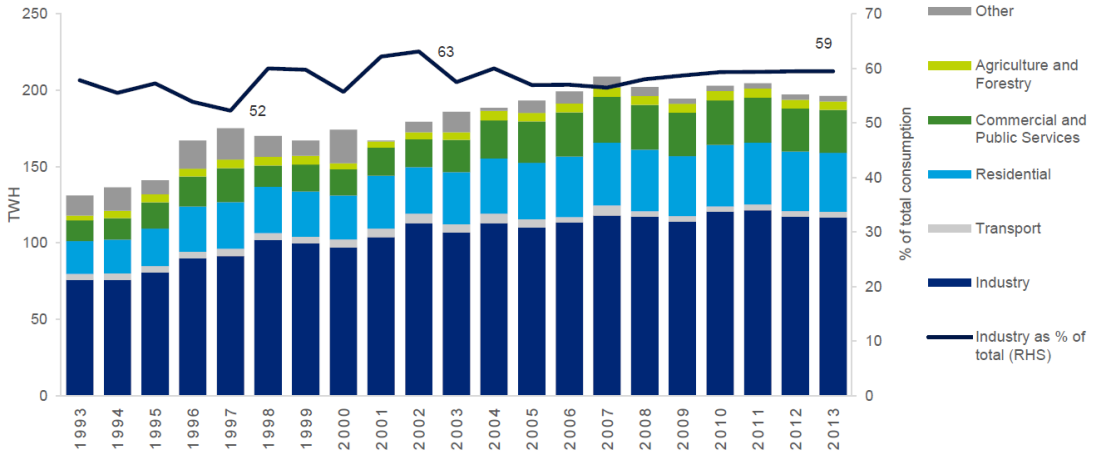

Figure 1. 2: Electricity consumption growth per sector (1993–2013) (Department of Energy, 2018a)

Moreover, most electricity produced is mainly by coal-fired power stations and consequently is responsible for about 1.1 % of global carbon emissions. According to (Pollet, Staffell & Adamson, 2015), 84 % of South Africa's total emissions in 2012 was dominated by emissions from the energy sector, which accounted for 60 %. This is about 40 % of emissions in sub-Saharan Africa, even though South Africa has less than 5% of the continent's population (Curry, Cherni & Mapako, 2017; Donev, Sark, Blok & Dintchev, 2012; Pegels, 2010) (refer to Figure 1.3). Moreover, emissions are steadily increasing, during the period 1990–2012, the total greenhouse gas (GHG) emissions grew 44% with an average annual change of 1.7%. Based on Figure 1.4, it can be increased from 325 to 452 MtCO2e during this period (USAID, 2014).

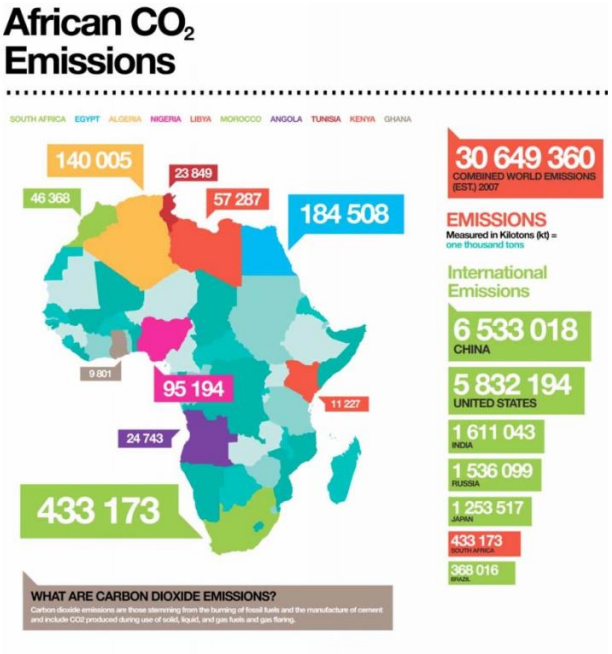

Figure 1. 3: African CO2 Emissions (USAID, 2014)

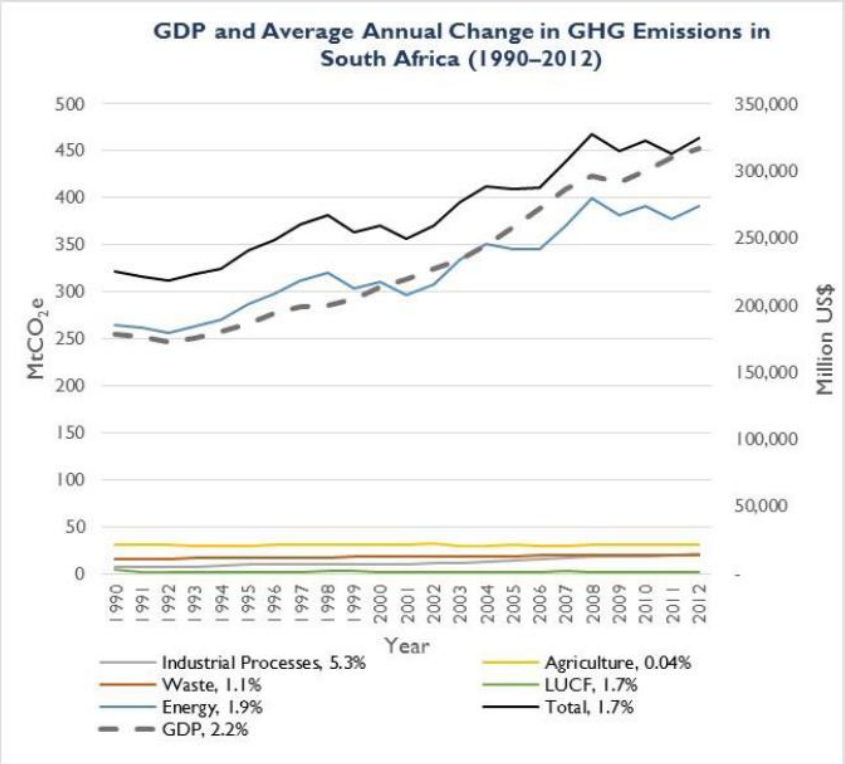

Figure 1. 4: GHG emissions in South Africa (USAID, 2014)

In addition to growth in electricity consumption and carbon emissions, the country is subjected to perpetual increasing costs for fossil fuel sources and electricity. For example, the price of coal has increased annually over the last 20 years by an average by 8.8% per annum, although it is the most affordable energy source in the country. The prices for petroleum, diesel and paraffin increased from January 2005 to March 2014 by an annual average of 15% (Joubert, Hess & Niekerk, 2016); and according to (Department of Energy, 2018b), the cost per kWh has significantly increased. For instance, in 2008 the price of domestic and street lighting rose from 53.43 cents/kWh in 2008/9 to 118.56 cents/kWh in 2018/19.

This trend is also applicable to other sectors (refer to Figure 1.5) which show annual average electricity prices by customer category. Consequently, this results in households spending more of their income on electricity. According to Bohlmann & Inglesi-lotz (2018), which conducted a review of the residential sector, the majority of households spent most of their income (75 %) on basic needs such as housing, electricity and water, food and transport.

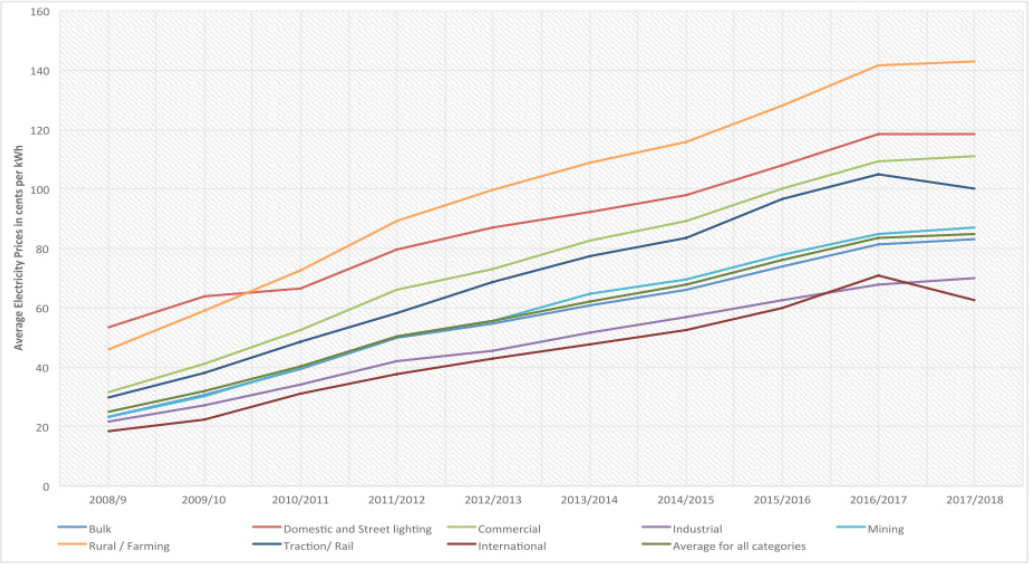

Figure 1. 5: Annual Average ESKOM prices by customer category in cents per kWh (2008-2018). (Department of Energy, 2018a)

The residential sector has accounted for approximately 23–27 % of annual energy consumption in South Africa as of 2015 and is second largest energy consumer in the economy (refer to Figure 1.6). Heating of water accounts for about 35–50 % of the total residential energy demand (Curry *et al.*, 2017; Donev *et al.*, 2012) as this is used for sanitary activities such as bathing, washing clothes and dishes, and cooking (refer to Figure 1.7). However, according to Bohlmann & Inglesi-lotz (2018), hot water heating can be as much as 50 % as majority of households do not use energy for space heating.

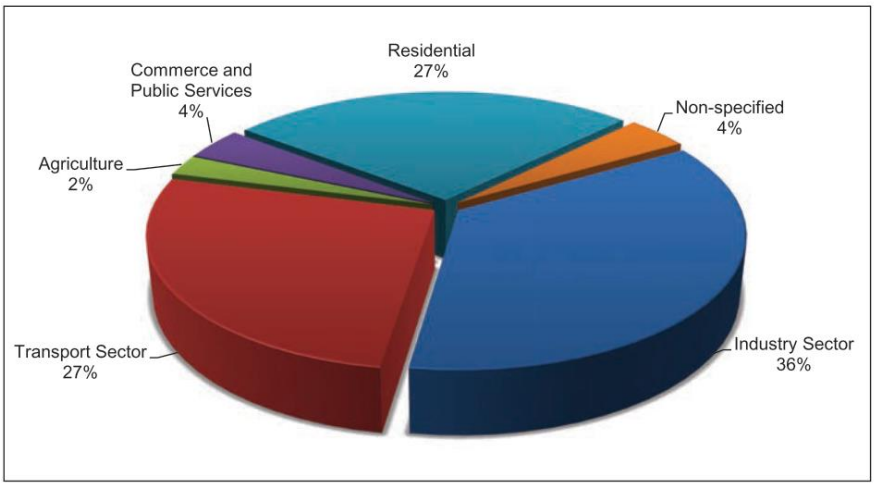

Figure 1. 6: Energy consumption by sector (Department of Energy, 2018b)

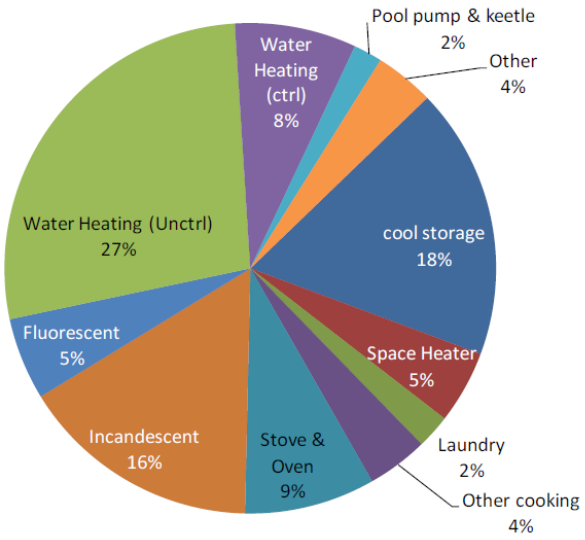

Figure 1. 7: Residential electrical end-use consumption (de la Rue du Can et al., 2013)

The primary technology used for for residential water heating within the country is currently electrical resistance water heaters (ERWH), commonly called “geysers” or “boilers”. These make up 98.85 % of all water heaters in the country, estimated to be over 5.4 million units (Nel, Booysen & van der Merwe, 2016). Moreover, more inefficient water heating methods are used in urban households which operate on the same energy principles as ERWH such as electric kettles and stoves or a combination of the two, and in the rural household biomass such wood and charcoal are used to meet hot water demand (Nel *et al.*, 2016).

ERWHs are cost-effective, convenient for installation and operation and possess low maintenance characteristics. However, the technology has several shortcomings, such as being energy extensive, inefficient as the overall efficiency of converting electrical energy to thermal energy is relatively low, and are mostly powered by fossil-fuelled energy sources (Hepbasli & Kalinci, 2009; Ibrahim, Fardoun & Louahlia-Gualous, 2014). Moreover, the use of fossil fuel based systems leads to both direct and indirect increased GHG.For instance, according to Chaturvedi, Gagrani & Abdel-Salam (2014), using a conventional gas water heater typically contributes about 2 tons of CO2 annually to the atmosphere, while ERWH are indirectly responsible for about three times more for each unit of electrical energy consumed.

Based on all the findings above, the South Africa government is currently aiming at decarbonising its energy sector through the establishment and the development of a modern renewable energy industry. This will assist in the mitigation of growth in electricity consumption and carbon emissions (CO2) . For example, the South African Department of Energy (DoE) published a White Paper on renewable energy in 2003, which aimed at an annual contribution of 10 000 GWh of renewable energy to be achieved over a 10 year period (Pegels, 2010). In 2010, the Integrated Resource Plan (IRP) proposed to generate 42 % of the total output, which

amounts to 17.8 GW of electricity by renewable energy, and plans to limit its CO2 emissions to below 275 million tons by 2025. This is planned to be met with renewable power generation technologies such as solar PV ,wind turbines and hydro-storage and non-power generation such as solar water heating (SWH) and biofuels. (Donev et al., 2012). A standard was published for " energy efficiency in building" which prescribes that for water heating, "a minimum of 50 % of the annual average-heating requirement for hot water must be provided by means other than electric resistance heating" (SANS, 2011). From the above perspective, there is sufficient motivation to investigate and explore alternative options for water heating, specifically renewable energy and sustainable approaches.

1.2 Statement of research problem

Multitudes of challenges face the energy sector in South Africa. To aid in alleviating these challenges, the country has adopted renewable energy perspectives by developing and implementing policies, standards, programmes and technologies.

In support of the country's newly adopted energy policies and perspectives, this study proposes to investigate the potential application of direct expansion solar-assisted heat pump (DX-SAHP) for water heating. The DX-SAHP is a confluence of heat pumps and solar thermal water heating systems. The system consists of a solar collector, compressor, a condensing heat exchanger and a throttling /expansion device. The solar collector serves as the evaporator for the system and thus the working fluid or refrigerant is directly vaporized by solar radiation, where the refrigerant stores the energy due the phase change from liquid to vapour. This configuration results in a few advantages, such as lower initial investment for the collector and energy consumption, extended collector life, and higher heat transfer coefficients due to direct vaporisation; further, using bare collectors results in higher efficiencies, anti-corrosive properties and night freezing. Moreover, it can extract energy from both solar and ambient air (Kara, Ulgen & Hepbasli, 2008).

DX-SAHPWH systems have been researched worldwide as an alternative to conventional water heating methods. Several authors (Anderson & Morrison, 2007; Huang & Lee, 2003; Soldo & Balen, 2004; Xu, Zhang & Deng, 2006), have investigated the efficiency of DX-SAHP systems compared to other water heating methods. Moreover, several review papers have been published, further accentuating the establishment of the field (Mohanraj, Belyayev, Jayaraj & Kaltayev, 2018a; Omojaro & Breitkopf, 2013; Poppi, Sommerfeldt, Bales, Madani & Lundqvist, 2018; Shi, Aye, Li & Du, 2019; Wang, Guo, Zhang, Yang & Mei, 2017). To accentuate its performance against conventional methods, a few publications will be

highlighted. For instance, (Sterling & Collins, 2012) compared the SAHP to conventional residential solar hot water (SHW) system and an ERWH system using a modelled approach via TRNSYS software. The modelling assumed the same hot water draw profile and delivery hot water temperature and the results indicated that the SAHP system proved to be the most energy efficient and exhibited the lowest annual operating cost of the three water heating systems. Further studies conducted by (Sun et al., 2015), stated that using the DX-SAHPWH can potentially yield COP about 2 to 3 times higher than conventional ASHPWH heat pumps. This is achieved because the solar evaporator of the system can supply energy at higher temperatures than the ambient outdoor air, which consequently results in a higher COP than that of a conventional air-source heat pump. More specifically, the COP in SAHP systems is around 4 as opposed to 2.5 in ASHP systems (Bellos & Tzivanidis, 2017).

Furthermore, unlike conventional solar water heating systems which are solely dependent on solar energy, the DX-SAHP system is highly efficient as water heating can occur in the absence of solar radiation, such as at night or during rainy days due to the direct expansion solar collector evaporator which allows both solar and ambient energy to be used as energy gains (Anderson & Morrison, 2007). In addition, the system carries economic benefits such as lowered heat pump operating costs compared to conventional heat pumps due to enhanced COP. For instance , according to (Tzivanidis et al., 2016), the DX-SAHP can potentially yield COP about 2 to 3 times higher than conventional heat pumps depending on climatic conditions; more specifically, the COP in DX-SAHP systems is around 4-6 versus 2.5-3.5 in conventional heat pump systems. Furthermore, the are economic and environmental benefits such as reduced initial investment and payback periods as bare collectors are primarily used (Chaturvedi *et al.*, 2014; Tagliafico, Scarpa & Valsuani, 2014). Moreover, switching from ERWH to DX-SAHP water heater systems can result in 75% greater reduction in carbon emissions, depending on climatic conditions (Malali, Chaturvedi & Abdel-salam, 2016).

Although DX-SAHP system has many advantages, however, its main shortcoming is the erratic collector-evaporator load due to diurnal and seasonal swings in meteorological conditions. Therefore, depending on the geographical location ,the DX-SAHP system performance will vary. Consequently, to discern whether it is a suitable technology for South Africa, an analysis is therefore required to evaluate the performance of the DX-SAHPWH system prior to implementation.

Research aim and objectives of the study

The aim of this dissertation is to develop a mathematical model of a DX-SAHPWH to determine the thermal performance characteristics in South Africa's meteorological conditions and to investigate the effects on the performance of the DX-SAHPWH system. The essential premise is to provide quantitative data in the form of performance metrics.

The objectives of this dissertation in support of the research aim are as follows:

- To conduct an extensive literature review on DX-SAHPWH systems highlighting the current level of knowledge, the system components and configuration and modelling approaches used.
- To develop a theoretical mathematical model of a DX-SAHPWH system based on the literature review.
- To simulate the theoretical mathematical model to assess the daily and annual performance of the DX-SAHPWH system by using the climatic conditions of South Africa. The daily performance must consider typical summer and winter performance.
- To conduct a parametric study with the mathematical model to investigate the effects of the meteorological parameters on the performance of the DX-SAHPWH system.

1.3 Research design and methodology

The nature of this study is theoretical and thus an analytical analysis was adopted This provides quantitative data to evaluate the performance of the DX-SAHP system. This consisted of the development of a *quasi-static* mathematical model that represented the DX-SAHPWH system and consisted of four sub/partial models i.e. solar collector evaporator, compressor, condenser and hot water storage which are a system of steady-state energy-balance algebraic equations that govern the components of the DX-SAHPWH system.

Thereafter, input data, i.e. the physical parameters, meteorological conditions and hot water tank temperature was used in the mathematical model and subsequently simulated to produce the anticipated performance metrics. The output data was used to assess the performance of the DX-SAHP water heater system; the performance criteria such as the COP, collector efficiency, solar fraction, and heating time were used. The research is based on modelling and simulation and thus most of the emphasis was placed on the design and programming of the mathematical model.

1.4 Delineation of research

The following delineations pertain to this research:

- The current study is based on theoretical model and thus the results presented were only for the simulated models. Consequently, a prototype must be correctly design, manufactured and tested to obtain accurate results.
- The performance data presented of the DX-SAHPWH system will only be viable for the specified location meteorological conditions (Stellenbosch, Western Cape); however, the same methodology or mathematical model could be easily applied to other regions of South Africa.
- The only meteorological conditions that were considered were ambient temperature, solar radiation and wind speeds

1.5 Significance of the study

The DX-SAHP water heater system is not a novel technology and has been researched by several authors worldwide**.** However, it has not been researched in the meteorological context of South Africa or Africa as a whole and therefore no existing qualitative performance data for this type of water heating system exists. This is supported by Shi et al. (2019) which notes that the research is predominately concentrated in the Asia and Europe. The significance of this research is to present this data to elucidate the thermal performance of the DX-SAHPWH system and the effect of meteorological parameters on system performance in the context of South Africa's climate.

1.6 Organisation of the dissertation

The dissertation is set out to achieve the aims and objectives in six chapters. The content of each chapter is summarized below.

Chapter 1 presents a holistic perspective of the proposed research to be conducted within the sphere of this dissertation. Contained in this chapter are the research background, research problem question, methodology, delineations and significance and anticipated contributions.

Chapter 2 presents a detailed review of recent literature of direct-expansion solar-assisted heat pump (DX-SAHP) systems. This chapter will be disseminated into 3 sections: the first section provides a general overview on solar- assisted heat pumps with regards to their

application, classification, and arrangement. The second delves into DX-SAHP water heating systems with an extensive review of literature only from the last two decades. It aimed to highlight typical daily and annual performance of the system, system components and configuration, working fluid used and the effects of meteorological, operational and design parameters on performance. The third section, which is focused on the mathematical modelling literature of DX-SAHP systems, aims to elucidate the various approaches used in such modelling. It describes the various components: collector-evaporator, compressor, expansion valve, condenser and hot water storage tank and refrigerant, their respective purposes within the system, and thereafter the various modelling approaches used.

Chapter 3 presents the mathematical model of the DX-SAHPWH system. The model was essentially based on the first law of thermodynamics and continuity of mass, which states that energy and mass are conserved. An analytical steady-state approach was adopted for all the system components which consist of four models of collector-evaporator, compressor, condenser, and water storage tank. In addition, it presents information about input data of the model and the system simulation procedure.

Chapter 4 presents the results and discussion of the simulation results. The hourly and annual performance of the system are presented and discussed. A summer and winter day were selected to provide disparate scenarios on system performance, and thereafter annual performance was simulated to give a holistic perspective on the system. Moreover, a parametric analysis was conducted to investigate the influence of the meteorological and operational conditions on the system performance.

Chapter 5: In this chapter, the research is concluded and recommendations are made to improve the mathematical model, and future work is suggested to further the increase the body of knowledge related to this research.

CHAPTER 2: LITERATURE REVIEW

2.1 Section One: Solar-assisted heat pumps

Solar-assisted heat pumps (SAHPs) were first proposed by Sporn and Ambrose in 1955 and extensive research on these systems only began in the 1970s (Omojaro & Breitkopf, 2013). SAHP is amalgamation of solar heating and heat pump technology which directly integrates the reverse-vapour compression refrigeration cycle that conventional heat pumps use, however, they also incorporate a solar thermal collector, which works as the evaporator of the system. SAHP is a versatile technology and can be employed in a plethora of applications for low temperature (<80 °C) applications like water heating and space heating in both commercial, residential and industrial sectors. Mohd & Hawlader (2015) investigated SAHP for desalination purposes, Bai et al. (2014) investigated SAHP for heating demands for a sports centre, Hawlader & Jahangeer (2006) for drying of green beans and Wang, Li & Qiu (2019) for mangoes. Liu et al. (2015) conducted simulation studies for space heating office buildings in severe cold areas. Furthermore, they can be multi-functional and provide both water and space heating. SAHPs can be generally be classified as either parallel and serial, are based on how the solar collector and heat pump evaporator are coupled (refer to Figure 2.1).

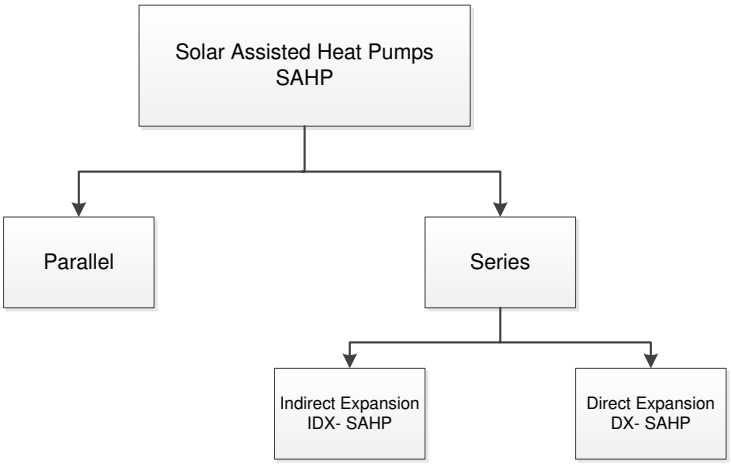

Figure 2. 1: Classification of solar-assisted heat pumps

In the parallel SAHP system in Figure 2.2, the solar thermal collector and heat pump units can independently supply thermal energy to heat the water. To supply a storage tank, the collectors charge the storage tank and if the amount of energy supplied by the collectors is insufficient,

then, an additional heat source can be operated in parallel to the solar thermal collector such as an air or ground source heat pump (Chu & Cruickshank, 2016; Kim, Choi, Han & Hyung, 2018). For instance, during the day, the solar collector can meet the demand, and during night or cloudy days (poor solar radiation conditions), an auxiliary heat source will begin to operate (Wang *et al.*, 2017). Moreover, the parallel systems are considered to be robust and reliable, as if one system breaks down, i.e. air source-evaporator, the solar collector will still be operational and has less complex hydraulic connections and system controls compared to series systems.

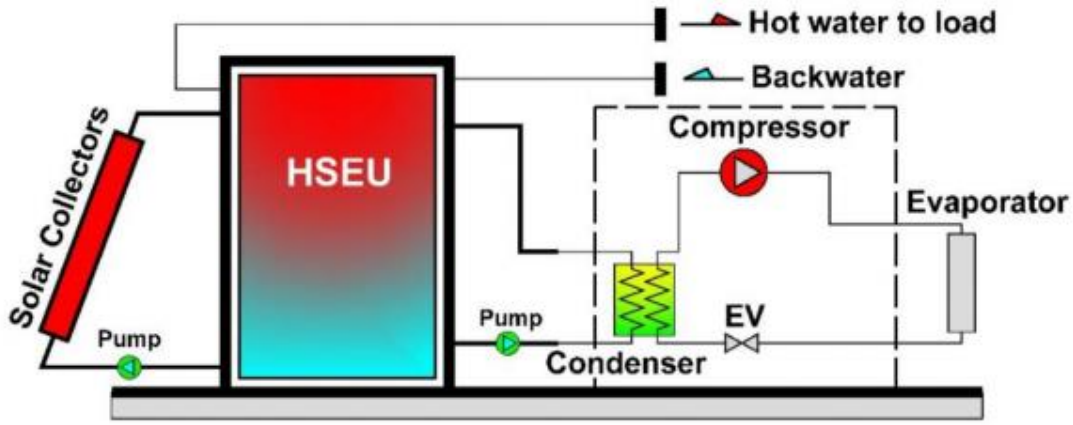

Figure 2. 2: Schematic of parallel SAHP (Fan, Zhao, Han, Li, Badiei, Golizadeh & Liu, 2021)

In the series SAHP system in Figure 2.3, the solar thermal collector acts the central thermal energy source of the heat pump unit. When an SAHP is configured this way, it concurrently increases the COP of the heat pump due to a higher evaporator temperature, and direct exposure to solar radiation improves the solar collector efficiency. The benefits of this arrangement are that in hot weather (summer or spring), the ambient temperature can higher than the temperature of the collector fluid, thus resulting in additional energy gain which increases the collector efficiency and increases the daily operation period of the collector. Moreover, in colder weather (winter or autumn) , a decreased heat transfer loss is typically expected as the temperature difference is small between the collector fluid and ambient temperature and thus an increase in collector efficiency (Chu & Cruickshank, 2016).

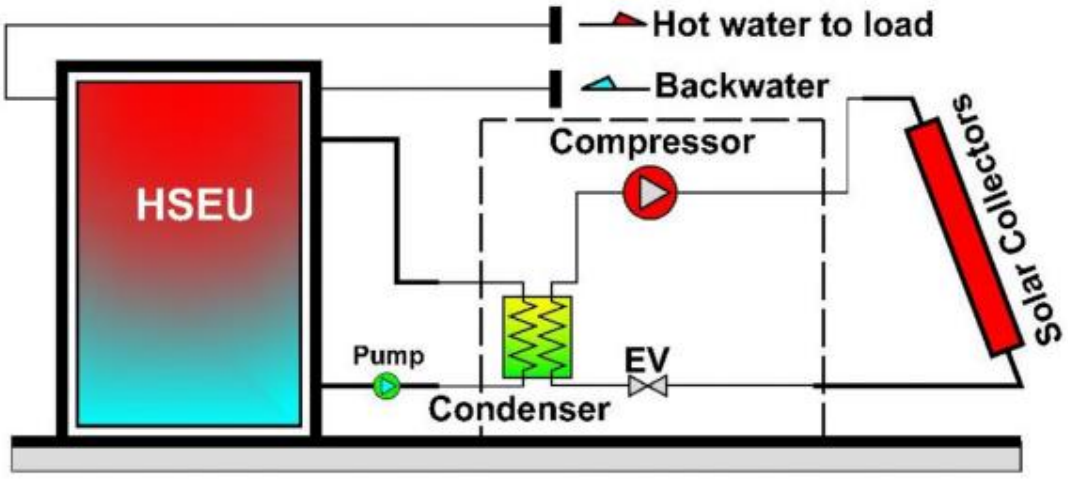

Figure 2. 3: Schematic of series SAHP (Fan *et al.*, 2021)

Furthermore, SAHP systems in series can be bifurcated into either a direct (DX-SAHP) or indirect (IDX-SAHP) configurations. This is based on how the solar thermal collector is coupled to the evaporator of the heat pump either direct or indirect. These are explained in the following paragraphs.

Indirect expansion SAHP (IDX-SAHP)

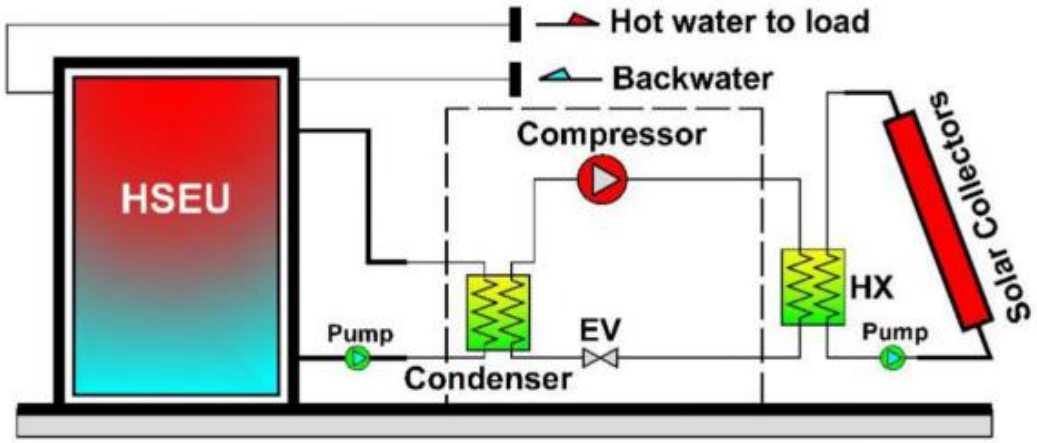

Figure 2. 4: Schematic diagram of a IDX-SAHP system (Fan *et al.*, 2021)

IDX-SAHP systems (see Figure 2.4) ,there are two individual circuits. One heat pump and solar collector circuit. The two circuits are amalgamated through an intermediate heat

exchanger for facilitating solar energy. The heat pump circuit consists of standard components such as compressor, condenser, expansion valve and an evaporator, which acts as an intermediate heat exchanger. The solar collector circuit consists of a solar collector, a pump, and an intermediate heat exchanger. The intermediate fluid is typically water or ethylene glycol, and is used to absorb solar radiation through the collector and transferred to the intermediate heat exchanger. The refrigerant in the heat pump circuit gains the heat from intermediate fluid during its evaporation and rejects the heat in the condenser for water heating (Mohanraj et al., 2017b). These systems more advantageous for countries which possess colder climate as a heat pump can provide thermal energy in the presence of poor solar radiation conditions.

Direct expansion SAHP (DX-SAHP)

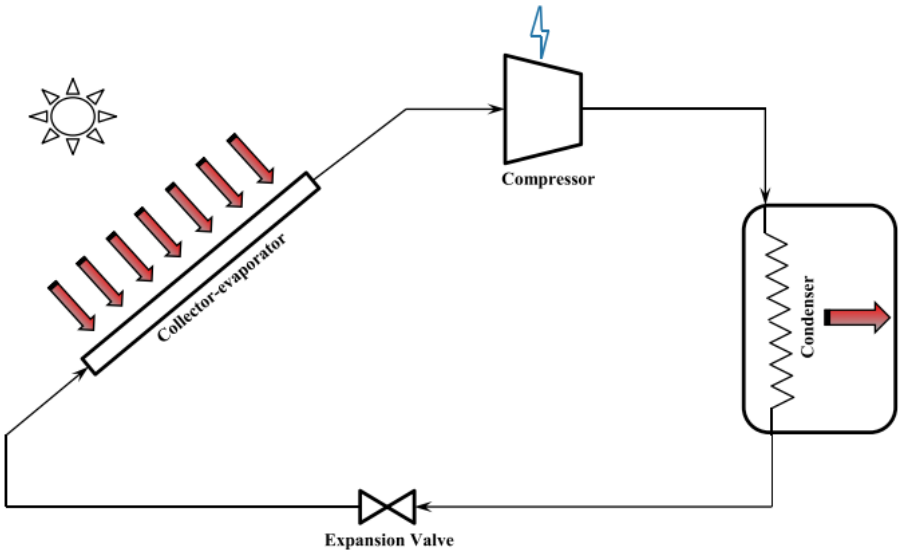

Figure 2. 5: Schematic diagram of a DX-SAHP system (Shi *et al.*, 2019)

In the DX-SAHP (see Figure 2.5), the solar collector and the heat pump evaporator are combined to form a collector-evaporator where the refrigerant is directly evaporated by absorbing solar radiation or ambient thermal energy. The vaporised refrigerant is driven by a compressor and then is condensed in an immersed condensing heat exchanger, passes through the expansion valve and returns to the collector-evaporator. When compared to IDX-SAHP, The DX-SAHP has a number of advantages such as higher evaporation temperature, lower solar collector energy losses which yield higher efficiencies, and improved collector

lifetime. Moreover, the direct evaporation/expansion of the refrigerant inside the solar collector eliminates the intermediate heat exchanger, thus eliminating the inherent inefficiency of an IDX-SAHP. The disadvantages of the DX-SAHP is that not suitable for large scale operation as it requires a large area of solar collectors which results in an a high extension of the refrigerant loop circuit, which may result in refrigerant leakage and trapping of the refrigerant in the evaporator and the condenser. Furthermore, the volatility of the systems compressor and performance due to fluctuation of solar radiation (Wang *et al.*, 2017). Therefore , this type of systems are suitable for smaller -scale /residential type applications and more suitable for countries with warmer climates and high solar radiation availability.

2.2 Section Two: Direct-expansion solar-assisted heat pump water heater review

This section presents a chronological review of the relevant work done on direct-expansion solar-assisted heat pump (DX-SAHP) systems. SAHP research began during the early 1970s. However, only literature from the last two decades will be rigorously reviewed. Furthermore, this review aims to highlight typical daily and annual performance of the system, system components and configuration, and the influence of meteorological, operational and design parameters on the performance of DX-SAHP systems. Several reviews have been published by authors (Badiei et al., 2020; Mohanraj et al., 2017b; Omojaro & Breitkopf, 2013; Poppi et al., 2018; Shi et al., 2019) outlining varying aspects of DXSAHPWH.

Hawlader, Chou & Ullah (2001) performed numerical, experimental and economical investigations of the DX-SAHP. Their system consisted of a 3 m^2 unglazed flat collector-evaporator, open type reciprocating-type hermetic compressor, thermostatic expansion, 250 L water tank with immersed helical coil condenser and R134a as the refrigerant of the system. Figure 2.6 illustrates their DX-SAHPWH. A quasi-steady state mathematical model was developed and simulated under the climatic conditions of Singapore to approximately predict the long-term thermal performance of the system. The results indicated that the COP ranged from 4 to 9 and collector efficiency 40 % and 70 % for a water tank with temperature varying from 30–50 C. To further provide insight into the elements which influence the performance of the system, a parametric study was conducted with the mathematical model. The results showed that increases in solar irradiation and ambient temperature had positive impacts on COP and collector efficiency. Furthermore, compressor speed decreases the COP and increases collector efficiency and thus have a conflicting system performance relationship . The effect of storage volume was also investigated and it was found that with increases in storage volume, both collector efficiency and COP increased. However, after a certain range of storage volume both collector efficiency and COP remained constant.

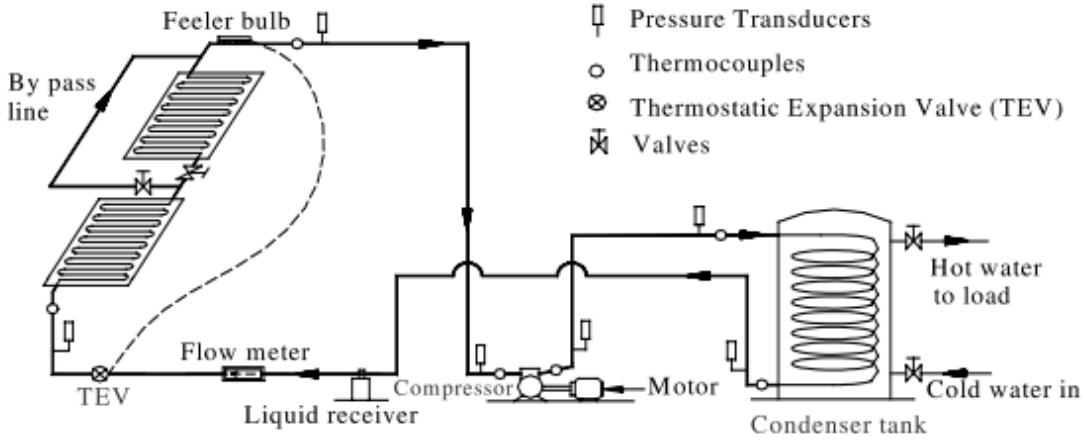

Figure 2. 6: Schematic diagram of a Hawlader DX-SAHP system (Hawlader *et al.*, 2001)

Kuang et al. (2003), conducted analytical and experimental studies on a DX-SAHPWH system using R22, which a 2 m^2 unglazed flat collector, a 150 L water storage tank with an immersed helical coil heat exchanger as condenser, a thermostatic expansion valve (TEV), and a small hermetic refrigeration compressor. A quasi-steady state simulation model was developed to predict the long-term thermal performance of the system by using FORTRAN and using the meteorological data of Singapore for typical summer, spring and winter days as input data. Their findings included monthly averaged COP values between 4 and 6 for solar radiation values above 250 W/m^2 while the collector efficiency ranged from 40 to 60% and the system could achieve COP of above 2.5 even at low ambient temperature and under poor solar radiation conditions **(**refer to Figure 2.7). They also conducted a parametric study similar to Hawlader et al. (2001) and obtained similar results. However, in addition, they specified that an optimum size of storage tank should be chosen for a given collector area; and also that if there is a mismatch between the fluctuating load on the collector and the constant capacity of the compressor on the COP and collector efficiency, to curtail such effects, a variable speed compressor or an electronic expansion valve with a controller should be employed in the system.

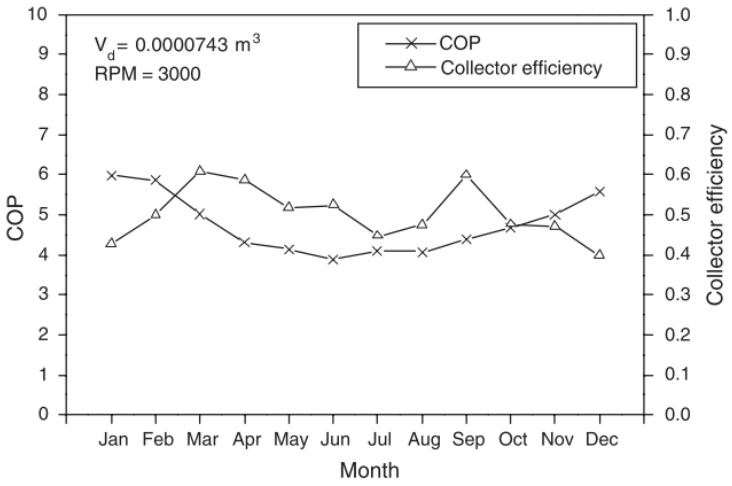

Figure 2. 7: Variation in the monthly averaged COP and collector efficiency in a year (Kuang et al., 2003).

Huang & Lee (2003) conducted an experimental analysis of different water heating methods, i.e. ERWH and conventional SWH, and showed that the DX-SAHP had the least energy consumption and possessed high reliability even under severe variations of solar incident radiation intensity, wind speed/direction, ambient temperature and rain. A similar study was conducted by Xu et al. (2006) by numerical simulation. The study compared DX-SAHP, solar thermosiphon system with electrical backup, and ERWH, in Nanjing, China. The DX-SAHP presented the best performance in terms of energy consumption and efficiency. Anderson & Morrison (2007) conducted an experimental analysis in Sydney, Australia, and the COP ranged from 5–7 in clear daytime conditions and from 3–5 under clear night-time conditions.

Li et al. (2007a) conducted an experimental analysis of the DX-SAHP for water heating in spring conditions in Shanghai, China. The system consisted of 4.2 m^2 collector-evaporator, 750 W rotary-type hermetic compressor using R22 and a 60m coil copper tube condenser immersed in a 150L domestic hot water tank insulated with 38mm polyurethane and a thermostatic expansion valve (see Figure 2.8). The results showed the COP of the system can reach 6.61 in conditions of average solar irradiation of 955 W/m^2 and ambient temperature of 20.6 ◦C. The system also reached a COP of 3.11 during rainy conditions with an average ambient temperature 17 ◦C. Overall, the seasonal performance of the system was COP of 5.25 and collector efficiency of 1.08 respectively. In addition, to identify the inefficient components of the system, a theoretical exergy analysis was conducted. The authors found that the highest exergy loss occurs in the compressor, followed by collector-evaporator, condenser and expansion valve. The same recommendations were given as Kuang et al (2003), i.e. variable speed compressor or an electronic expansion valve with a controller to improve system

performance/exergy losses. They conducted a follow-up study (Li et al., 2007b), which conducted more experiments in spring and autumn. Experimental results indicated that higher COP values around 6 are expected in spring due to higher evaporating temperatures, collector efficiencies of in the excess of 88 % and heating times around 90 minutes. In autumn, the COP was 4–5,collector efficiencies the same as spring, and longer heating times around 180 minutes.

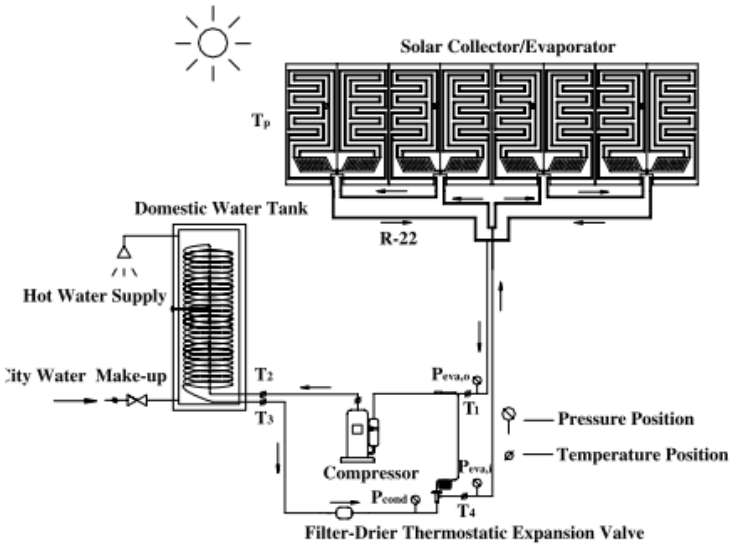

Figure 2. 8: Schematic of DX-SAHPWH (Li et al., 2007b)

Ji et al. (2008) conducted an experimental analysis, followed up in Ji et al. (2009) with a dynamic modelling of DX-SAHPWH with a solar photovoltaic (PV) as the evaporator, also called a PV-SAHP (see Figure 2.9). The aim of this design is to convert the incoming solar radiation into electricity to power the compressor and concurrently evaporate the refrigerant in the heat pump component. Moreover, the system also increases PV efficiency as the evaporation temperature of the refrigerant is normally lower than the PV cells. The studies' results indicated the COP could reach as high as 10.4 with an average value of 5.4. The design consisted of PV cells laminated on the front surface of the thermal absorber, air evaporator, R22 variable-frequency compressor, air and water-cooled condenser and electronic expansion valve. The PV-evaporator power was able to provide 85% of the compressor's, with an average photovoltaic efficiency of 13%.

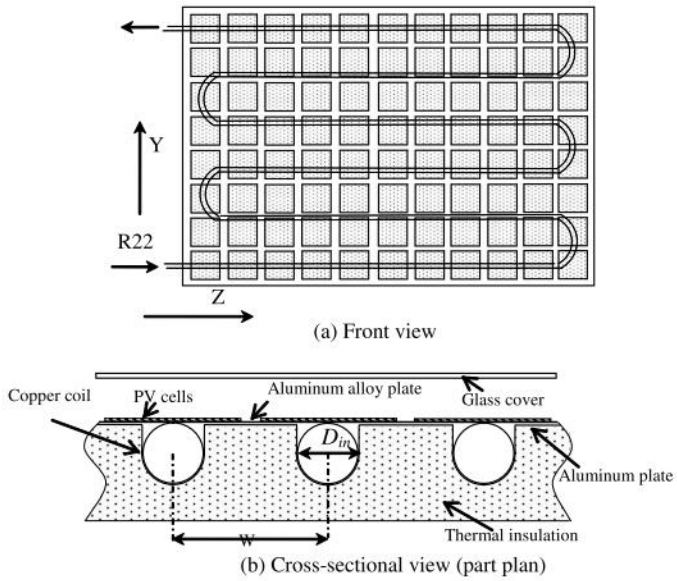

Figure 2. 9: PV-Thermal Collector-Evaporator (Ji et al., 2008)

Chow et al. (2010) conducted a theoretical analysis and investigated the annual performance of a residential-scale DX-SAHPWH system in Hong Kong's sub-tropical climate. A numerical mathematical model of the system was developed and consisted of serpentine collector-evaporator, a water tank with immersed condenser, 1KW variable speed reciprocating compressor, capillary tube and R134a as the refrigerant of the system. Subsequently, numerical simulations were performed using Hong Kong typical meteorological year (TMY) hourly data, which were used to predict the daily and year-round performance of the system. The results displayed an annual average COP of 6.46, annual hot water generation of 360 300 kg and the system performed better and generated more hot water in the summer, with COP values up to 10 and higher due the higher ambient temperature and better availability of solar radiation during the period. In winter, the monthly average COP values were 7.5. It is noteworthy that compressor power consumption was higher in summer periods compared to winter, which is corroborated by Kuang et al. (2003). Furthermore, the COP varied throughout the day and was significantly influenced by the solar radiation (see Figure 2.10) .Chow et al. (2010) conducted a follow up study (Chow, Fong, *et al.*, 2010) by investigating a PV-SAHP as an alternative evaporator. The results indicated that is possible to achieve a yearly average COP of 5.93 and PV efficiency of 12.1 %. Moreover, the system has a better performance in summer compared to winter, with the monthly average values of COP of 6.89 and double the hot water production of winter. Moreover, they compared DX-SAHPWH with their system and found that the annual water heat gain of DX-SAHP is 25.4% higher than PV-SAHP but has about 15% higher compressor power consumption. The monthly COP of DX-SAHP is also slightly higher with an annual average COP of 6.46, compared to 5.93 in the case of PV-SAHP.

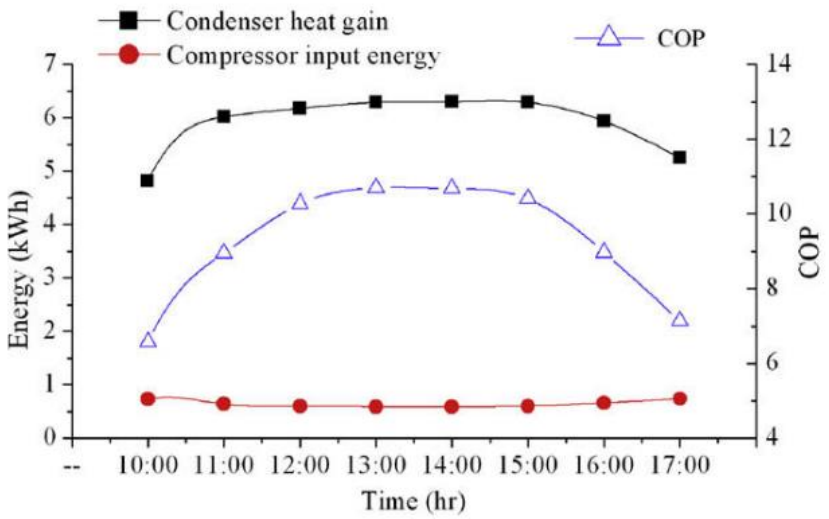

Figure 2.10: Daily variation of condenser heat gain, compressor input power, and system COP on a typical summer day (Chow et al., 2010).

Kong et al. (2011) performed numerical simulations to predict the thermal performance of the system, with aim of comparing it to the experimental results published by Li et al. (2007b). A mathematical model of the system was developed using C++ and they investigated the effects of solar radiation, ambient temperature, wind speed, and compressor speed on the thermal performance of the system. The mathematical model of the system comprised four partial steady-state energy balance models of collector-evaporator, compressor, condenser and thermostatic expansion valve. The lumped parameter approach was used for the compressor and expansion valve models, whereas the distributed parameter approach was used to model the collector-evaporator .Moreover, refrigerant charge and mass flow rate were also modelled through each component which was used for the model convergence. The results indicated that solar radiation increases the COP while decreasing the collector efficiency. The authors stated that that was due to the increase of solar radiation results in a higher evaporating temperature of the refrigerant, consequently resulting in an increase in COP. Moreover, the ambient temperature also increased the COP and collector efficiency, which lowers the heat transfer loss from the collector and concurrently increases the refrigerant temperature in the collector (see Figure 2.11). The wind speed on the other hand slightly increases the COP and collector efficiency if the absorber temperature is less than the ambient, which enables the collector to harvest more energy from the environment. Overall, this showed good agreement between the simulation and experimental results by Li et al. (2007), and the simulated values of the COP displayed the same trend with the average relative error of 7.41 %.

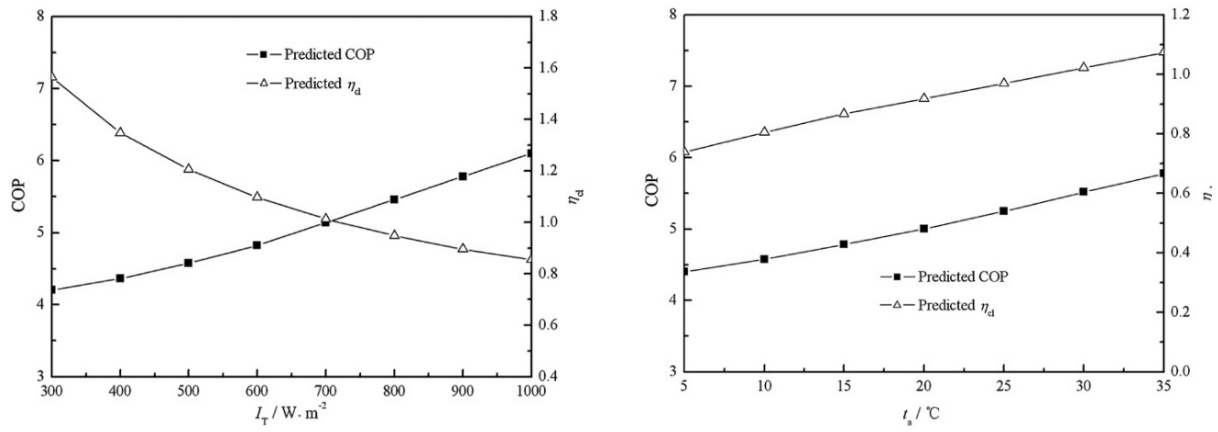

Figure 2. 11: Effect of solar radiation and ambient temperature on system performance (Kong et al. 2011)

Zhang et al. (2014) investigated the effect of refrigerant charge and structural parameters on the performance of DX-SAHPWH by performing a numerical analysis with the same system as Kong et al. (2011). The results showed that most of the refrigerant was in the heat exchangers. The condenser contained 50% refrigerant and about 30% in the collector-evaporator. Furthermore, increases in the refrigerant charge had positive impacts on COP and collector efficiency; for instance, when the refrigerant charge increased from 1.2 kg to 1.8 kg, the COP increased by 36.7% and the collector efficiency 42.3% respectively. For the structural parameters, It was clearly seen that COP increased and collector efficiency decreased rapidly with the increase of solar collector area, which is in agreement with Ito, Miura & Wang (1999) and Yang et al. (2011). The effects of the collector plate thickness and internal diameter of collector tube were also investigated. The results indicated that increases in collector plate thickness had positive impacts on COP and collector efficiency for 2 mm and less, however, from 2 mm to 10 mm they both remained constant. Lastly, increases in internal diameter of tube of the condenser and length of the tube had negative impacts on the COP and collector (see Figure 2.12).

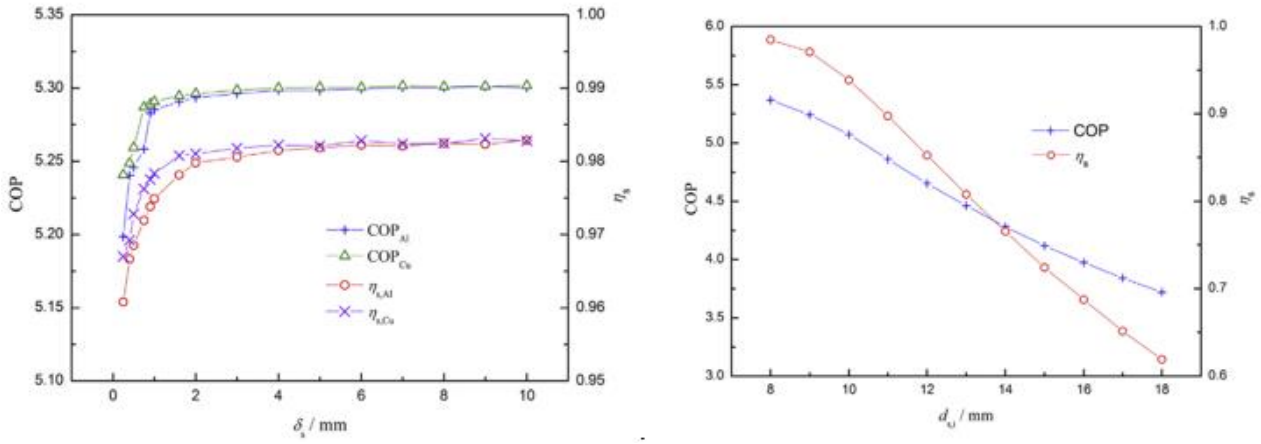

Figure 2. 12: Effect of solar collector plate thickness and internal diameter of collector tube on system performance (Zhang et al., 2014)

Sun et al. (2015) analysed a conventional heat pump (ASHPWH) compared to a DX-SAHP for water heating under various operating conditions in Shanghai, China. They investigated conditions such as clear day and night and overcast night and day both for daily and annual performance, and concluded that the DX-SAHP system has a higher COP in clear daytime conditions, as it is able to harness energy from both ambient air and radiation. In overcast conditions, they both performed equally to an ASHP. They conducted an annual simulation and found that the DX-SAHP has higher monthly average COP of 4–6 compared to the 2.5–4 of the conventional ASHPWH system (see Figure 2.13). However, during night-time conditions the ASHPWH system performed better than the DX-SAHPWH.

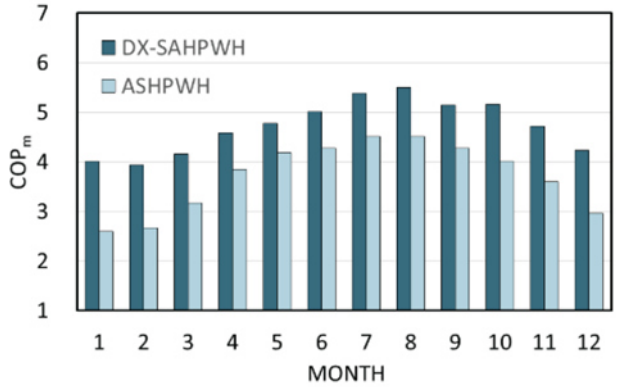

Figure 2. 13: Comparison of annual performance of ASHPWH and DX-SAHPWH (Sun *et al.*, 2015)

Kong et al. (2017) conducted a theoretical parametric study on DX-SAHPWH using R410 as the refrigerant in the system. A numerical model was developed to investigate the effects of refrigerant charge and meteorological conditions on the performance of the system. The results indicated that increases in refrigerant charge , resulted in an increased the energy gain in the collector, energy consumed by the compressor and the heating time of the water decreased while the collector efficiency increased significantly, but had a minute effect on the COP. Moreover, they reported that the meteorological parameters had a significant impact on system performance. The ambient temperature increased both the COP by 56.4 % and collector efficiency by 55 %, with a 74 % decrease in heating time for a range of temperatures from 0–35 °C. The solar radiation increased the COP by 32 % and decreased the collector efficiency and heating by 110 % and 25 % respectively for range of 300–900 W/m^2 (refer to Figure 2.14). The operational parameters indicated that when the compressor speed increases, decreases occurred in both the heating time by 46 % and COP by 59 % respectively, with a slight increase in the collector efficiency for the range of speeds of 1500–3300 rpm. As the initial water temperature increased, it decreases both the COP and heating time by 7.7 % and 53.9 % respectively, with negligible effect on the collector efficiency for the range of temperatures of 0–35 °C.

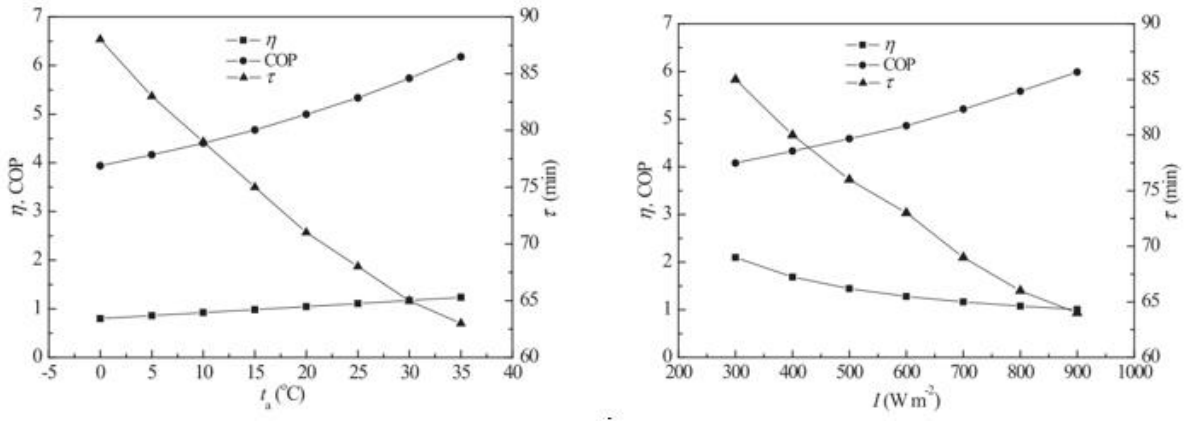

Figure 2. 14: Effect of ambient temperature and solar radiation on system performance.(Kong et al, 2017)

(Kong, Sun, Li, Jiang & Dong, 2018a) and (Kong, Sun, Li, Jiang & Dong, 2018b) and conducted a follow up studies based it on the recommendations of Kong et al. (2011) . They now used a bare flat-plate collector-evaporator with an area of 2.1 m^2, a variable-frequency rotary-type R134a hermetic compressor, a 200 L hot water tank surrounded by a micro-channel condenser, and an electronic expansion valve. The premise of the study was to experimentally investigate the DX-SAHPWH in summer, winter, and autumn conditions. In the first study, they

investigated typical summer conditions where the solar radiation varied from 58–634 W /m^2 and ambient temperature from 28–34 °C. The effects of various parameters, including ambient temperature, solar radiation intensity, compressor speed and final water temperature were analysed experimentally. The metrics used for investigation were the COP, compressor consumption and heating time. As the solar radiation increased from 258-634 W/m^2, the COP increased by 28.3 % and the heating time by 18.2 %. The compressor consumption increased during the morning and slightly decreased but behaved linearly throughout the day, thus showcasing the improvement of the variable-frequency compressor. The ambient temperature varied from 28–36 °C, the COP increased by 6.6 % and the heating time decreased by 6.6 %. The compressor consumption decreased by about 5 %. In the second study, where they studied winter and autumn conditions, they concluded that the average COP was higher than 4.0 and 3.0 in summer and overcast days respectively. Even in the winter conditions, the average COP was also higher than 2.5.

2.3 Section Three: Mathematical modelling of DX-SAHPWH components

Prior to the development of the mathematical model, a review of previous models by other authors was important. This section of the literature reviews modelling approaches of the components in DX-SAHP systems . Generally, DX-SAHP systems are made up of four main elements*:* collector–evaporator, compressor, expansion valve and condenser and hot storage tank. Moreover, in this dissertation, the working fluid or refrigerant was also considered as an element of the system. This part of the review will begin by introducing each respective component and its types, its purpose within the system and thereafter the modelling approaches used.

2.3.1 Mathematical modelling of collector–evaporator

The collector–evaporator is the central element in a DX-SAPWH system. It acts as a heat exchanger that converts solar radiation into thermal energy, which is then transferred to the refrigerant. Normally, unglazed or bare collectors are predominantly employed in DX-SAPWH systems as they are able to absorb energy in various forms, such as solar energy in the form of radiation, sensible heat from ambient air via convection, and latent heat of water vapour in the case of condensation of moisture within the air. Therefore, to quantify these thermal energy gains several models were developed.

- Steady State Approach

The most prominent method used to evaluate the performance of flat plate collectors is a thermal energy analysis approach, namely the Hottel & Whillier-Bliss model (Duffie & Beckman, 2013). This approach relies on the mass-energy balance/conservation of the collector in steady state conditions or instantaneous heat gain, and is simplified to reduce computational time. The model indicates the distribution of incident solar energy into useful energy gain in one-dimensional, and thermal losses due to conduction, convection and radiation and optical losses which cumulate into a simplified overall heat loss coefficient are considered (Duffie & Beckman, 2013). Furthermore, the model depends on the collector characteristics such as geometrical properties, the arrangement of absorber to collector tube, internal convection and mass flow rate flow and efficiency of the absorbers. To model the collector heat transfer losses, all modes of heat transfer are considered, namely conduction, convection and radiation. Several authors have published reviews such as Kumar & Mullick (2010), which looked at wind heat transfer coefficient loss; Matuska & Zmrhal (2009), a software manual which reviewed all types of heat transfer coefficients through a typical solar thermal collector; and Bhatt & Channiwala (2001) who reviewed several top loss coefficients of solar collectors. Normally, researchers neglect the edge and sides of the collector and assume that it is perfectly insulated.

The steady-state approach allows fast computational time due to its simplicity, as thermal resistances are neglected, and is beneficial only with long-time simulations, as highlighted by Tagliafico, Scarpa & De Rosa (2014). Conversely, it is not suitable for control or regulation analysis as it is not very detailed. Moreover, this model is exclusively used for solar radiation energy transfer/gains and does not consider sensible heat from ambient air via convection and latent heat of water vapour in the case of condensation of moisture within the air.

In addition, the steady-state approach can further be classified into single, two-phase or separated flow models which describe the state of the refrigerant (Shi *et al.*, 2019). As the collector- evaporator acts as a heat exchanger, the refrigerant will change state from liquid to vapour and this means its thermo-physical properties will change. Normally, in the collector-evaporator the refrigerant is a saturated liquid and then becomes a superheated/saturated vapour. For the modelling approaches, in the single-phase model, pressure drop is neglected and the outlet state of the refrigerant is assumed to be in the saturated vapour phase and thus the heat absorbed can be calculated easily. The second is the two-phase flow theory. In this approach, the pressure drop is taken into account and both phases are taken into account. It assumes that the liquid refrigerant and the vapour refrigerant are in thermal equilibrium and

now the combined vapour-liquid refrigerant in the collector is considered as a special fluid with specific properties. In DX-SAHPWH modelling, many authors have adopted this approach such as Hawlader et al. (2001) and Kuang et al. (2003). The separated flow model subdivides the refrigerant into a two-phase region, a superheated vapour region and a liquid region. This model represents the actual fluid flow and heat transfer of refrigerant in the collector-evaporator. However, it takes more computation time as the numerical solution needs to converge.

- Dynamic Models

Two approaches are normally used to model dynamic interactions in solar collectors, the Lumped capacitance and discretized models. In the lumped capacitance approach, the collector is lumped model into one section where it consists of one energy balance differential equation, or it is lumped into two-sections where the collector is modelled as two regions, namely: (i) the absorber plate and the heat removing fluid, and (ii) the cover plates lumped together in a single equivalent cover. Both approaches are used ,when there is small variation in data of meteorological conditions and initial water temperature. For instance, during a cloudy or partially cloudy day where the collector is subjected to high variations of solar radiation, it is unable to predict the outlet temperature compared to sunny days (constant solar radiation). The discretized model address the shortcoming of the lumped approach and is able to model collectors are subjected to strong variation of the operating conditions (solar radiation, wind speeds etc.). This is achieved by the discretization of the solar collector along the fluid direction, and an unsteady energy balance equation is written for each node. It is thus able to accurately model the fluid temperature profile and calculate the outlet fluid temperature. Consequently, these models are computationally extensive, and a more complex implementation is required.

2.3.2 Mathematical Modelling of Compressor

The purpose of the compressor in the DX-SAPWH is to compress the low-pressure vapour from the evaporator and raise its pressure and temperature to ensure that adequate heat will be supplied to the condenser to heat the water Omojaro & Breitkopf (2013). Furthermore, it can be also considered the heart of the vapour compression cycle (VCC) and DX-SAPWH systems as it is used to determine both condenser and evaporating capacities. The

compressor model is critical in DX-SAPWH simulations and performance analysis as it is responsible for three parameters. This is of high significance as it should be calculated accurately to predict the performance of DX-SAPWH systems (Ding, 2007). For instance, if refrigerant mass flow rate prediction is incorrect, it will be propagated to other component models such as the evaporator and condenser heat exchangers, which are normally oversized for practical design.

There are many different approaches to model a compressor and the suitable method is selected based on the desired outputs and available data. Generally, they can be categorized into three groups: black box or map-based models; grey box or efficiency-based models; and white box or detail-based models (Qiao & Radermacher, 2010).

- Black box models

Black box models are based on extensive empirical data from compressor tests and have highly accurate performance analysis in term of mass-flow rate, power consumption and the discharge temperature. These models are estimated by using single variable or multi-variable regression analysis carried out between measured data such as suction, discharge evaporators and condensing temperature energy consumption and COP. Moreover, these models are suitable for system simulation as they do not consider geometric and physical parameters of the compressor, which results in quicker computational time. However, they do possess limitations such as being only valid for certain ranges, they are unable to extrapolate accurately are is not able to describe any physical processes within the compressor. In DX-SAHPWH modelling, a large number of authors have used this approach (Duarte et al., 2019; Faca & Joa, 2014; Kim et al., 2018; Kumar et al., 2016; Miguel et al., 2018).

- White box models

White box models are based on the fundamental equations only, e.g. conservation of mass, energy, and momentum. The compressor is divided into several control volumes and simulates each individual process: compression process, internal refrigerant leakage, heat transfer between refrigerant and compressor components, etc. This approach is suitable for compressor design and not is not suitable for system simulation due to its complexity and

slow computational time (Qiao & Radermacher, 2010). In DX-SAHPWH modelling, no authors have used this approach.

- Grey Box Models

Grey box models fall between the two categories mentioned above, hence the name. These models combine both empirical and physical relations to describe the compressor. They are based on the ideal compression process and utilise the volumetric and isentropic efficiency via semi-empirical and empirical models to predict compressor performance and parameters similar to the black box models (Qiao & Radermacher, 2010; Vindenes, 2018). The advantage of using this model approach is that it results in better accuracy and extrapolation compared to black-box models and better computational time than white box models. In DX-SAHPWH modelling, most authors (Hawlader *et al.*, 2001; Kong *et al.*, 2011; Kuang, Wang & Yu, 2003) initially used these models, which require the mass flow rate through refrigerant properties which are then computed assuming a polytropic compression in the compressor.

2.3.3 Mathematical modelling of condenser-helical coil

The condenser is another central element in the DX-SAPWH system, which acts as a heat exchanger that latent energy gained from the refrigerant is released to the water in the storage tank. Moreover, its purpose is to the receive high pressure and temperature refrigerant vapour from the compressor and condense it back to liquid form. There are several types of condensers used in standard DX-SAPWH systems, and in predominantly all DX-SAPWH literature. Helically coiled tubes are commonly used as heat exchangers inside hot water storage tanks (Chow, *et al.,* 2010; Deng & Yu, 2016; Kong et al., 2011; Kuang et al., 2003; Mohd & Hawlader, 2013; Yousefi, Masoud & Misagh, 2015; Zhou et al., 2016). Other authors used microchannel, concentric counter flow heat exchangers (Miguel *et al.*, 2018) . However, these types will not be discussed in this review as they are not employed in the model. The steady state models for condensers can be classified into three types: single-node or lumped parameter model, zone or moving boundary model, and multi-node or distributed parameter model (Ding, 2007; Qiao & Radermacher, 2010).

- The single-node model or lumped parameter

In this approach, the entire condenser is treated as a single control volume(single-mass body) and the logarithmic mean temperature difference method (LMTD) or NTU-effectiveness method is used to compute the condenser heat gain. These models compute the overall heat transfer coefficient without regard to any phase change. This approach is suitable for system simulation due to its simplicity; however, the limitation is that these models do not account for the variation in refrigerant properties and phase change that occur and therefore their accuracy cannot be ensured. In DX-SAHPWH modelling, many authors have used this approach (Kuang, Wang, *et al.*, 2003).

- Distributed parameter model

In this approach, the condenser is divided into a specified number of segments, which are independent of any phase change, like the lumped parameter approach. The segments are calculated along the direction of flow and thereafter, using the inlet condition to the condenser, all thermophysical properties are then used to calculate the overall heat transfer coefficient. If a phase transition occurs within a segment, it can be further subdivided to model the different parts of the segment. This approach is very accurate; however, it is not suitable for system simulation as increasing the number of segments will not improve accuracy and will increase computational time. In DX-SAHPWH modelling it is not a popular approach, although it is utilised to some degree.

- Zone model or moving boundary.

In this approach, the condenser is sectioned into three zones i.e. a superheated zone, two-phase zone and subcooled zone. The central idea of this approach is to determine the physical properties and consequently, an average heat transfer coefficient for each phase. These models are more accurate than the lumped approach and computational speed lies between that of the lumped parameter model and the distributed parameter model. Furthermore, there is slight difference in accuracy between the distributed parameter and zone model, which makes the zone model a suitable model for system simulation when the accuracy is not critical, with no compromise on computational speed.

2.3.4 Mathematical modelling of expansion valve

The purpose of the expansion valve in the DX-SAPWH system is to reduce the pressure of the refrigerant from the condenser to the evaporator and to regulate the flow rate of the refrigerant. There are a few types which are used in DX-SAHPWH systems; a majority of researchers have used thermostatic types, capillary tubes and orifices. However, electronic expansion valves are recommended by several authors (Kuang et al, 2003; Chaturvedi, 1998) as it allows the DX-SAPWH to maintain a proper matching between the power consumption of the compressor and the evaporative heat gain of the collector–evaporator under widely varying climatic conditions.

There are two modelling approaches used in expansion valves, correlation-based and distributed parameter models. Correlation based models are used to compute the mass flow rate at specific inlet and outlet pressures. These models use basic equations and have adequate accuracy; however, the disadvantage of these models is the unpredictable accuracy of extrapolation. Furthermore, these models are refrigerant-dependant and work inconsistently well, depending on which refrigerant is selected.

Distributed parameter models are much more complex than correlation-based models as they focus on two-phase flow (combined liquid and vapour states) and on whether the flow is homogenous or not. These models can be further classified into homogenous or separated flow models. In the homogeneous models the slip ratio between fluid and vapour phase is unity, and void fraction can be computed analytically. In the separated flow model, the two phase flow is considered and the void fraction is approximated via semi-empirical relationships. The correlation-based approach is predominantly used for modelling DX-SAPWH systems as it is less computationally extensive and requires minimal thermo-physical properties. For instance, Guo, Wu, Wang & Li (2011), Kong et al. (2018), Kong et al. (2011) and Mohamed et al. (2017) modelled the thermostatic expansion valve as an orifice through which the liquid is expanded from condensing to evaporating pressures. The mass flow rate and flow coefficient were correlated according to empirical equations.

2.3.5 Mathematical modelling of refrigerant properties

One essential element of the simulation of a DX-SAPWH system is the determination of the refrigerant's thermodynamic properties. These properties constitute an important delineation on the system's behaviour as it is constrained at any point during each process. Moreover, once the state is constrained, all other thermo-physical properties of the refrigerant viscosity, thermal conductivity, specific enthalpy, entropy volume and can be computed (Laughman et al., 2012)

- The EOS (equation of state) method

Refrigerant properties can be fundamentally calculated using an appropriate equation of state (EOS), which is an equation that relates the pressure, temperature, and specific volume of a substance. There are several equations such as the van der Waals equation, Strobridge-Viral, Beattie-Bridgeman, and best known (and reasonably accurate) equation is the Benedict-Webb-Rubin equation as it was recently developed (Cengel & Boles, 2011). Moreover, these EOSs can predict with high range and accuracy refrigerant thermodynamic properties. However, the EOS method is not miscible for simulation of refrigeration systems as they are computationally expensive as the calculation speed and stability are limited by unavoidable iterations in calculation. In DX-SAHP modelling, a limited amount of authors have used this approach (Chow, Pei, *et al.*, 2010; Yamaguchi, Kato, Saito & Kawai, 2011).

- The explicit polynomial regression method

The explicit polynomial regression method is a rudimentary but efficient calculation method for refrigerant thermodynamic properties and is the most popular technique used in DX-SAHP modelling (Hawlader & Jahangeer, 2006; Miguel *et al.*, 2018; Zhang *et al.*, 2014). Moreover, the method is more stable than the EOS method with adequate accuracy, it is less computationally extensive, and the calculation reversibility of the formulae for saturation pressure and temperature is ensured. One of the first published studies focusing on this method was Cleland (1986) who proposed the use of various polynomials forms/correlations for R12, R22, R114, R502, and R717 for calculation of saturated liquid and vapour properties such as enthalpy, specific volumes and saturation temperature and pressures. He further extended his work in Cleland (1994) by providing correlations for R134a up to saturation temperatures of -60 to 60 ℃. Charters & Safadi (1987) developed polynomial

forms/correlations for R22 for all thermodynamic properties from enthalpy, thermal conductivity, heat capacity, and viscosity, etc. In comparison to Cleland (1986), it provides a more coherent and holistic view in terms of saturated property values but does not provide correlations for superheated ones Furthermore, other authors used the same method to obtain additional R134a properties such as Scalabrin & Marchi (2006) to calculate thermal conductivity; Cristofoli et al. (2002) to calculate the viscosity; and Tillner-Roth and Baehr (1994) to calculate the enthalpy, pressure and specific heat capacity. Martin-Dominguez (2014) proposed another explicit method for calculating refrigerant properties of R22. He proposed the use of various polynomial forms similar to Cleland (1986). Although, the method has its advantages, it is susceptible to divergence in simulations unless a high regression accuracy is applied, and the application range may exclude the region near the critical point. Moreover, it cannot be directly used for zeotropic refrigerant mixtures.

- Implicit regression and explicit calculation method

In this method, an implicit polynomial equation is mathematically regressed by the piecewise smooth regression method and the analytical solutions of the equation are used as the correlations for calculating refrigerant thermodynamic properties. From the implicit polynomial equation, an explicit polynomial equation is calculated by converting the dependent variable of the explicit polynomial equation into an independent variable. Moreover, in these equations the highest degree of the equation is not greater than fourth order, which means that that the equation can be solved analytically which consequently results in better accuracy. The method is miscible for both pure refrigerants and refrigerant mixtures. The deviations from the original property values for regression can be neglected while the computation speed is increased by three times. Authors who have proposed this work are Ding et al. (2005) and Ding et al. (2007) who presented the method for calculation of refrigeration thermodynamic properties and demonstrated application to R22 and R407C.

2.4 Chapter Summary

Based on the literature review, the main points of each section are highlighted as follows:

The first section presented a general overview on solar-assisted heat pumps with regard to their application, classification, and arrangement.

- Solar-assisted heat pumps have various applications such as space and water heating, desalination and drying for all types of sectors.

- Solar-assisted heat pumps are classified into two types, series and parallel which depend on whether the heat pump and solar collector can operate dependently or independently. The series types are further bifurcated into indirect and direct-expansion types, which are based on how the solar thermal collector-evaporator is coupled to the heat pump. In the indirect type, the heat pump and evaporator are separate units. When adequate solar radiation is available, the solar collector is used for hot water demand and when solar radiation is insufficient (e.g., during night or cloudy days), the heat pump starts to operate.

- The direct-expansion type is more suitable for climates with warmer and higher solar radiation values, whereas the indirect type is suitable for colder climates with low solar radiation. When comparing the two, direct expansion types have advantages as they are more economical because the system is amalgamated into one system (one refrigeration loop) versus two systems with an intermediate heat exchanger.

The second section focused on DX-SAHP water heating systems only, with an extensive review only of literature from the last two decades. It aimed to highlight typical hourly and annual performance of the system, system components and configuration used and the effects of meteorological, operational and design parameters on the performance of DX-SAHP systems.

- Most studies conducted are experimental and numerical with aims of discerning the performance under various meteorological conditions, specifically in Singapore and China.
- Most traditional systems have bare flat collector-evaporator (2-10 m^2), reciprocating-type hermetic compressor (300 W -1 KW), thermostatic expansion valves or capillary tubes, hot water storage tank (150- 250 L) with immersed helical coil condensers. The modern systems typically have electronic expansion valves and variable speed compressors.
- Most systems used R22, R134a and R410a and R404a for the working fluids.
- COP values range from 4–10 and collector efficiencies from 40 to over 100%, depending on meteorological conditions and system configurations.
- The system performance varies throughout the day, with better performance when solar radiation is present.
- The system performance is generally higher in summer compared to winter, however COP values are higher compared to conventional heat pumps.

- DX-SAHPWH systems can be incorporated with Solar PV systems to power the compressor.
- Meteorological parameters influences the system performance, Increases in ambient temperature result in higher COP and collector efficiency and decreased water heating time. Increases in solar radiation result in higher COP, decreased collector efficiency and decreased water heating times. Increases in wind speed results in slight decreases in COP and decreases in collector efficiency.
- Structural parameters influence system performances as well. Increases in collector area results in increased COP and decreased collector efficiency. The effects of the collector plate thickness, increases the COP and collector efficiency for 2 mm and less, however, from 2 mm to 10 mm have negligible effects. Increases in internal diameter of the collector tube and the length of condenser tube had negative impacts on the COP and collector efficiency. The effect of storage volume was also investigated and it was found that with increases in storage volume, both collector efficiency and COP increased. However, after a certain range of storage volume both collector efficiency and COP remained constant.
- Operational parameters influence system performance. Compressor speed decreases the COP and increases collector efficiency and thus have a conflicting system performance relationship. Increases in initial water temperature result in increased COP and have negligible effects on collector efficiency and decreases heating time. The refrigerant charge had significant influence of system performance. Typically, most of the refrigerant was in the heat exchangers. The condenser contained 50% refrigerant and about 30% in the collector-evaporator. Furthermore, increases in the refrigerant charge had positive impacts on COP and collector efficiency.

The third section, which is focused on the mathematical modelling literature of DX-SAHP systems, aims to elucidate the various approaches used in modelling DX-SAHP system.

- Mathematical modelling approaches for DX-SAHP for the solar thermal collector-evaporator can be divided into typically steady-state and dynamic (transient) approaches.
- Steady-state approaches are based on the first law of thermodynamics and continuity of mass principles and various modes of heat transfers, namely conduction, convection and radiation. They can be further classified into single and two-phase models which describe the state of the refrigerant and are less computationally extensive compared to dynamic simulations, and thus good for long-term and holistic predictions.
- Compressor modelling approaches for DX-SAHP can be divided into black, white and grey box models. Black box models are based on extensive empirical data from

compressor tests and have highly accurate performance analysis in term of mass-flow rate, power consumption and the discharge temperature. They are suitable for system simulation as they do not consider geometric and physical parameters of the compressor, which results in quicker computational time. White box models are based on the fundamental equations only, for example, conservation of mass, energy, and momentum are used for compressor design. Grey box models are between the two categories mentioned above, hence the name. These models combine both empirical and physical relations to describe the compressor. Most authors have used black and grey models in their modelling and simulation studies.

- Condenser modelling approaches can be divided into three types: single-node model or lumped parameter, zone or moving boundary models, and multi-node or distributed parameter models.

CHAPTER 3: MATHEMATICAL MODELLING OF DX-SAHPWH SYSTEM

Mathematical modelling is one of the most prominent methods to assess the basic behaviour of various components and the holistic relationship of thermodynamic systems amongst others. Moreover, it is an initial step towards simulation. Simulation is the process of predicting performance parameters such as temperature and energy/heat interactions**.** This chapter presents the development of a mathematical model of the DX-SAHPWH system. This involved the formulation of physical laws that govern the dynamics of the system's interactions into equations using variables and constant parameters. The model was based on the first law of thermodynamics and continuity of mass, which states that energy and mass are conserved. Furthermore, several heat transfer concepts are included as the DX-SAHPWH is a thermal machine. An analytical steady-state approach was adopted for all the system components. MATLAB software was used for modelling and simulation.

3.1 Description of the DX-SAHPWH system

The theoretical DX-SAHPWH system was predominantly designed and inspired based essentially on systems designed by Kuang et al. (2003) , Li et al. (2007a) and Franklin (1989). However , a few modifications were made based on recommendations of various authors (see Figure 3.1 below). The system is designed to be installed in the roof of a residential home, where ERWHs are typically situated (refer to Figure 3.2).

The system consists of 2 bare/unglazed solar collectors used as the evaporator-heat exchanger with an area of 4.2 m^2, the solar collector dimensions are 2 m long and 0.8 m wide, and they are made of two aluminium sheets which is coated black to ensure high absorptivity. The collector acting as the solar radiation absorber has refrigerant copper tubes running underneath in a serpentine configuration. The choice of this configuration was based on a study by Allan et al. (2015). The copper tube pitch was 50 mm. The whole is cased in aluminium and is insulated on the lateral, top and bottom surfaces, which are covered with high impact polystyrene. rotary-type hermetic R22 compressor (P12TN). A input power rated 680 W was selected.

A vertical stainless steel cylindrical heat storage tank was considered in the present study. The tank volume is 150 L, and the tank height and diameter are 1.085 m and 0.5 m with a 2 mm thick vertical cylindrical body and caps respectively. The storage tank is assumed to fully insulated with 50 mm thick polyurethane. In the tank, an immersed helical coil acts as the heat

exchanger which is located vertically 0.975 m from the bottom of the hot water storage tank. The condenser is made up of a copper tube outer tube; diameter and thickness are 9.90 mm and 0.75 mm respectively, with a length of 2000 mm (Ji et al., 2010)

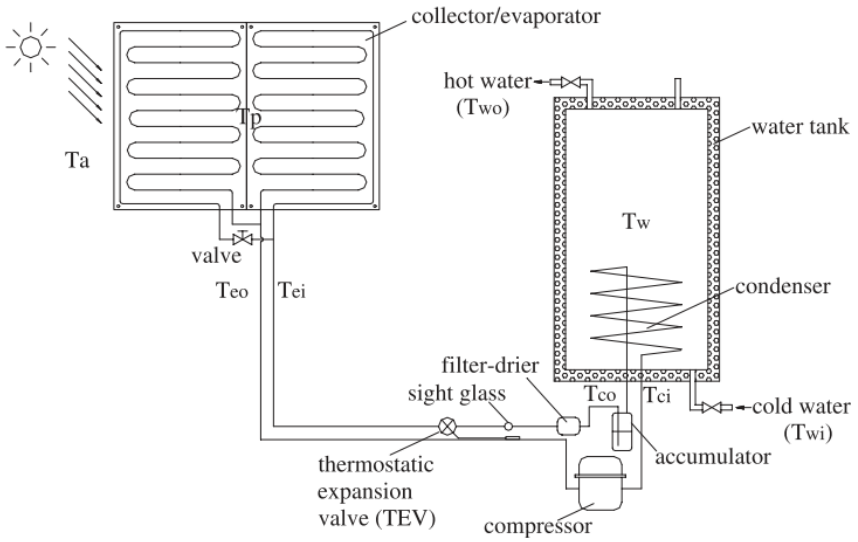

Figure 3. 1: Schematic diagram of the DX-SAHPWH (Kuang et al., 2003)

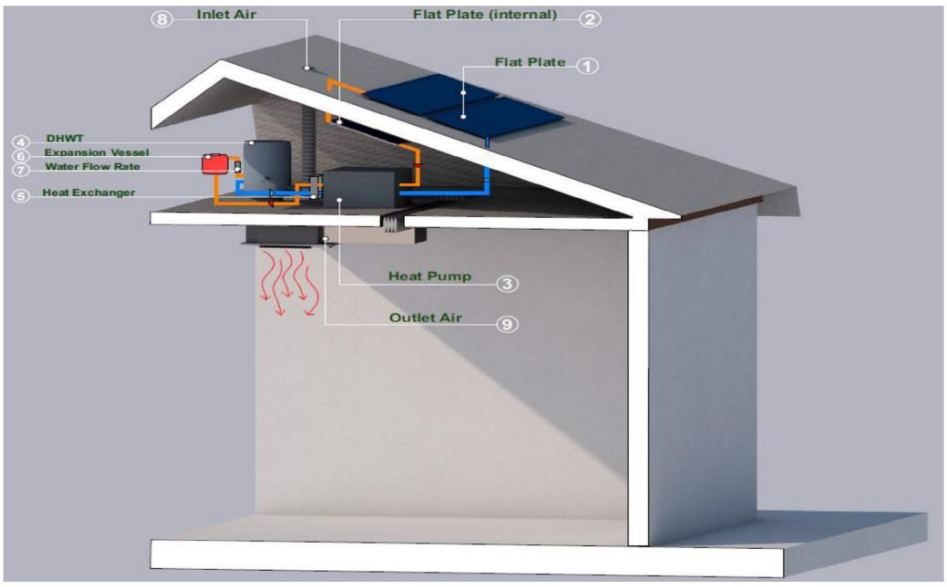

Figure 3. 2: DX-SAHPWH system configurations in typical residential home (Mohamed, Riffat & Omer, 2017)

3.1.1 Operation of the DX-SAHPWH system

The DX-SAHPWH employs the conventional vapour compression cycle system and operates as follows:

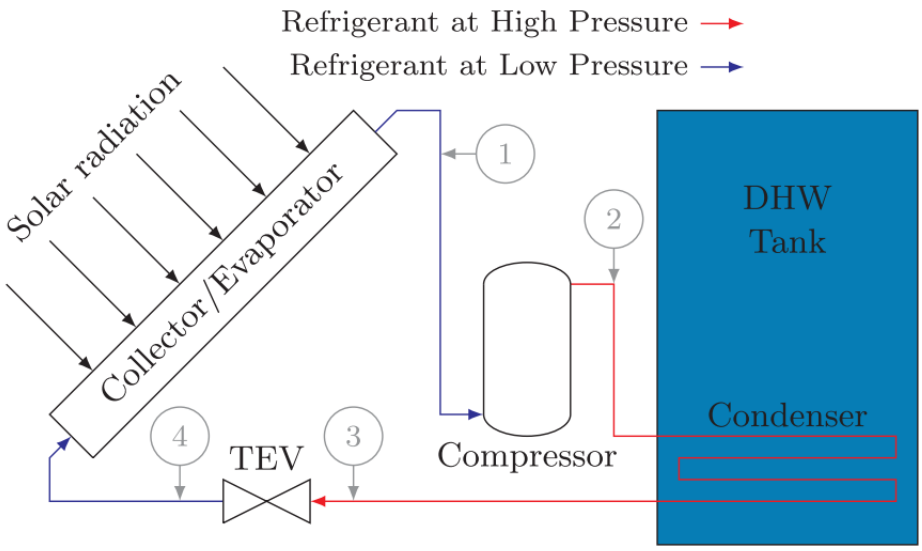

Figure 3. 3: Schematic diagram of the DX-SAHPWH system (Rabelo et al., 2019)

Initially,(see Fig.3.3) the saturated or superheated vapor refrigerant is at a low pressure and temperature which enters the solar collector-evaporator and is evaporated by absorbing solar energy and/or ambient air energy (process 4–1). This is dependent on whether the refrigerant temperature is higher or lower than that of ambient. Subsequently, the vaporized refrigerant passes through the compressor, where the temperature and pressure is increased.(process 1–2).

Subsequently, the high pressure, high temperature vapor is condensed into liquid and transfers thermal energy (heat) to the lower temperature water in the hot water storage tank by means of an immersed heat exchanger (condenser) (process 2–3). The resulting condensed refrigerant flows out of the condenser into the thermostatic expansion valve, where the high-pressure liquid is throttled to a lower pressure, which causes some of the refrigerant to vaporize as its temperature is reduced (process 3–4). The low-pressure, low-temperature refrigerant returns to the collector-evaporator and the cycle is re-initiated.

3.2 Thermodynamic steady state modelling of DX-SAHPWH system

3.2.1 Vapour compression cycle modelling

The DX-SAHPWH system can be modelled as a vapour compression cycle (VCC) which is the most commonly used principle for heat pump water heating applications (Omojaro & Breitkopf, 2013; Wang *et al.*, 2017). The model compartmentalizes the system into the four main components. An energy balance was conducted from the first law of thermodynamics and continuity of mass, which states that energy and mass are conserved. Figure 3.4 shows the basic components of a heat pump and energy interactions in the VCC. Assuming a steady state process for a constant time interval, the energy balance is shown in Eq.3-1 and 3-2.

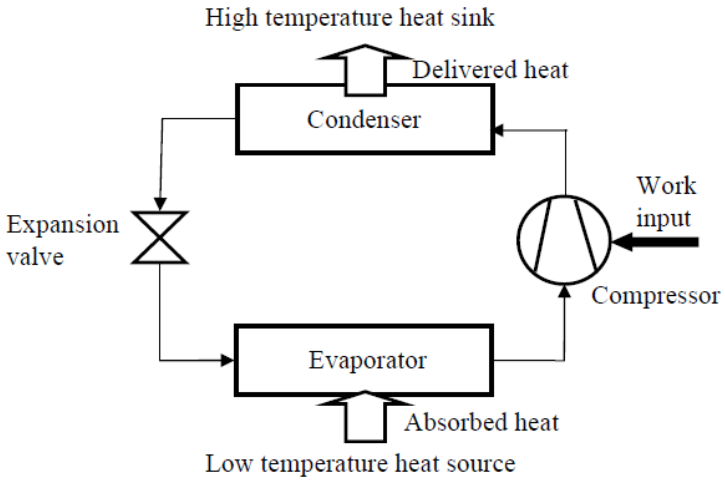

Figure 3.4: Heat Pump components and energy interactions

$$\mathrm{Q_{in}} + \mathrm{W_{in}} + \mathrm{m_{in}}(\mathrm{h_{in}} + \frac{v_{in}{}^2}{2} + \mathrm{g}Z_{in}) = \mathrm{Q_{out}} + \mathrm{W_{out}} + \mathrm{m_{out}}(\mathrm{h_{out}} + \frac{v_{out}{}^2}{2} + \mathrm{g}Z_{out}) \quad (3.1)$$

where Q is heat transfer rate, $\dot{W}$ is work transfer rate, $\dot{m}$ is the mass flow rate, h is the specific enthalpy of the flowing fluid or the internal energy component, v is the velocity of the fluid or the kinetic energy component, Z is the height of the fluid in relation to some reference height or the potential energy due to gravitation component, and g is the gravitational acceleration. Considering the following assumptions as: inlet and outlet kinetic and potential energy differences are insignificant, and no work is done at outlet of the system. The equation can be simplified and rearranged as Eq. 3.2.

$$\mathrm{Q_e} + \mathrm{W_{comp}} = \mathrm{Q_{con}} \quad (3.2)$$

Considering equation 3.2 , the energy input to the DX-SAHPWH system is Q_e is the collector-evaporator heat gain by either solar or ambient energy and the energy consumption by the compressor W_{comp}. The energy output is the heat gained the condenser, Q_{con} which is dissipated to the water in the storage tank.

3.3. DX-SAHPWH system components

3.3.1 Solar thermal collector-evaporator

The incident solar radiation which impinges on the collector-evaporator can be expressed as:

$$Q_{in} = A_{cl}\, I_T \tag{3.3}$$

However, as the unglazed solar collector-evaporator absorbs the solar radiation, the temperature of the absorber increases and thus becomes higher than ambient temperature, which consequently results in heat losses through convection and radiation.

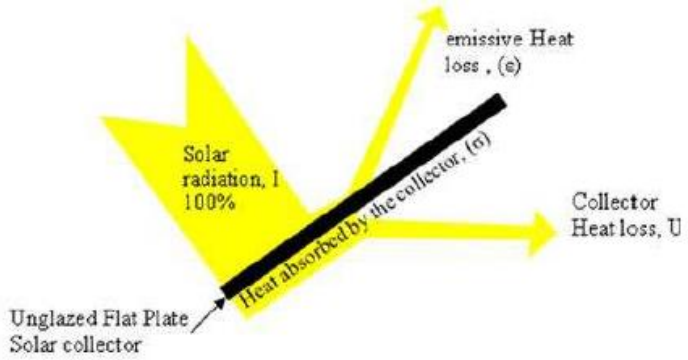

Figure 3. 5: Schematic diagram of the energy distribution in the unglazed solar collector-evaporator

The useful solar energy (Q_e) gained by the unglazed solar collector-evaporator, operating under steady-state conditions, can now be expressed as follows, assuming no significant pressure drop due to the refrigerant flow (Duffie & Beckman, 2013; Hawlader *et al.*, 2001):

$$Q_{coll} = A_{cl}F'(I_T(\alpha) - U_{CL}(T_e - T_a)) \tag{3.4}$$

where A_{cl} is the area of the solar collector, F' is the collector effiiency factor, I_T is the solar irradition, α, is the absorptivity of the solar collector-evaporator, U_{CL} is overall collector heat transfer loss coefficient from the collector to the ambient air, T_e is the evaporating temperature of the refrigerant which also is the average temperature of the refrigerant fluid/collector-evaporator unit, and T_a is the ambient air temperature (Deng & Yu, 2016).

The overall collector heat transfer loss coefficient U_{CL} is mainly due to the convection and radiation heat-transfer from the top surface of the collector to the surroundings. Ignoring the losses at the edges and bottom of the collector, it can be expressed (if well-insulated) as:

$$U_{CL} = h_w + h_r \tag{3.5}$$

Where h_w is the convection heat transfer coefficient which is approximated as a function of wind speed, which is determined using the following empirical model developed by McAdams for wind speeds less and greater than $5\ m/s$ (Sartori, 2006):

$$h_w = 5.7 + 3.8\, u_w \quad \text{if } u_w \leq 5 \tag{3.6}$$

$$h_w = 6.47\ {u_w}^{0.78} \quad \text{if } u_w > 5$$

Where u_w is the wind speed.

The radiation heat transfer coefficient h_r, assuming that the sky temperature, to which the plate will radiate back, is the same as the ambient temperature, can be expressed as : (Ji *et al.*, 2009)

$$h_r = \varepsilon\sigma({T_p}^2 + {T_{sky}}^2)(T_p + T_{sky}) \tag{3.7}$$

Where ε is the emissivity, σ is the Stefan–Boltzmann constant, T_p is the plate temperature, and T_a is the ambient air temperature. However, thermal resistance between the solar collector and refrigerant is negligible since losses are very small, therefore $T_p = T_e$.

To model, the sky temperature, the following equation is used:

$$T_{sky} = \varepsilon_{sky} {T_a}^{0.25} \tag{3.8}$$

Because the emissivity of the sky changes depending on day and night conditions, the following models are used (Dobson, 2005):

$$\varepsilon_{sky} = 0.741 + 0.0162\,T_{dp} \quad \text{if } I \leq 0.25 \quad (\text{Night}) \tag{3.9}$$
$$\varepsilon_{sky} = 0.727 + 0.0016\,T_{dp} \quad \text{if } I > 0.25 \quad (\text{Day})$$

Where T_{dp} is the dewpoint temperature of the air, and I is the solar irradiation which is dependent on day and night periods.

The dewpoint temperature is a function of the relative humidity and can be expressed by the emprical model as :

$$T_{dp} = \frac{237.7\,(\frac{17.27T_a}{237.7+T_a} + \ln RH)}{17.27 - (\frac{17.27T_a}{237.7+T_a} + \ln RH)} \tag{3.10}$$

Where RH is the relativte humidity of the air.

The collector efficiency factor (F´) indicates the efficiency of heat transfer from the absorber to the refrigerant and is based on the configuration of the absorber to pipe. Figure 3.6 shows the arrangement used for this design. It can determined by the following formula, and assuming that conduction heat transfer through the tube is negligible, it can be expressed as:

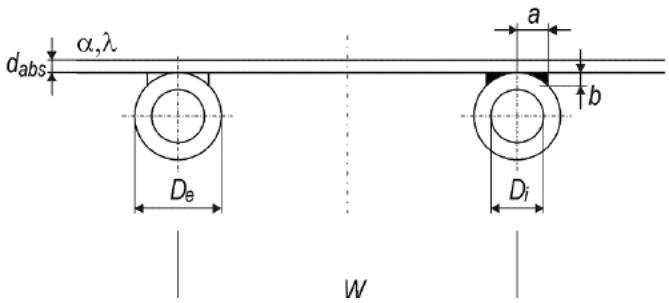

Fig.3.6 : Absorber–pipe upper bond configuration

$$F' = \frac{\frac{1}{U_{CL}}}{W[\frac{1}{U_{CL}(D+(W-D_o)F)} + \frac{1}{C_b} + \frac{1}{\pi D_i h_f}]} \tag{3.11}$$

Where F is the fin efficiency, D_o is the external diameter of the tube, W is the pitch of the tube, C_b is the bond conductance and h_f is the internal heat transfer coefficient.

The fin efficiency (F) for a straight fin with a rectangular profile can be expressed as:

$$F = \frac{\tanh\left[\sqrt{\frac{U_{CL}}{\lambda_p \delta_p \left(\frac{(W-D)}{2}\right)}}\right]}{\sqrt{\frac{U_{CL}}{\lambda_p \delta_p \left(\frac{(W-D)}{2}\right)}}} \quad (3.12)$$

Where δ_p is the thickness is λ_p and thermal conductivity of the collector plate.

Assuming the flow is laminar, the single-phase convection heat transfer coefficient inside the collector is approximated assuming laminar flow (Re < 2300) in a circular tube (Hajabdollahi & Hajabdollahi, 2017):

$$h_f = 4.36 \frac{\lambda_r}{D_i} \quad (3.13)$$

Where the λ_r and thermal conductivity of the refrigerant and D_i is the internal diameter of the tube.

To calculate the thermal conductivity of the refrigerant, the following curve-fitted polynomial equation is used (Charters & Safadi, 1987):

$$\lambda_r = 9.38378\text{-}6.40858E\text{-}2T_e + 9.604716T_e^2 - 4.4717T_e^3 - 5.677792T_e^3 + 1.85558T_e^4 \quad (3.14)$$

Assuming the absence of any heat loss between solar collector and the refrigerant, the optimal evaporating temperature was developed by Reyes & Ez (1998) and can be expressed as:

$$T_e = T_1 = \sqrt{T_a} \times \sqrt{\left[\left(\frac{I_T \alpha}{U_{CL}} + T_a\right)\right]} \quad (3.15)$$

3.3.2 Compressor Model

A rotary-type hermetic R22 compressor (P12TN), rated input power 680 W, was selected. Empirical black box models which were provided on the technical data sheet were used (Danfoss, 2020).The power consumption of the compressor and mass flow rate are a function of evaporator and condenser temperature, and are available from compressor manufacturer data.

For a small-scaled rotary-type compressor, the refrigerant mass flow rate is given by:

$$m_{r\_com} = 41.08571+1.51698\ T_e - 0.2754085\ T_c + 0.01482619\ (T_e)^2 - 0.0072828\ T_e T_c \quad (3.16)$$

Where m_r is the mass flow of the refrigerant in kg/h, and T_e is the suction temperature (before compression) which is equal to T_e in Kelvin and where T_c is the condensing temperature of the refrigerant.

The electrical power consumption of the compressor W_{comp} in watts can also be found using the black box model:

$$W_{comp} = 272.07685 - 1.68116\ T_e + 6.41352\ T_c + 0.0025426(T_e)^2 + 0.2316861\ T_e T_c \quad (3.17)$$

3.3.3 Condenser and hot water storage tank model

For the optimal condensing temperature of the condenser refrigerant, the following equation was used, based on Cervantes & Torres-Reyes (2002):

$$T_c = \frac{1}{2} T_a + \left[\frac{Ta^2}{4} + \frac{\lambda_r}{C_{pr}}\ T_a\right]^{\frac{1}{2}} \quad (3.18)$$

To calculate the specific heat capacity of the refrigerant, the following curve-fitted polynomial equation is used (Charters & Safadi, 1987):

$$C_{pr} = = \ 0.721311 - 4.323487E - 3T_e \ + 3.8380479E - 5T_e^{\ 2} - 3.736462E - 7T_e^{\ 3} - 2.1617922E - 9T_e^{\ 3} + 2.6628872E - 10T_e^{\ 4} \quad (3.19)$$

For the condenser heat gain, a first-law approach is used. Thus the heat dissipated to the water in the storage tank from the condenser is the algebraic sum of the energy gain at the collector-evaporator and the energy consumed by the compressor, and can also be expressed as:

$$Q_{con} = Q_{coll} + W_{comp} \quad (3.20)$$

To model the hot water storage tank, the one node-lumped parameter model was used which is focused on the energy balance equation and considers the body of water contained within the EWH as a single node (refer to Figure 3.7). For a non-stratified water storage tank mode, the heat gain of the water in the storage tank can be further expressed as :

$$\frac{Q_w}{\tau} = Q_{con} - Q_{st} - Q_{load} \quad (3.21)$$

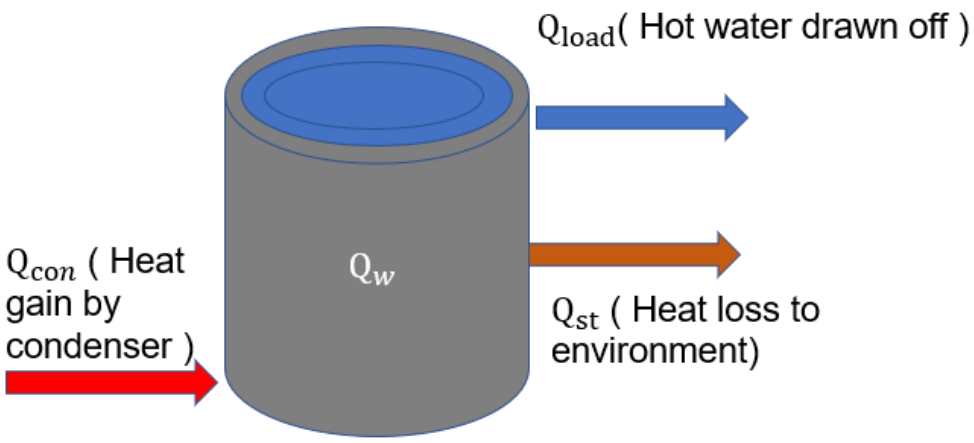

Figure 3. 6: Hot water storage tank energy interactions

The thermal energy required to heat the water is expressed as:

$$Q_w = m_w C_{pw} (T_{wo} - T_{wi}) \quad (3.22)$$

Where Q_w is the heat gain of the water in the storage tank, m_w is the mass of the water, C_{pw} is the specific heat capacity of water, T_{wo} is the set point temperature (hot water out), T_{win} is inlet water temperature, Q_{con} is the heat rejected by the condenser, Q_{st} is the total heat transfer loss by the storage tank and τ is the heating time or working hours.

Moreover, the m_w is the mass of the water can be further expressed as :

$$m_w = \rho_w V_{st} \quad (3.23)$$

Where ρ_w is the density of water at ambient temperature and V_{st} is the vulume of the hot water storage tank.

The density of water is a function of the water temperature and can be expressed as (Khin, Sint, Choudhury, Masjuki & Aoyama, 2017):

$$\rho_w = 1.0005776E+3\text{-}7.0629371E\text{-}2t_w \text{ -}3.5666433E\text{-}3t_w{}^2 \quad (3.24)$$

Moreover, the specific heat capacity of water is also a function of the water temperature and can be expressed as (Khin *et al.*, 2017):

$$C_{pw} = 4.2152727 - 1.6342424E - 3t_w + 1.651515E - 5t_w{}^2 \quad (3.25)$$

Referring to Figure 3.2, the hot storage tank is typically situated inside a house, roof or some storage room. The room will most likely be at a different temperature than the hot storage tank temperature and will not not perfectly insulated, consequently, heat transfer will occur. The type of heat transfer which will occur in this case is assumed to be a combination of convection loss between stationary tank water and ambient air, conduction loss through the tank walls and insulation and radiation from the tank walls to the room.

The heat transfer loss by the hot water storage tank can be further expressed as :

$$Q_{st} = Q_{cond\,(st)} + Q_{conv\,(st)} + Q_{rad\,(st)} \quad (3.26)$$

The heat loss by conduction loss through the tank walls and insualtion can be expressed as:

$$Q_{cond\,(st)} = \frac{(T_{wo} - T_a)}{R_{con}} \quad (3.27)$$

Where R_{con} is the conductive thermal resistance of the tank and insulation.

$$R_{con} = \frac{\ln\left(\frac{R_o}{R_i}\right)}{2\pi\,\lambda_{st}\,L} + \frac{\ln\left(\frac{R_{ins}}{R_o}\right)}{2\pi\,\lambda_{ins}L} \quad (3.28)$$

Where λ_{st} and λ_{ins} is the thermal conductivity of the tank and insulation, and *L* the length of the tank.

The heat loss by convection loss between stationary tank water and ambient air can be expressed as:

$$Q_{conv\,(st)} = h_{conv(st)} A_{st}\,(T_{wo} - T_a) \quad (3.29)$$

The superficial area of the water tank can be expressed as :

$$A_{st} = 1.845\,(2+\frac{h}{d})V_{st}^{\frac{2}{3}} \quad (3.30)$$

Where h_{st}, is the tank height, d_{st} tank diameter and volume is V_{st}.

To calculate the natural convection heat transfer coefficent tank $(h_{conv(st)})$ of the ambient air surrounding the tank:

$$h_{conv(st)} = Nu\,\frac{\lambda_{air}}{L} \quad (3.31)$$

The Nusselt Number is defined as the ratio of convection to conduction fluid heat transfer and can be expressed as :

$$Nu = \left(0.825 + \frac{0.387Ra^{\frac{1}{6}}}{\left[1+\left(\frac{0.492}{Pr}\right)^{\frac{9}{16}}\right]^{\frac{8}{27}}} \right)^2 \quad (3.32)$$

To calculate the thermal conductivity of the air, the following curve-fitted polynomial equation is used (Shitzer, 2014),

$$\lambda_{\text{air}} = -3.06E-4 + 9.89089E-4\text{T}_\text{a} - 3.46571E-8-5\text{T}_\text{a}^{\,2} \quad (3.33)$$

The Prandtl number, Pr, a dimensionless number, is defined as the ratio of kinematic viscosity to thermal diffusivity. To calculate the Prandtl number of the air, the following curve-fitted polynomial equation is used (Shitzer, 2014).

$$\text{Pr}_{\text{air}} = 0.80040 - 0.00031\text{T}_\text{a} \quad (3.34)$$

To calculate the Grashoff number of the air, the following equation is used :

$$Gr = \frac{g\beta(\text{T}_{\text{wo}}-\text{T}_\text{a})L^3}{\upsilon^2} \quad (3.35)$$

Where g is the gravitational accelaration constant, β coefficient of volume expansion and υ kinematic viscosity of the fluid.

The kinematic viscosity is the ratio of the dynamic viscosity to the density of the fluid and can be expressed as:

$$\upsilon = \frac{\mu_{air}}{\rho_{air}} \quad (3.36)$$

The Raleigh number is a dimensionless quantity used in modelling natural convection and is the product of the Grashoff and Prandtl numbers and can be expressed as:

$$Ra = GrPr \quad (3.37)$$

The radiation heat loss from the tank walls to the room:

$$Q_{rad\,(st)} = \varepsilon\sigma A_{st}(T_{wo}{}^4 - T_a{}^4) \quad (3.38)$$

To model the annual initial water temperature annually using the following equation (Popoola, 2014):

$$T_{win} = \frac{T_{min} - T_{max}}{2} - \frac{T_{max} - T_{min}}{2} \times h(\cos 2\pi \times \frac{N-2}{N}) \quad (3.39)$$

Where T_{min} and T_{max} are the value of maximal and minimal cold water and estimated to be 20 ◦C and 15 ◦C respectively; h is the location, if it is in the southern or northern hemisphere (1 if northern or -1 if southern hemisphere) and N is the number of the hours or months.

3.4 Performance indicators

The performance metrics used in this study to evaluate the entire system efficiency are the COP, collector efficiency, solar fraction, and the heating time. These are all described below:

3.4.1 Collector thermal efficiency (η_{coll})

The collector efficiency represents the ratio of the heat energy provided by the collector to the product of a defined collector area and the incident solar irradiation on the collector for a certain time period under steady conditions (Shi *et al.*, 2019).

$$\eta_{coll} = \frac{Q_{coll}}{A_{cl}\, I_T} \quad (3.40)$$

3.4.2 Coefficient of performance (COP):

The COP of the heat pump represents the ratio between its heating capacity and the overall electricity consumption, both measured under steady-state operating conditions (Shi *et al.*, 2019). It indicates how efficient the energy transfer is in the system, and is essentially the ratio of energy produced by energy received.

$$COP = \frac{Q_{con}}{W_{comp}} = \frac{Q_e + W_{comp}}{W_{comp}} \quad (3.41)$$

3.4.3 Solar fraction (f_{solar}):

The solar fraction is a system performance figure representing the ratio of the thermal energy provided by the solar system to the total system load for the same period of time:

$$f_{solar} = \frac{Q_{coll}}{Q_w} = \frac{Q_{coll}}{Q_{con} - Q_{st}} \quad (3.42)$$

3.4.4 Heating time (τ):

The time taken to heat the water under steady-state conditions is the ratio of thermal energy in joules (J) required to heat the water to the total amount of energy provided in watts (W) to the system. This is also referred to the working or operating hours according to Chow et al. (2010):

$$\tau = \frac{Q_w}{Q_{con} - Q_{st} - Q_L} \quad (3.43)$$

3.5 System simulation

To solve the mathematical model in Chapter 3, MATLAB R2016a was used. The MATLAB code developed for the model is presented in Appendix B. The objective was to assess daily and annual performance. For the daily performance, two days were considered, one in the summer and one in the winter season, and for the annual performance, 8760 runs were conducted for each hour of the year. In this study, it is assumed that the set-point temperature of the water is at 55° C and that no water is drawn off from the storage tank during daytime, and thus $Q_{Load} = 0$. In addition, the simulation assumes that the refrigerant temperature will always be higher than ambient temperature, $T_e > T_a$ and thus no ambient energy gains are quantified.

3.5.1 Model assumptions

To predict the performance of the proposed DX-SAHPWH system, the modelling is simplified based on the following assumptions:

`

(i) The DX-SAHP system is at quasi-steady-state conditions which are approximated within the chosen time interval (constant solar radiation and ambient temperature during heating).
(ii) Heat transfer loss from the collector sides and back are negligible.
(iii) Two-phase flow convection in the collector-evaporator and condenser is not considered.
(iv) Pressure drop is negligible in the collector-evaporator and condenser.
(v) The hot water storage tank is assumed to be non-stratified.
(vi) Thermal losses to the surroundings are negligible in the R22 circulation loop.

3.5.2 Physical parameters

The following parameters used as inputs in the performance analysis of the DX-SAHPWH system:

Table 3. 1: Physical parameters of DXSAHPWH

Parameter	Value
Collector area (A_{cl})	4.2 m^2
Absorptivity of the collector plate (α)	0.9
Emissivity of the collector plate (ε)	0.1
Thermal conductivity of collector plate (λ_p)	236 W/m.K
Thickness of collector plate (δ_p)	4 mm
External diameter of the tube in collector plate(D)	9.4 mm
Pitch of the tube (W)	40 mm
Bond conductance. (C_b)	15 W/m.k
Volume of storage tank (V_{st})	150 L
Height of storage tank	1805 mm
Diameter of storage tank	500 mm
Polyurethane insulation thickness of hot water tank (δ_i)	38 mm
Thermal conductivity Polyurethane insulation (λ_i)	0.055 W/m.K
Final water temperature in the water tank	55 ℃
Initial water temperature	Summer : 20 ℃ & Winter : 15 ℃

3.5.3 Meteorological parameters

The meteorological parameters were obtained from the South African Universities Radiomentric Network Station (SAURAN) station located at Stellenbosch University, in Stellenbosch, South Africa (-33.9281° E, **;** 18.8654° S). The instruments are positioned on the roof of an engineering building at an elevation of 119m. For more details on the weather station see Appendix C (SAURAN, 2019). The data is presented in an Excel spreadsheet and contains ambient temperature, solar radiation, wind speed and relative humidity in hourly increments for the year 2018. For the hourly data, 02 January 2018 was considered for summer and 31 July 2018 for winter.

3.5.4 Simulation procedure

The MATLAB program was used to solve the above equations to obtain the theoretical results and predictions of the system performance. The algorithm of the program is sequential with no loops is described below:

1. To start the simulation, the meteorological parameters (ambient temperature, solar radiation, wind speed and relative humidity) are imported from an Excel spreadsheet.
2. The initial water temperature model must be adjusted depending on whether an annual or hourly simulation is conducted.
3. Physical and design parameters of the collector-evaporator are declared as per Table 4.1 above
4. The convection and radiative heat transfer coefficients and collector efficiency factor (F′) are calculated.
5. Evaporating and condensing temperature of refrigerant (T_e and T_c) are calculated.
6. The collector-evaporator heat gain is then calculated.
7. The compressor mass flow rate and power consumption are calculated.
8. The physical parameters of the storage tank are declared as per Table 4.1 above.
9. Storage tank required thermal energy and heat loss to the environment are calculated.
10. The simulation ends, COP, collector efficiency, solar fraction and heating time are the outputs.
11. Data is cleaned up, any impractical values are not considered.
12. Plots of time vs COP, collector efficiency, solar fraction and heating time are generated for data presentation and analysis.

CHAPTER 4 – RESULTS & DISCUSSION

This chapter examines the results of the daily and annual simulation. For the daily performance, two days are selected, one in summer and one in winter to provide disparate meteorological conditions to discern the system performance. The annual performance provided a holistic view of the system performance. Thereafter, a parametric analysis was conducted to investigate the influence of the meteorological conditions (ambient temperature, solar irradiation, and wind speed) on the system performance.

4.1 Daily performance

4.1.1 Summer meteorological conditions

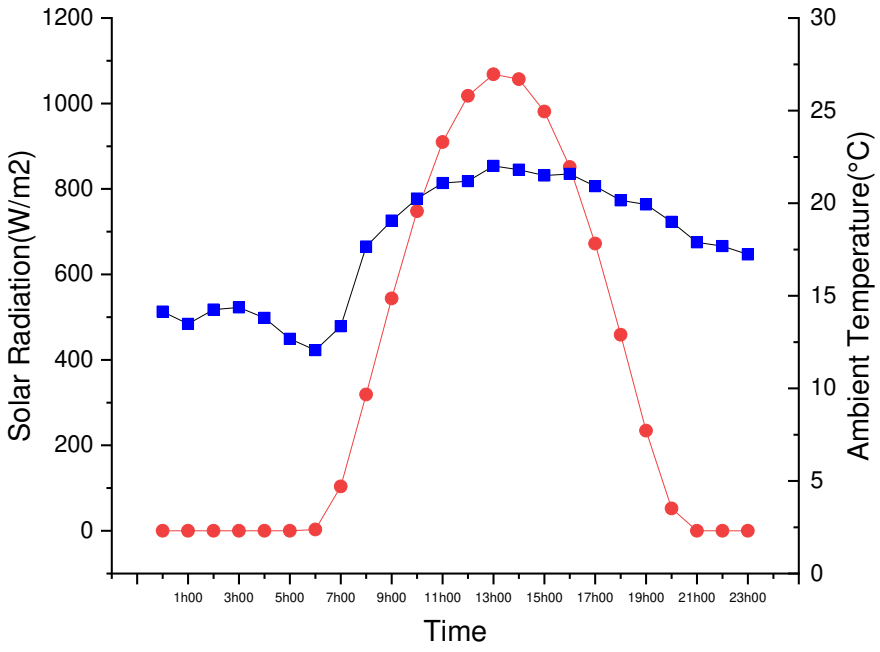

Figure 4.1: Summer meteorological conditions (solar radiation and ambient temperature)

The date 02 January 2018 was selected to represent the summer day for the hourly simulation. The solar irradiation, ambient temperature, and wind speed for the period from 6:00 to 20:00 is shown in Fig. 4.1. The solar irradiation ranged from 0 to 1068 /m^2 and had the maximum value at 13:00. The ambient temperature increased from 14 to 22 °C with a maximum at about 13:00 as well. In Figure 4.2, The wind speed varied from about 0.5 to 6.3 m/s, increasing towards the evening. The relative humidity varied from about 51% to 80%, decreasing when

solar radiation becomes more prominent during the day. For this particular day, the average temperature, solar radiation, wind speed and relative humidity during the sunshine hour period are 20 °C, 690 W/m^2, 3.8 m/s and 68 % respectively. It is assumed that the initial water temperature is 20 °C for this day.

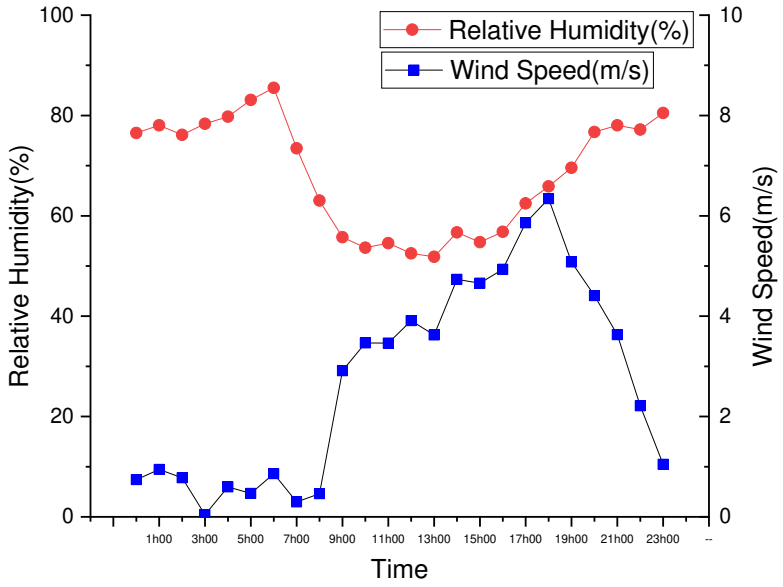

Figure 4. 2: Summer meteorological conditions (wind speed and relative humidity)

4.1.2 Instantaneous energy performance (summer)

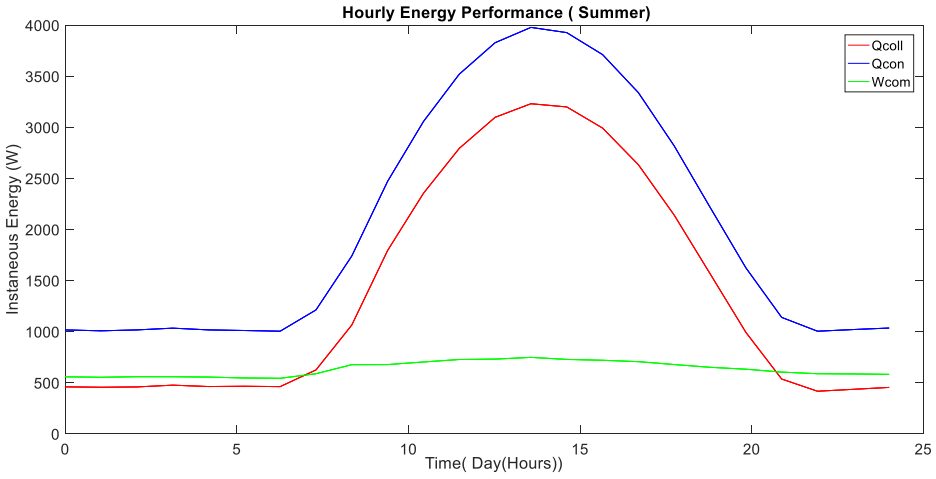

Figure 4. 3: Instantaneous energy performance: Summer

Figure 4.3 shows the variations in the condenser heat gain, collector-heat gain, and power consumption of the DX-SAHWH system operating in the solar-assisted heat-pump mode. Compared with Fig. 4.1, both the condenser heat gain and collector heat gain are shown to have very similar patterns to the solar radiation. Moreover, these trends are smiliar to Chow, et al. (2010) who investigated daily perforomance.The condenser heat gain increased from 1200 W to 3900 W from about 8:00 to solar noon and then decreased to 1600 W in the late afternoon.The power consumption of the compressor increased almost linearly from 550 to 750 W from 8:00 to 15:00. However, after 15:00, as the solar radiation weakened and the collector-evaporator was unable to absorb sufficient energy for the heat-pump system, and thus the power consumption decreased. Furthermore, this was a result of higher ambient temperature and solar radiation, which resulted in an increase in evaporator temperature and the refrigerant mass flow rate. This consequently resulted in an the increase in energy consumption. These findings corroborated with Huang, Ji, Modjinou & Qin (2017). Based on a 24-hour average, the condenser heat gain was 2000 W, collector-heat gain was 1400 W and compressor power consumption was 632 W.

4.1.3 COP and collector efficiency (summer)

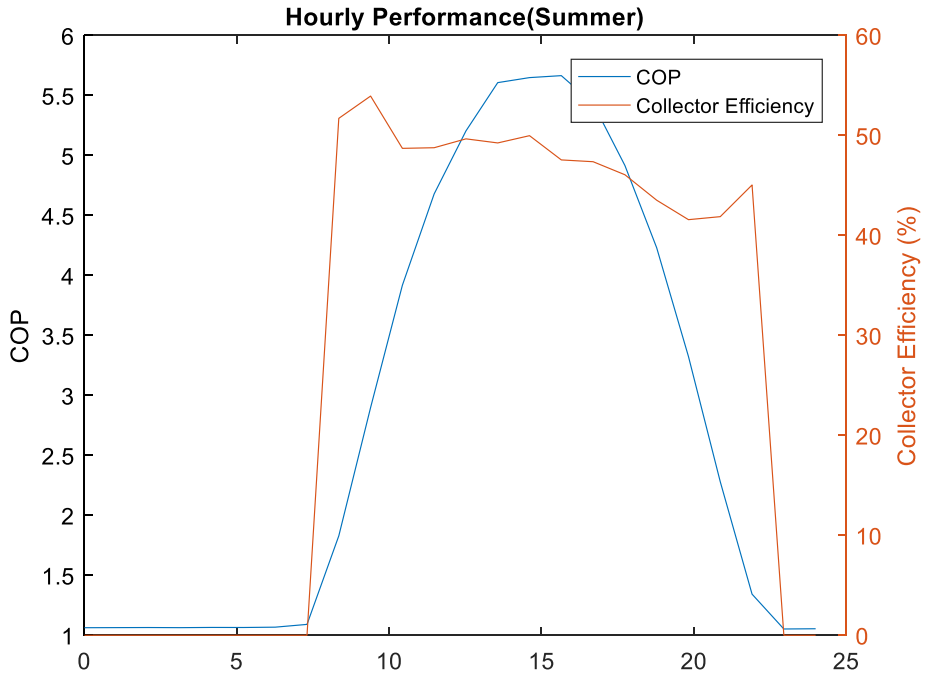

Figure 4. 4: Summer hourly performance: COP and collector efficiency

The summer hourly COP and solar collector efficiency was investigated in Figure 4.4. For this particular day, the COP of the system varied parabolically with the amount of solar radiation

available throughout the day and varied during the day from 1.83 - 5.65. The COP therefore increases with solar radiation and will be more efficient when operated during the day, when more solar radiation is present. Moreover, it is worth accentuating that the minimum COP of 1.04 is possible during periods with no solar radiation. The COP graph follows the trend by Chow et al., (2010); however, the magnitude of the COP is less due to climatic conditions.

The collector efficiency ranged from about 45–51 % and varies due to convective and radiative heat transfer losses to the environment, which is a function of wind speeds and ambient temperature. It is noteworthy that at midday when solar radiation was at a maximum, the collector efficiency was at minimum. This indicates that there is a contrasting relationship between the COP and collector efficiency at specified solar radiation values. During a summer day, it is not expected that the ambient temperature will be higher than that of the refrigerant which means that no additional heat is being gained from the ambient. Therefore, an increase in collector efficiency will not occur.

4.1.4 Heating time and solar fraction (summer)

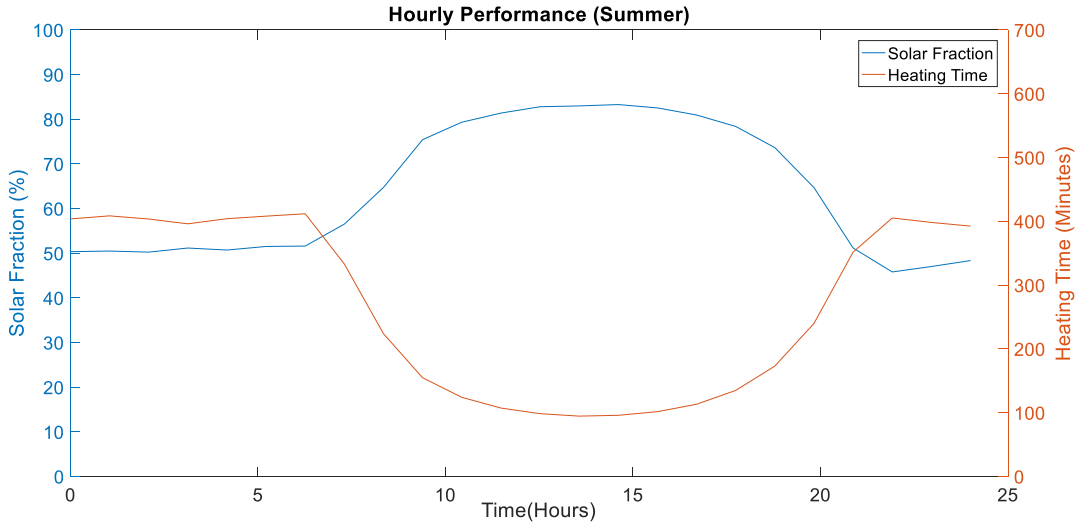

Figure 4. 5: Summer hourly performance: Solar fraction and heating time

The summer hourly solar fraction and heating time investigated are shown in Figure 4.5. Similar to the COP, the solar fraction is a function of solar radiation, which varies throughout the day from 0–82 % and peaks at midday which is also due to solar radiation. Conversely, the heating time ranges from 403 to 94 minutes due to more solar energy being available during throughout the day. Therefore, when the system is operated when more solar radiation is present, the water heating time will improve. These results are in corroboration with Kong

et al., (2017) who stated that higher solar radiation values improve the heating time. The average heating time is about 265 minutes during this particular day.

4.1.5 Winter meteorological conditions

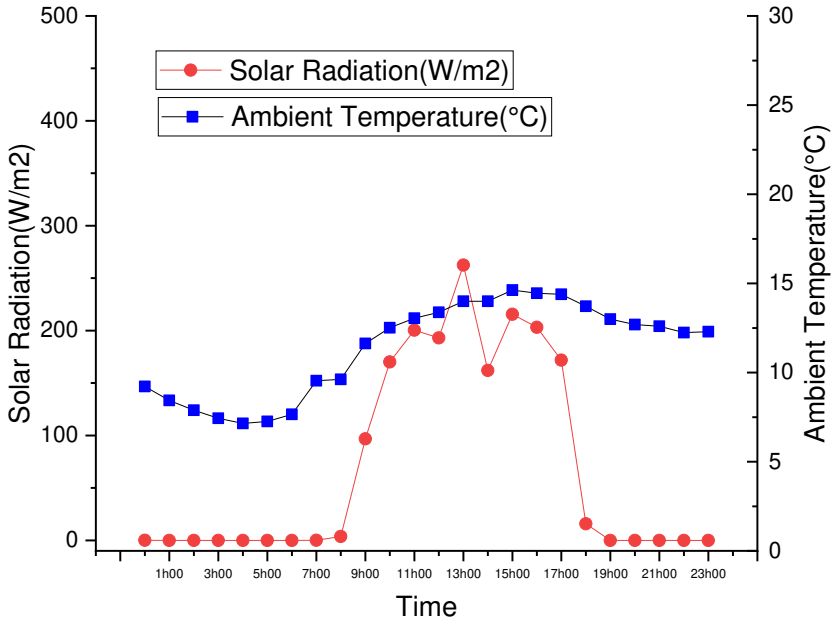

Figure 4. 6: Winter meteorological conditions (solar radiation and ambient temperature)

The date 31 July 2018 was selected to represent the winter day for the hourly simulation. The solar irradiation, ambient temperature and wind speed for the period from 6:00 to 20:00 are shown in Figure.4.6. The solar irradiation ranged from 0 to 262 W/m^2 and had a maximum value at 13:00. Furthermore, the inconsistent curve is attributed to probable cloud cover for this day. The ambient temperature increased from 7 to 14°C with a maximum at about 16:00. In Figure.4.7, the wind speed varied from about 0.5 to 3.65 m/s with no distinct trend, whereas the relative humidity remained fairly constant with values between 77- 80 %. The average temperature, solar radiation, wind speed and relative humidity during the sunshine hour period were 13 °C, 130 W/ m^2,2.7 m/s and 80 % respectively. It is assumed that the initial water temperature was 15 °C for this day.

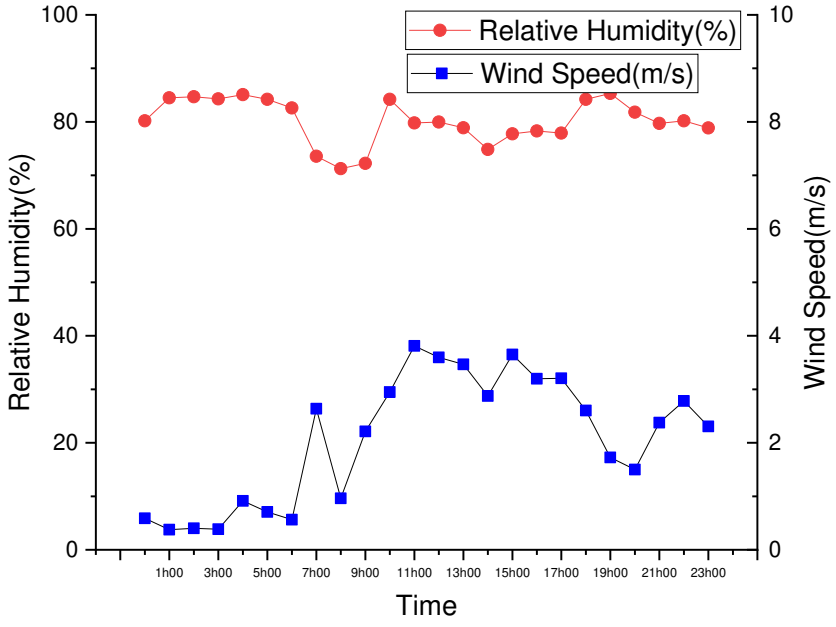

Figure 4. 7: Winter meteorological conditions (wind speed and relative humidity)

4.1.6 Instantaneous energy performance (winter)

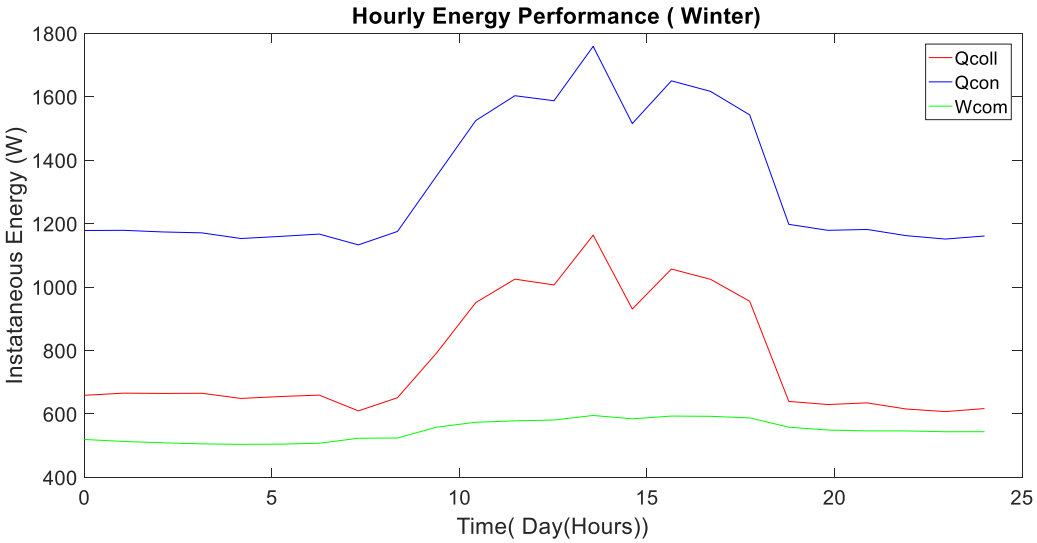

Figure 4. 8: Instantaneous energy performance: winter

Fig 4.8 shows the variations in the condenser heat gain, collector heat gain, and power consumption of the DX-SAHWH system operating in the solar-assisted heat-pump mode. Compared with Fig. 4.6, both the condenser heat gain and collector heat gain are shown to

have very similar patterns to the solar radiation. The condenser heat gain increased from 1100 W to 1800 W from about 8:00 to solar noon and then decreased to 1100 W in the late afternoon again.The power consumption of the compressor increased from 520 W to 595 W from 8:00 to 18:00. In comparison to summer, the compressor power consumption remained fairly constant. This was expected as the condensing and evaporating temperature had a smaller difference. Moreover, these trends are similar to Chow et al. (2010) who investigated daily performance. Based on a 24-hour average, the condenser heat gain was 1320 W, collector heat gain was 772 W and compressor power consumption is 547 W.

4.1.7 COP and collector efficiency (winter)

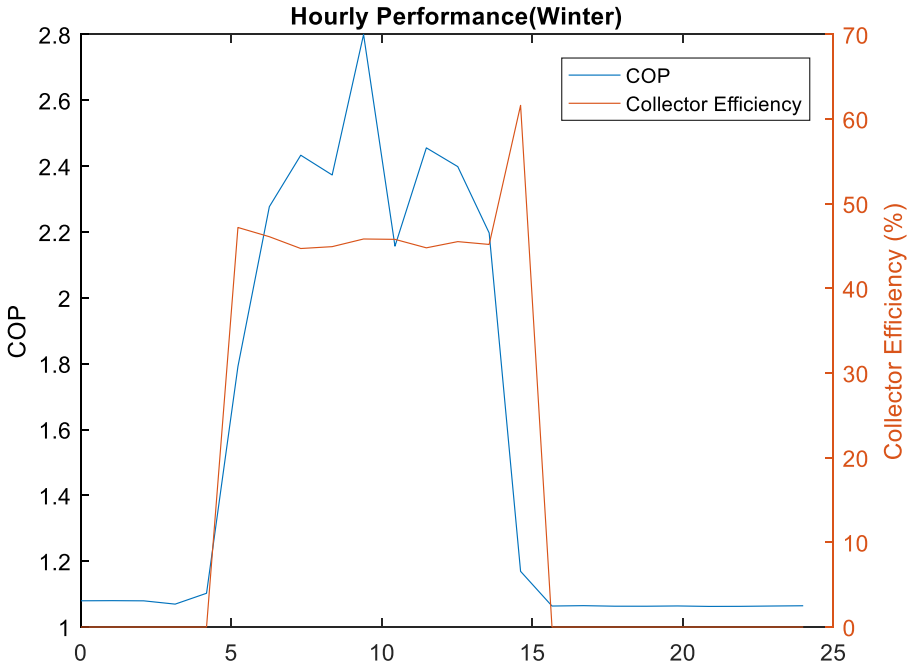

Figure 4. 9: Winter hourly performance: COP and collector efficiency

The winter hourly COP and solar collector efficiency is shown in Figure 4.9. For this particular day, the COP of the system varied during the day from 1.07–2.8 and followed the solar radiation curve. The collector efficiency ranged from about 45-60% and followed the same trend. In comparison to the summer day, the COP was expected to be less as the magnitude and presence of solar radiation was smaller and the initial water temperature was colder, which meant that the system required more energy to heat the water. These results are supported by Kong et al. (2018), Kong et al. (2017), and Sun et al. (2015) which found that the COP decreases when solar radiation is less and the initial water temperature is colder.

4.1.8 Heating time and solar fraction (winter)

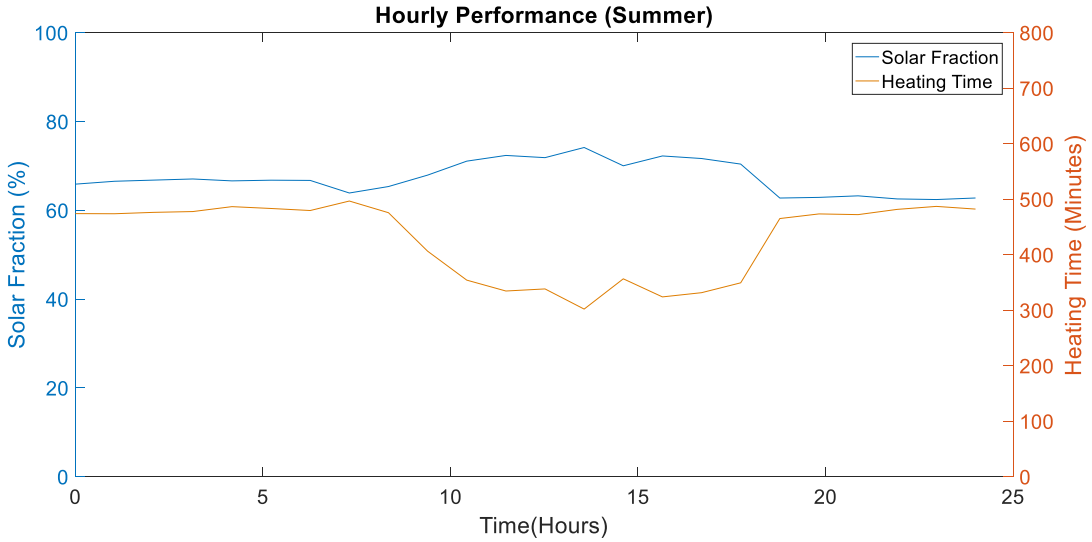

Figure 4. 10: Winter hourly performance: solar fraction and heating time

The winter hourly solar fraction and heating time is shown in Figure 4.10. Like the COP, the solar fraction varies erratically from 0 -74 % which is also due inconsistent solar radiation. The heating time ranges from 300 to 480 minutes, which is greater than summer and thus further accentuates the significance of ambient temperature, initial water temperature and solar radiation on system performance. These results are supported by Kong et al. (2018), Kong et al. (2017) and Sun et al. (2015) which found that the heating time increases when solar radiation is less and the initial water temperature is colder. The average heating time was about 428 minutes during this day. Based on these results, a back-up heating device would be required as heating time would be about 7 hours to reach 55 °C; however, it has been reported that during raining days or nights a DXSAHPWH is able to absorb ambient energy via convection or in essence behave as a standard conventional heat pump and thus improve heating times.

4.1.9 Summary of daily performance results

The following tables highlight the salient features of the daily performance analysis.

Table 4. 1: Daily performance metrics

Performance Indicator	COP	Collector efficiency (%)	Solar fraction(%)	Heating time (minutes)
Summer	1.83 - 5.65	45-51	0-82	94 to 403
Winter	1.07 – 2.8	45-60	0-74	300 to 480

Table 4. 2: Daily energy performance

Heat Gain	Condenser heat gain (W)	Collector heat gain (W)	Compressor power consumption (W)
Summer	1200 to 3900	500 – 3150	550 to 750
Winter	100 to 1800	620-1110	520 to 595

The system performance is generally better in the summer day than in the winter day due to the variation in ambient temperature, initial water temperature and solar radiation. For “summer”, the COP ranged from 1.83 - 5.65 and in “winter” ,it ranged from 1.07 – 2.8. These values are supported by Kuang et al. (2003) and Sun et al. (2015) which stated that the COP can range from 4–6 during summer conditions and a COP above 2.5 in low ambient temperature and solar radiation .i.e; winter conditions. The collector efficiency for “summer” ranged from 45-51% and “winter” 45-60% ,which indicates that the collector performs better in “winter”. These values are in the range reported by Hawlader *et al* (2001) and Kuang *et al*. (2003) who obtained collector efficiencies from 40 % and 70 %.

To consolidates results above, It means that system should ideally run during the day when solar radiation is abundant. These values could vary in practice, as it is not expected during a summer day that the ambient temperature would be higher than that of the refrigerant, which means that no additional heat would be gained from the ambient. However, in winter it is expected that there would be additional energy gained from the ambient environment , improving both COP and collector efficiency.

4.2 Annual performance

This section deals with the annual performance of the DX-SAHPWH system. The performance metrics, COP, collector efficiency, solar fraction and heating time were investigated for a year, or 8760 hours.

4.2.1 COP annual performance

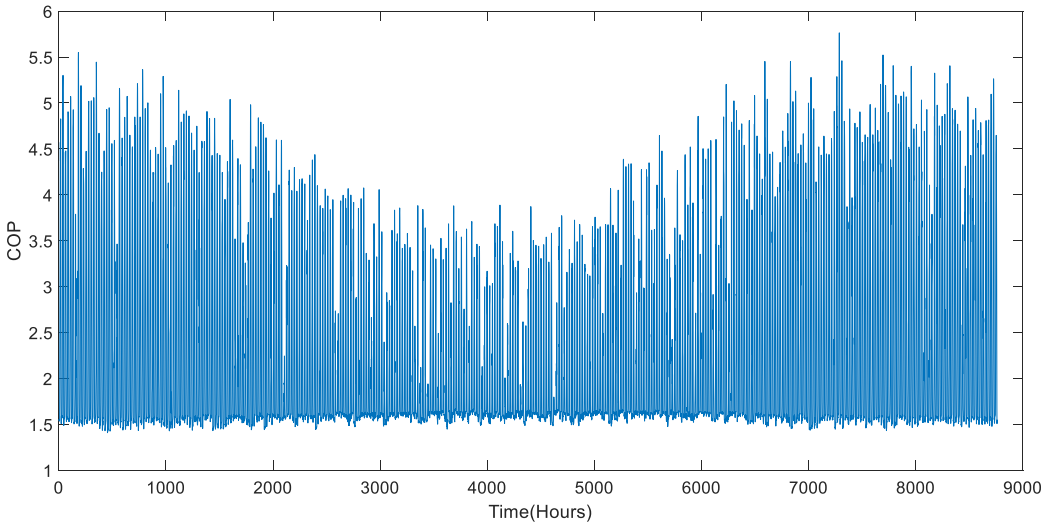

Figure 4. 11: Annual COP performance

The annual COP and collector efficiency are shown in Figure 4.11. The minimum (min) and maximum (max) COP expected are 1.4 and 5.75 respectively, with an annual average of 2.3. These values are similar to the range stated by Kuang & Wang (2006) and Sun et al.(2015) which is between 4–6. The COP is higher during the summer, spring and autumn seasons which is attributed to higher ambient temperatures, solar radiation, and higher initial water temperatures, which is the converse for the winter seasons. These results are in agreement with Chow et al. (2010) and Kong et al. (2018) who reported that higher COPs are to be expected in summer months. In contrast, Kuang et al. (2003) state that summer COP is expected to be lower due to higher temperature gradient between the evaporation and

condensation of the refrigerant, which results in higher compressor consumption, which consequently leads to a lower COP of the system.

4.2.2 Collector efficiency annual performance

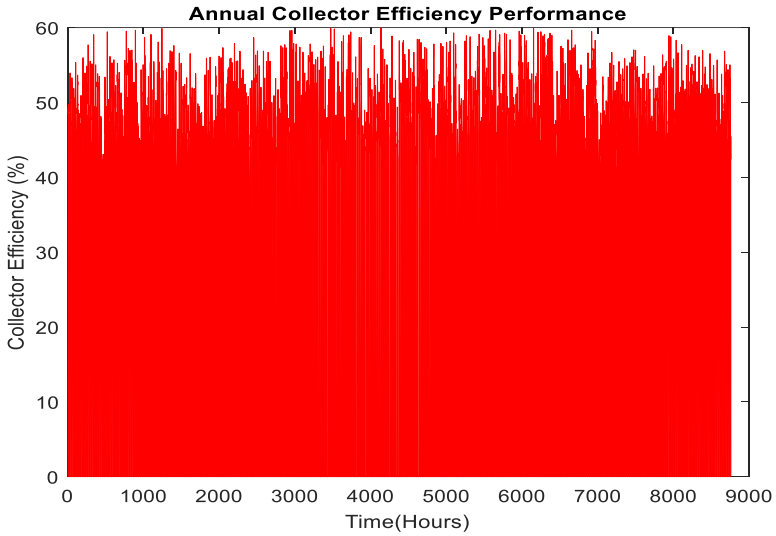

Figure 4. 12: Annual collector efficiency performance

The min and max collector efficiency are 0 and 60 % respectively. As seen in Figure 4.12, the collector efficiency remains constant throughout the year. These values are similar to the range stated by Hawlader et al. (2001) and Kuang et al. (2003) which is between 40–70%.The values remain constant which can be attributed to the temperature gradient between the collector and the ambient temperatures, which do not vary significantly annually. However, according to Li et al. (2007a), the collector efficiency can increase above 100 % during colder seasons where ambient temperatures are expected to be lower than the evaporating temperature of the refrigerant, which results in additional convective heat gain from the ambient air. This is dependent on climate conditions and thus requires further investigation and analysis.

4.4.3 Solar fraction annual performance

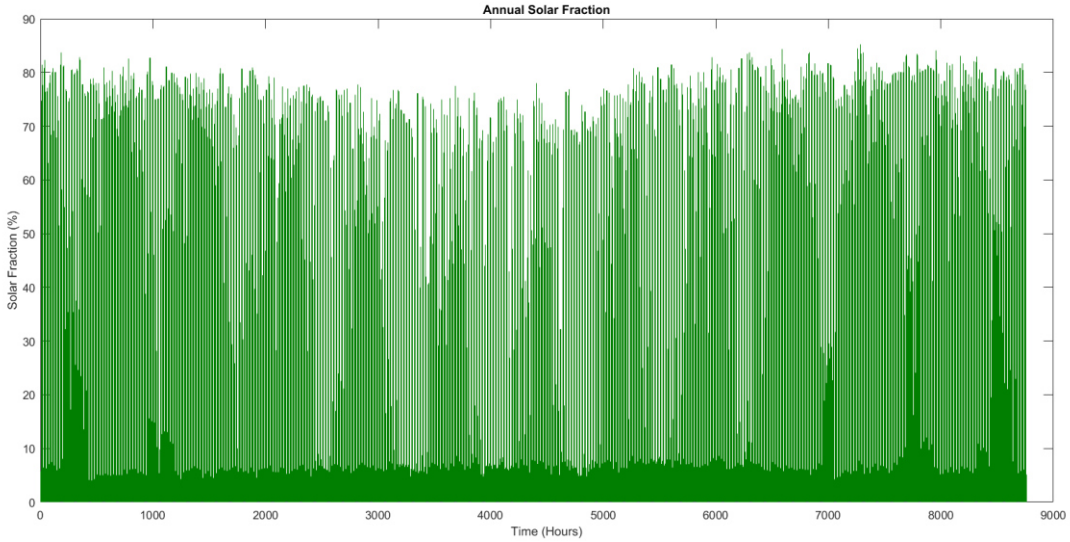

Figure 4. 13: Annual solar fraction performance

The annual solar fraction and heating time is shown in Figure 4.13. The min and max solar fraction are 0 and 86.47 %. The variations axiomatically occur due the variation of solar radiation throughout the year, and higher solar fractions are expected during the summer period that exhibits higher solar radiation values compared to other periods. There are slight decreases in the other colder months; however, it remains above 50 %. Moreover, more ambient energy gains are expected in winter, further decreasing the solar fractions but increasing the COP, as reported by (Zhang *et al.*, 2014)

4.4.4 Heating time annual performance

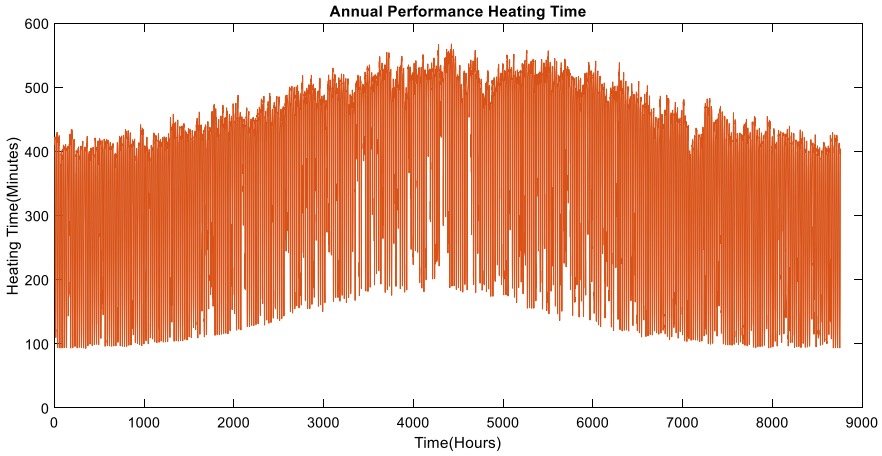

Figure 4. 14: Annual heating time performance

The heating time min and max are 92 and 570 minutes with an annual average of 355 minutes. In Figure 4.14, it can be seen that winter has the highest heating times which is attributed to lower ambient, initial water temperatures and solar radiation values, in contrast with the warmer summer. These results are further corroborated by Kong et al. (2017), who stated that higher solar radiation, initial water ambient and temperatures results in improved heating times. This attributed to the fact that more solar energy can be harvested by the collector-evaporator, and less energy is required to heat the water to the desired temperature. It has been reported that during inadequate solar radiation, the DXSAHPWH is able to absorb ambient energy via convection and thus improving heating times in “winter” or “night-time conditions”.

4.5 Parametric analysis

In this analysis, the effect of ambient temperature, solar irradiation and wind speed was investigated with regards to DXSAHPWH performance metrics . In the parametric study, specific variables were kept constant to investigate the relationship between performance and meteorological conditions. The figure caption states which values were kept constant during the parametric analysis. It must be noted that the parametric study was based on Duarte et al. (2019), Kong et al. (2018), Kong et al. (2017, 2011) and Kuang et al. (2003) to discern whether the trends are similar.

4.5.1 Effects of the ambient temperature

4.5.1.1 COP and collector efficiency

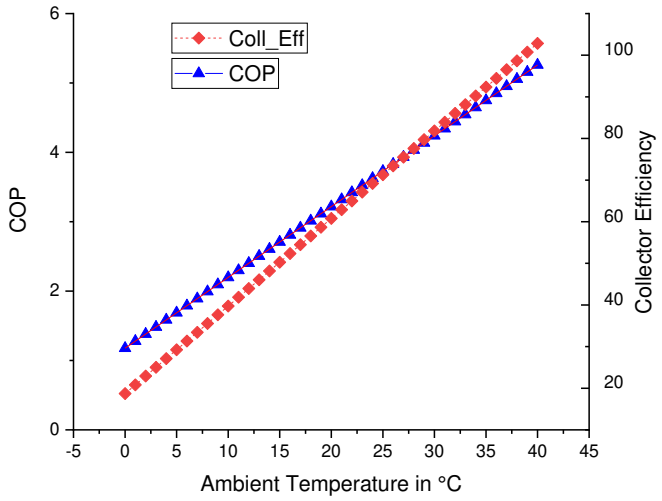

Figure 4. 15: Effect of ambient air temperature on the COP and collector efficiency (A_c= 4.2 m^2, V=0.15 m^3, T_{win} = 20 °C , u_w = 3 m/s and I = 700 W/m^2)

The effect of in ambient temperature on the system performance is shown in Figure 4.15. The increase in ambient temperature results in a linear increase in both the COP and collector efficiency. These results are supported by other studies (Duarte et al., 2019; Hawlader et al., 2001; Kong et al., 2017; Kong et al., 2011; Kuang et al., 2003). For instance, when the ambient temperature was 0 °C, the COP was 1.2. As the temperature increased to 40 °C, the COP was 5.25, an increase of 77 %. Furthermore, the collector efficiency increased from 19 to 100 %, an increase of 81 % for the same range of ambient temperatures. This is a result of a lower overall heat transfer loss to the ambient surroundings from the collector, thus increasing both COP and collector efficiency. It is noteworthy that the collector efficiency could exceed 100 % ,this occurs when the ambient temperature is higher than the refrigerant temperature and thus additional ambient energy via convection is harvested Kong et al. (2011).Moreover, increases in ambient temperature relates to increases in the refrigerant evaporating temperature, which reduces the compressor work, thereby contributing to higher COP.

4.5.1.2 Solar fraction and heating time

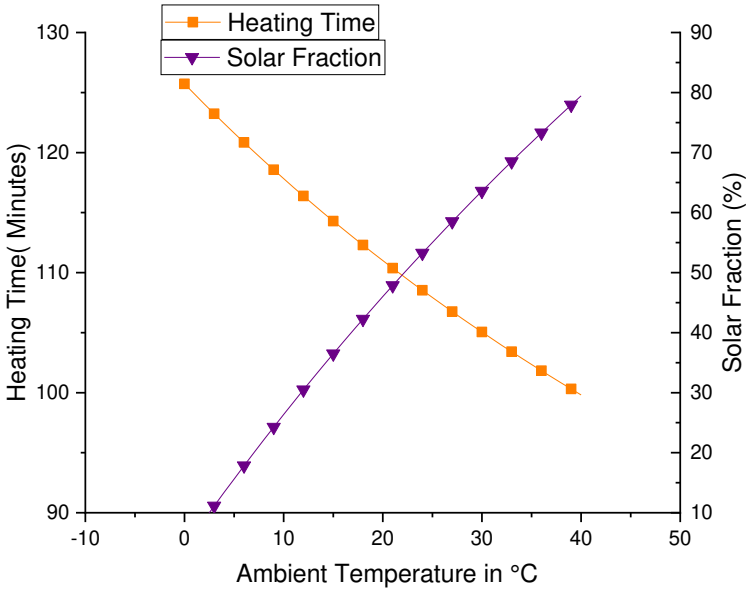

Figure 4. 16: Effect of ambient air temperature on the heating time and solar fraction(A_c= 4.2 m^2, V=0.15 m^3, T_{win} = 20 °C , u_w = 3 m/s and I = 700 W/m^2)

The effect of ambient temperature on the heating time and solar fraction is shown in Figure 4.16. The increase of in ambient temperature results in an increase in the solar fraction (SF)

and a decrease in the heating time (HT). These results are supported by other studies (Kong et al., 2018; Kong et al., 2017; Sun et al., 2015). For instance, when the ambient temperature is 0°C, the SF is 4 %. As the temperature increases to 40°C, the SF becomes 80 %.This represents an increase of 95 %. Furthermore, the heating time decreases from 125 minutes to 100 minutes, a decrease of 25 % for the same range of ambient temperatures. Both these results are a consequence of a lower overall heat transfer loss from the collector to the ambient surroundings as the temperature gradient is reduced.

4.5.2 Effects of the solar radiation

4.5.2.1 COP and collector efficiency

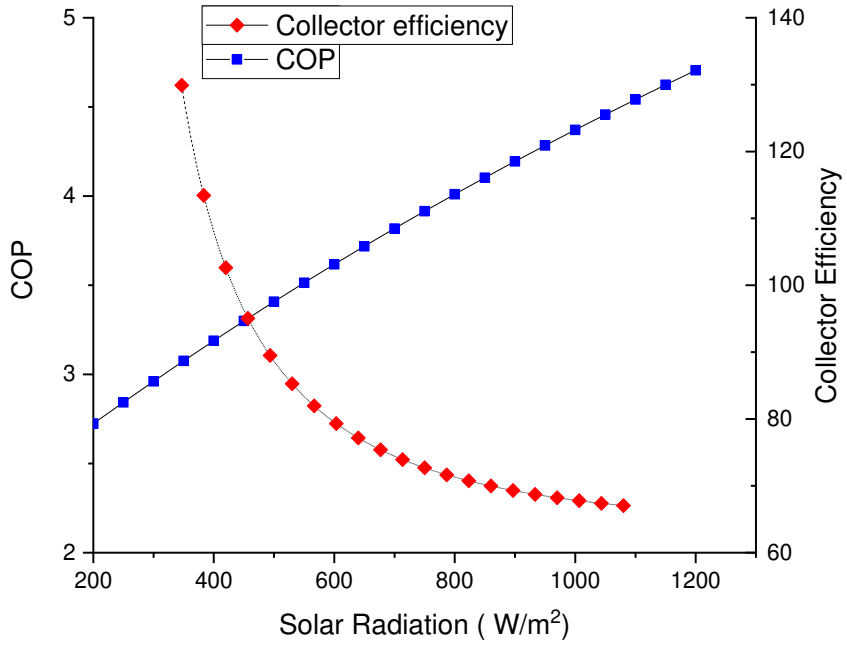

Figure 4. 17: Effect of solar radiation on the COP and collector efficiency (A_c= 4.2 m^2, V=0.15 m^3, T_{win} = 20 °C , u_w = 3 m/s and T_a = 25 °C)

Figure 4.17 shows that the increase in solar radiation results in an increase of COP and a decrease in collector efficiency which is supported by the results of various studies (Duarte et al., 2019; Hawlader et al., 2001; Kong et al., 2017; Kong et al., 2011; Kuang et al., 2003). For instance, when the solar radiation is 200 W/m^2, the COP is 2.72. As the solar radiation increases to 1200 W/$m^{2,}$, the COP becomes 4.71, an increase of 73 %. This further corroborates with the hourly performance results which show that COP increases with solar radiation.

Furthermore, the collector efficiency decreased from 130 to 67 %, a decrease of 48 % for the same range of solar radiation values. The increase in COP is due to more solar energy being harvested by the collector-evaporator; secondly increases in solar radiation result in a higher evaporating temperature of the refrigerant, consequently resulting in a higher system COP. The decrease in collector efficiency is due to the increase in temperature difference between the refrigerant and ambient, which increases heat transfer losses to the surroundings.

4.5.2.2 Solar Fraction and Heating Time

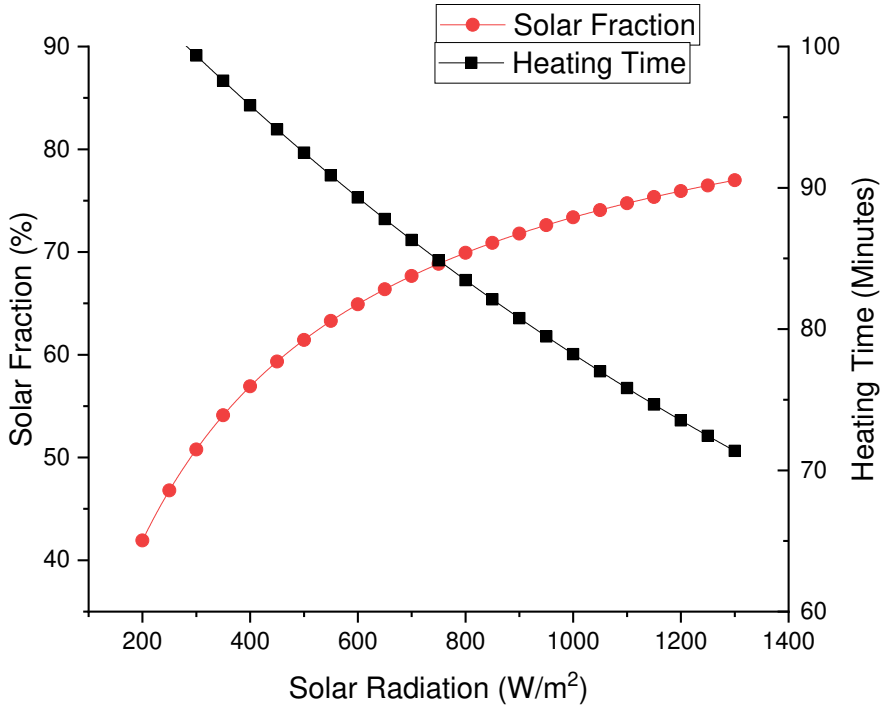

Figure 4. 18: Effect of solar irradiation on the solar fraction and heating time (A_c= 4.2 m^2, V=0.15 m^3, T_{win} = 20 °C , u_w = 3 m/s and T_a = 25 °C)

The effect of solar irradiation on the heating time and solar fraction is shown in Figure 4.18. The increase in solar irradiation results in an increase in the solar fraction (SF) and a decrease in the heating time (HT). This results are supported by other studies (Kong et al., 2018; Kong et al., 2017; Sun et al., 2015). For instance, when the solar irradiation is 200 W/m^2, the SF is 40 %. As the solar irradiation increases to 1200 W/m^2, the SF reaches about 75 %, an increase of 88 %. This further corroborates with the hourly performance results, which show that solar fraction increases with solar radiation. This is a consequence of more solar energy being harvested by the collector-evaporator to contribute to water heating. It is important to note that

the maximum solar radiation possible for South Africa is 1200 W/m^2 which thus indicates that a maximum SF of 80 % is possible. The remaining of 20 % of energy is lost to the surroundings. In the case of the heating time, it decreases from 104 minutes to 73 minutes, a decrease of 43 % for the same range of solar radiation values, which is also due to solar energy being harvested by the collector-evaporator which accelerates the heating time process.

4.5.3 Effects of wind speed

4.5.3.1 COP and Collector Efficiency

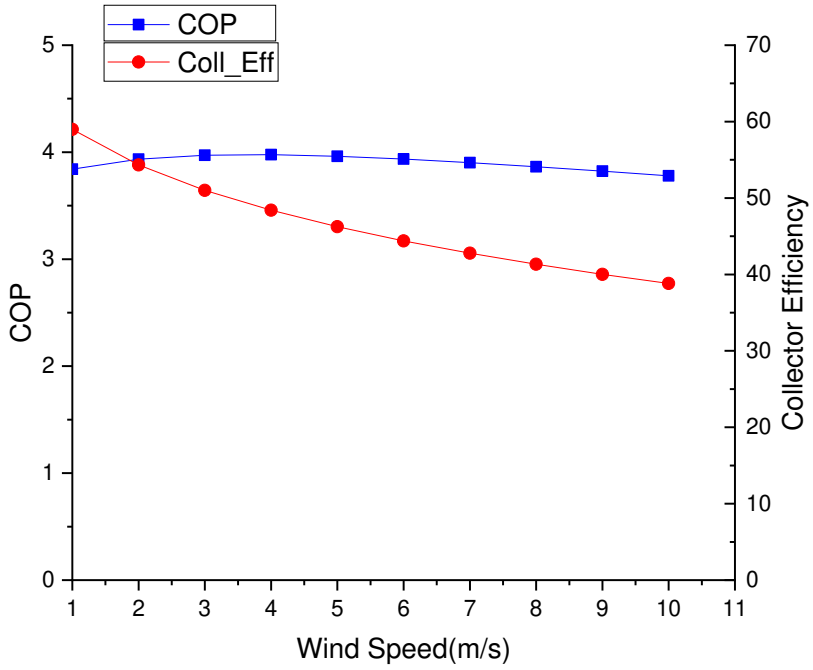

Figure 4. 19: Effect of wind speed on COP and collector efficiency (A_c= 4.2 m^2, V=0.15 m^3, T_{win} = 20 °C , u_w = 3 m/s ,T_a = 25 °C and I = 700 W/m^2)

The effect of wind speed was investigated on the system performance in Figure 4.19. The increase of wind speed, results in a slight increase in COP and decrease in collector efficiency but both eventually gradually becomes constant. For instance, when the wind speed is 1 m/s, the COP was 3.84. As the wind speed decreased to 10 m/s, the COP was 3.78 ,which attributes to a 15.6 % decrease. These results which corroborates with (Duarte *et al.*, 2019; Kong *et al.*, 2011) Moreover, the collector efficiency decreased from 59 % to 39 %,which is a 34 % decrease for the same range of wind speeds. This is a result of enhanced heat transfer between the collector-evaporator and the ambient surroundings, which also depends on the relation between evaporating and ambient temperature. When the evaporating temperature is lower than the ambient, increases in wind speed allows the collector-evaporator to harvest

more energy from the surroundings. The collector efficiency has a slight decrease, due to convective heat transfer loss from the wind. In this case, the evaporating temperature is higher than ambient due to South Africa's subtropical climate and therefore a decrease in collector efficiency. These results are supported by (Duarte *et al.*, 2019; Kong *et al.*, 2011) which state that the wind speed has a minuet effect compared to ambient temperature and solar radiation on system performance.

4.5.3.2 Solar Fraction and Heating Time

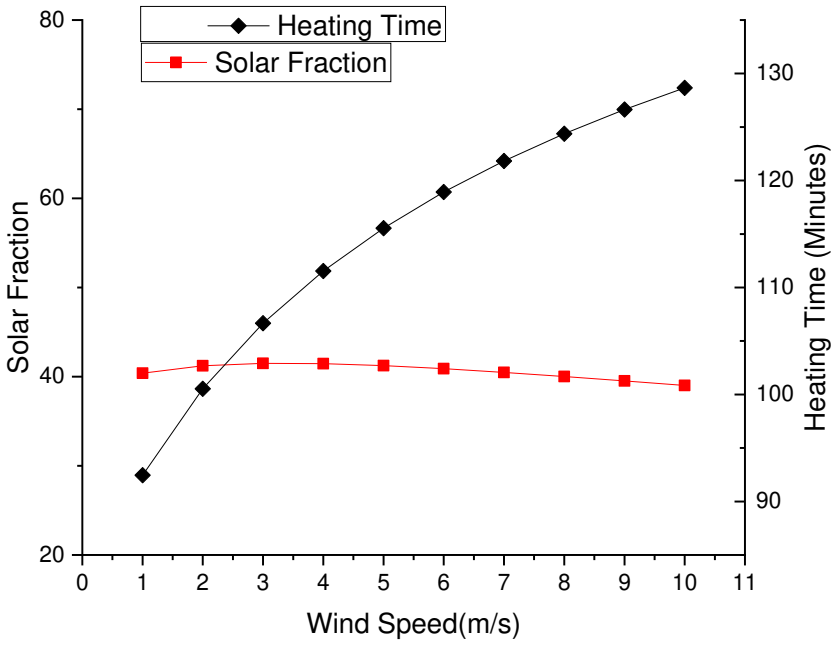

Figure 4. 20: Effect of wind speed on the solar fraction and heating time (A_c= 4.2 m^2, V=0.15 m^3, T_{win} = 20 °C , u_w = 3 m/s ,T_a = 25 °C and I = 700 W/m^2)

The effect of wind speed on the heating time and solar fraction is shown in Figure 4.20. There is a slight decrease in the solar fraction. For instance, when the wind speed is 1 m/s, the solar fraction is 40.38 % and as the wind speed decreases to 10 m/s, it becomes 38.82 %, which is a decrease of 3.7 %. Based on these results, it seems that wind speed has a negligible effect on the solar fraction. Moreover, the heating time increases from 92.5 to 128.6 minutes, which is a 37 % increase for the same range of wind speeds. This occurs because of increased forced convective heat transfer loss from the wind.

4.5.4 Summary of Parametric Results

The following table highlights the salient features of the meteorological parametric analysis.

Table 4. 3 : Summary of Parametric Results

Meteorological Parameter	COP	Collector Efficiency (%)	Solar Fraction(%)	Heating Time (Minutes)
Ambient Temperature	Increase	Increase	Increase	Decrease
Solar Radiation	Increase	Decrease	Increase	Decrease
Wind Speeds	Decrease	Decrease	Decrease	Increase

Based on these results, the following extrapolation can be made with regards to the South African context. The geographical locations with higher ambient and solar radiation values will have higher COPs and lower heating times, which are the essential elements which. In addition, locations with high wind speeds will experience lower COP and collector efficiencies.

CHAPTER 5 – CONCLUSION & RECOMMENDATIONS

5.1 Conclusion

This dissertation aimed to investigate the potential application of DXSAHPWH in South Africa's meteorological conditions through theoretical analysis. This was carried out by running daily and annual simulations to provide qualitative data in the form of performance metrics. Moreover, it aimed to investigate the effects on the performance of the DX-SAHPWH system. To meet this aim, the following objectives were addressed.

The first objective of this dissertation was to conduct an extensive literature review on DX-SAHPWH systems highlighting the current level of knowledge, the modelling used for the system components and configuration, and in addition, the effects of various parameters of the performance on the DX-SAHPWH system. Most such systems used a bare-unglazed collector as it has both capabilities of solar radiation and ambient energy depending on ambient and evaporating temperature gradients. Most systems used R22 and R134a compressors, helical coil condensers immersed in storage tanks and thermostatic expansion valves. In terms of modelling approaches, most authors used a quasi-steady state approach and conducted parametric studies to investigate system performance. Meteorological parameters had significant effects solar irradiation, ambient temperature and wind speeds.

The second objective was to develop a theoretical mathematical model of a DX-SAHPWH system, and this was achieved through converting formulation of physical laws that govern the dynamics of the system's interactions into equations using variables and constant parameters. The model was based on several heat transfers concepts, the first law of thermodynamics and continuity of mass, which state that energy and mass are conserved.

The third objective was to simulate the theoretical mathematical model to assess the daily and annual performance of the DX-SAHPWH system by using the climatic conditions of South Africa. The daily results indicate that the system performance is generally better in the summer day than in the winter day due to the higher ambient temperature, initial water temperature and solar radiation. Moreover, the specific results indicated for the summer condition showed that the system could produce 1700–4000 W of thermal energy, and compressor consumption from 550 to 750 W based on a 24-hour average. Condenser heat gain was 2000 W, collector heat

gain was 1400 W and compressor power consumption was 632 W. The COP and collector efficiency ranged from 1.83–5.65 and 45–51 % respectively. The solar fraction and heating time varied from 0–82 % and 94 to 403 minutes.

In the winter condition, the results showed that the system could produce 1100–1800 W of thermal energy and a compressor consumption from 550 to 585 W; based on a 24-hour average, the condenser heat gain was 1320 W, collector heat gain was 772 W and compressor power consumption was 547 W. The COP and collector efficiency ranged from 1.07–2.80 and 45–60 % respectively. The solar fraction and heating time varied from 0–74 % and 300 to 480 minutes. The system performance was generally better in the summer day than in the winter day due to the variation ambient temperature, initial water temperature and solar radiation. Moreover, during a summer day, the ambient temperature is not expected to be higher than that of the refrigerant, which means that no additional heat is being gained from the ambient. However, in winter it is expected that there will be additional energy gained from ambient, improving both COP and collector efficiency. However, the model is unable to quantify these improvements at this stage.

The annual performance results indicated that the minimum (min) and maximum (max) COP expected are 1.4 and 5.75 respectively, with an annual average of 2.3. The COP is higher during the periods with higher ambient temperatures, solar radiation and higher initial water temperatures which is the converse for the colder seasons. The min and max collector efficiency are 0 and 59.96 % respectively; the collector efficiency remains fairly constant throughout the year, because the temperature gradient between the collector and the ambient temperatures does not vary annually. The min and max solar fraction are 0 and 86.47 % with an annual average of 34.81 %. It is axiomatic that higher solar fractions are expected during the summer period that exhibits higher solar radiation values compared to other seasons. The heating time min and max are 92 and 570 minutes with an annual average of 355 minutes. It was found that periods with lower ambient, initial water temperatures and solar radiation values exhibited higher heat times.

The fourth objective was to conduct a parametric study with the mathematical model to investigate the effects of the meteorological parameters on the performance of the DX-SAHPWH system. The effect of the ambient temperature was investigated on the performance metrics. A range of 0–40°C was selected in this present study. The results indicated a linear increase in both the COP and collector efficiency by 77 and 81 % respectively. In addition, an increase in the solar fraction and a decrease in the heating time was found to be 95% and 25

% respectively. This occurs because of a lower overall heat transfer loss and increases in the refrigerant evaporating temperature. Moreover, it was concluded that the ambient temperature had the most positive effects on system performance.

The effect of solar radiation on the performance metrics was investigated. A range of 200–1200 W/m^2 was selected in this present study. The results indicated an increase in solar radiation, resulting in an increase of COP and a decrease in collector efficiency by 73 % and 48 % respectively, as well as an increase in the solar fraction and a decrease in the heating time by 88 % and 43 % respectively. This is attributed to the higher evaporating temperature of the refrigerant and more solar energy being harvested by collector-evaporator. The decreases in collector efficiency are attributed to an increase in temperature difference between the refrigerant and ambient, which increases heat transfer losses to the surroundings. Moreover, it was concluded that solar radiation had the second most positive effects on system performance.

The effect of the wind speed on the performance metrics was investigated. A range of 1–10 m/s was selected in this present study. Lastly, the wind speed was investigated for a range 1–10 m/s. As the wind speed increases, the COP and collector efficiency decreased by 15.6 % and 34 % respectively . In addition, a decrease was noted in solar fraction and heating time of 3.7 % and 37 % respectively. Moreover, it was concluded that the wind speed had mostly negative effects on system performance.

This research aimed to provide an initial benchmark for the performance of a DX-SAHPWH system in South Africa. Moreover, the research undertaken was conducted as a preliminary stage and was meant to theoretical gauge the feasibility of the specific DX-SAHPWH system. The thermal performance metrics such as COP, collector efficiency, heating time and solar fraction provided a quantitative measure of how these systems will perform for the specific geographical location. Although the analytical modelling approach is not entirely novel and complete, it does provide a guide to the theoretical analysis of the DX-SAHPWH system, which can be used for design and manufacture purposes. The parametric analysis further provides performance insight, so that one might understand how the meteorological conditions affect performance and where the system will best be implemented. Furthermore, it must be highlighted that the results presented were only for the simulated models and thus a prototype must be correctly design, manufactured and tested to obtain accurate results. Based on the results of this dissertation, the author highly recommends the implementation of the DX-SAHPWH system in South Africa.

5.2 Recommendations

The author suggests the model be used to quantity all provinces of South Africa to provide a holistic performance analysis of the DX-SAHPWH system and determine where its best suited to be implemented. Moreover, techno-economic study of the DX-SAHPWH is highly recommended so that a comparison can be made with current water heating systems in South Africa.

For the parametric analysis, other meteorological parameters should be investigated to evaluate the performance of the system such as relative humidity, precipitation, and atmospheric pressure. Moreover, the influence of collector area, compressor speed, initial water temperature and storage volume on system performance should be investigated. However, while the study uses R22 as the refrigerant, it is expected to be banned internationally by 2030. Therefore, modern refrigerants such R134a, R410a, R404a and R744 should be investigated.

To improve mathematical model capabilities, the following is recommended:

- Higher resolution meteorological data can be used to improve to obtain more accurate predictions. For instance, instead of hourly period data, minute increments would be better.
- A solar radiation meteorological model can be developed such as the Angstrom & Prescott correlations instead of using measured data.
- When solar radiation reaches values below 250 W/m^2, the DX-SAHPWH acts as a conventional heat pump. Therefore, a new refrigerant evaporating temperature should be implemented within the model. This is specifically for the conditions with low solar radiation, as additional thermal energy is expected from ambient air via convection, thus improving both COP and collector efficiency.
- To predict the performance of the system more accurately, both air and frost phenomena should be considered in the heat transfer analysis of the collector-evaporator
- Two-phase flow heat transfer coefficients should be considered in heat exchangers: collector-evaporator & helical coil-condenser.

References

[1] Allan, J., Dehouche, Z., Stankovic, S. & Mauricette, L. 2015. Performance testing of thermal and photovoltaic thermal solar collectors. *Energy Science & Engineering*. 3(4):310–326.

[2] Anderson, T.N. & Morrison, G.L. 2007. Effect of load pattern on solar-boosted heat pump water heater performance. *Solar Energy*. 81:1386–1395.

[3] Badiei, A., Akhlaghi, Y.G., Zhao, X., Shittu, S., Xiao, X., Li, J., Fan, Y. & Li, G. 2020. A chronological review of advances in solar assisted heat pump technology in 21st century. 132(July).

[4] Bai, Y., Chow, T., Menezo, C., Dupeyrat, P., Bai, Y., Chow, T., Menezo, C. & Dupeyrat, P. 2014. Analysis of a hybrid PV / thermal solar-assisted heat pump system for sports center water heating application To cite this version : Research Article Analysis of a Hybrid PV / Thermal Solar-Assisted Heat Pump System for Sports Center Water Heating Applica. *International Journal of Photoenergy*. 1–13.

[5] Bellos, E. & Tzivanidis, C. 2017. Energetic and fi nancial sustainability of solar assisted heat pump heating systems in Europe. *Sustainable Cities and Society*. 33(June):70–84.

[6] Bhatt, M.K. & Channiwala, S.A. 2001. REVIEW OF TOP LOSS COEFFICIENT CORRELATIONS FOR FLAT PLATE COLLECTOR. *4th International Conference on Mechanical Engineering*. 7–12.

[7] Bohlmann, J.A. & Inglesi-lotz, R. 2018. Analysing the South African residential sector ' s energy pro fi le. *Renewable and Sustainable Energy Reviews*. 96(December 2017):240–252.

[8] Cengel, Y.A. & Boles, M.A. 2011. Thermodynamics : An Engineering Approach Seventh Edition Chapter 8 EXERGY – A MEASURE OF WORK POTENTIAL. 1–153.

[9] Cervantes, J G & Torres-Reyes, E. 2002. Experiments on a solar-assisted heat pump and an exergy analysis of the system. *Applied Thermal Engineering*. 22:1289–1297.

[10] Charters, W.W.. & Safadi, H.. 1987. Saturation property equations for R22. *International Journal of Refrigeration*. 10:301–304.

[11] Chaturvedi, S.K., Gagrani, V.D. & Abdel-salam, T.M. 2014. Solar-assisted heat pump – A sustainable system for low-temperature water heating applications. *ENERGY CONVERSION AND MANAGEMENT*. 77:550–557.

[12] Chow, T.T., Pei, G., Fong, K.F., Lin, Z., Chan, A.L.S. & He, M. 2010. Modeling and application of direct-expansion solar-assisted heat pump for water heating in subtropical Hong Kong. *Applied Energy*. 87(2):643–649.

[13] Chow, T.T., Fong, K.F., Pei, G., Ji, J. & He, M. 2010. Potential use of photovoltaic-integrated solar heat pump system in Hong Kong. *Applied Thermal Engineering*. 30(8–9):1066–1072.

[14] Chu, J. & Cruickshank, C.A. 2016. Solar-Assisted Heat Pump Systems : A Review of Existing Studies and Their Applicability to the Canadian Residential Sector. *Journal of Solar Energy Engineering*. 136(041013):1–9.

[15] Cleland, A.C. 1986. Computer subroutines for rapid evaluation of refrigerant thermodynamic properties Sous-programmes d ' ordinateur pour l ' bvaluation rapide des propri t & thermodynamiques des frigorigenes. *International Journal of Refrigeration*. 9(June):346–351.

[16] Cleland, A.C. 1994. Polynomial curve-fits for refrigerant thermodynamic properties : extension to include R134a Interpolations polynomiales pour les propri6t6s thermodynamiques des frigorig nes " elargissement pour inclure le R 134. 17:245–249.

[17] Curry, C., Cherni, J.A. & Mapako, M. 2017. The potential and reality of the solar water heater programme in South African townships : Lessons from the City of Tshwane. *Energy Policy*. 106(June 2016):75–84.

[18] Danfoss. 2020. *Technical Data Sheet Compressor model P12TN*. Danfoss.

[19] Deng, W. & Yu, J. 2016. Simulation analysis on dynamic performance of a combined solar / air dual source heat pump water heater. *Energy Conversion and Management*. 120:378–387.

[20] Department of Energy. 2018a. *2018 South African Energy Sector Report*. [Online], Available: http://www.energy.gov.za.

[21] Department of Energy. 2018b. *2018 South African energy prices statistics*.

[22] Ding, G. 2007. Recent developments in simulation techniques for vapour-compression refrigeration systems ´ veloppements re ´ cents dans les techniques de simulation des De ` mes frigorifiques a ` compression de vapeur syste. *International Journal of Refrigeration*. 30:1119–1133.

[23] Ding, G., Wu, Z., Liu, J., Inagaki, T., Wang, K. & Fukaya, M. 2005. An implicit curve-fitting method for fast calculation of thermal properties of pure and mixed refrigerants ` nes purs et me ´ langes de frigorige ` nes : me ´ thode rapide de Frigorige ´ te ´ s avec interpolation

implicite calcul des proprie. 28:921–932.

[24] Ding, G., Wu, Z., Wang, K. & Fukaya, M. 2007. Extension of the applicable range of the implicit curve-fitting method for refrigerant thermodynamic properties to critical pressure ´ ventail d ' application de la me ´ thode a ` interpolation Extension de l ' e ´ e pour les proprie ´ te ´ s thermodynami. 30:418–432.

[25] Dobson, R.T. 2005. Thermal modelling of a night sky radiation cooling system. *Journal of Energy in Southern Africa*. 16(2):56–67.

[26] Donev, G., Sark, W.G.J.H.M. Van, Blok, K. & Dintchev, O. 2012. Solar water heating potential in South Africa in dynamic energy market conditions. *Renewable and Sustainable Energy Reviews*. 16(5):3002–3013.

[27] Duarte, W.M., Paulino, T.F., Pabon, J.J.G., Sawalha, S. & Machado, L. 2019. Refrigerants selection for a direct expansion solar assisted heat pump for domestic hot water. *Solar Energy*. 184(April):527–538.

[28] Duffie & Beckman, W.A. 2013. *Solar Engineering of Thermal Processes*. Fourth ed. Wisconsin-Madison: John Wiley & Sons.

[29] Faca, J. & Joa, M. 2014. New test methodologies to analyse direct expansion solar assisted heat pumps for domestic hot water. *Solar Energy*. 100:66–75.

[30] Fan, Y., Zhao, X., Han, Z., Li, J., Badiei, A., Golizadeh, Y. & Liu, Z. 2021. Scienti fi c and technological progress and future perspectives of the solar assisted heat pump (SAHP) system. *Energy*. 229(2021):120719.

[31] Franklin, J.. 1989. *Patent No. 4789056*. United States of America.

[32] Guo, J.J., Wu, J.Y., Wang, R.Z. & Li, S. 2011. Experimental research and operation optimization of an air-source heat pump water heater. *Applied Energy*. 88:4128–4138.

[33] Hajabdollahi, Z. & Hajabdollahi, H. 2017. Thermo-economic modeling and multi-objective optimization of solar water heater using flat plate collectors. *Solar Energy*. 155:191–202.

[34] Hawlader, M.N.A. & Jahangeer, K.A. 2006. Solar heat pump drying and water heating in the tropics. *Solar Energy*. 80:492–499.

[35] Hawlader, M.N.A., Chou, S.K. & Ullah, M.Z. 2001. The performance of a solar assisted heat pump water heating system. *Applied Thermal Engineering*. 21:1049–1065.

[36] Hepbasli, A. & Kalinci, Y. 2009. A review of heat pump water heating systems. *Renewable*

and Sustainable Energy Reviews. 13:1211–1229.

[37] Huang, B.J.Ã. & Lee, C.P. 2003. Long-term performance of solar-assisted heat pump water heater. *Renewable Energy*. 29(2003):633–639.

[38] Huang, W., Ji, J., Modjinou, M. & Qin, J. 2017. Effects of Ambient Parameters on the Performance of a Direct-Expansion Solar-Assisted Heat Pump with Bare Plate Evaporators for Space Heating. *International Journal of Photoenergy*. 2017:1–10.

[39] Ibrahim, O., Fardoun, F. & Louahlia-gualous, H. 2014. Review of water-heating systems : General selection approach based on energy and environmental aspects. *Building and Environment*. 72(2014):259–286.

[40] Ito, S., Miura, N. & Wang, K. 1999. PERFORMANCE OF A HEAT PUMP USING DIRECT EXPANSION SOLAR COLLECTORS †. *Solar Energy*. 65(3):189–196.

[41] Ji, J., Pei, G., Chow, T., Liu, K. & He, H. 2008. Experimental study of photovoltaic solar assisted heat pump system. 82:43–52.

[42] Ji, J., He, H., Chow, T., Pei, G., He, W. & Liu, K. 2009. Distributed dynamic modeling and experimental study of PV evaporator in a PV / T solar-assisted heat pump. *International Journal of Heat and Mass Transfer*. 52(5–6):1365–1373.

[43] Jie JI, Huide FU, Hanfeng HE, G.P. & Performance. 2010. Performance analysis of an air-source heat pump using an immersed water condenser. *Front. Energy Power Eng. China*. 4(2):234–245.

[44] Joubert, E.C., Hess, S. & Niekerk, J.L. Van. 2016. Large-scale solar water heating in South Africa : Status , barriers and recommendations. *Renewable Energy*. 97:809–822.

[45] Kara, O., Ulgen, K. & Hepbasli, A. 2008. Exergetic assessment of direct-expansion solar-assisted heat pump systems : Review and modeling. *REmap 2030 programme*. 12(2008):1383–1401.

[46] Khin, N., Sint, C., Choudhury, I.A., Masjuki, H.H. & Aoyama, H. 2017. Theoretical analysis to determine the efficiency of a CuO-water nanofluid based-flat plate solar collector for domestic solar water heating system in Myanmar. *Solar Energy*. 155:608–619.

[47] Kim, T., Choi, B., Han, Y. & Hyung, K. 2018. A comparative investigation of solar-assisted heat pumps with solar thermal collectors for a hot water supply system. *Energy Conversion and Management*. 172(April):472–484.

[48] Kong, X., Sun, P., Li, Y., Jiang, K. & Dong, S. 2018a. Experimental performance analysis of a direct-expansion solar-assisted heat pump water heater with R134a in summer Analyse expérimentale des performances d ' un chauffe-eau à pompe à chaleur à détente directe assistée par l ' énergie solaire fonctionnant. *International Journal of Refrigeration*. 91:12–19.

[49] Kong, X., Sun, P., Li, Y., Jiang, K. & Dong, S. 2018b. Experimental studies of a variable capacity direct-expansion solar-assisted heat pump water heater in autumn and winter conditions. *Solar Energy*. 170(February):352–357.

[50] Kong, X.Q., Zhang, D., Li, Y. & Yang, Q.M. 2011. Thermal performance analysis of a direct-expansion solar-assisted heat pump water heater. *Energy*. 36(12):6830–6838.

[51] Kong, X.Q., Li, Y., Lin, L. & Yang, Y.G. 2017. Modeling evaluation of a direct-expansion solar-assisted heat pump water heater using R410A Évaluation par modélisation d ' un chauffe-eau à pompe à chaleur solaire à détente directe fonctionnant au R410A. *International Journal of Refrigeration*. 76(2017):136–146.

[52] Kong et al. 2017. Modeling evaluation of a direct- expansion solar-assisted heat pump water heater using R410A,. *International Journal of Refrigeration (2017)*.

[53] Kuang, Y.H. & Wang, R.Z. 2006. Performance of a multi-functional direct-expansion solar assisted heat pump system. *Solar Energy*. 80(2006):795–803.

[54] Kuang, Y.H., Sumathy, K. & Wang, R.Z. 2003. Study on a direct-expansion solar-assisted heat pump water heating system. *International Journal of Energy Research*. 27(October 2002):531–548.

[55] Kuang, Y.H., Wang, R.Z. & Yu, L.Q. 2003. Experimental study on solar assisted heat pump system for heat supply. *Energy Conversion and Management*. 44(2003):1089–1098.

[56] Kumar, S. & Mullick, S.C. 2010. Wind heat transfer coefficient in solar collectors in outdoor conditions. *Solar Energy*. 84(6):956–963.

[57] Kumar, K.V., Paradeshi, L., Srinivas, M. & Jayaraj, S. 2016. Parametric Studies of a Simple Direct Expansion Solar Assisted Heat Pump Using ANN and GA. *Energy Procedia*. 90(December 2015):625–634.

[58] Laughman, C.R.; Zhao, Y.; Nikovski, D. 2012. Fast Refrigerant Property Calculations Using Interpolation-Based Methods. In *International Refrigeration and Air Conditioning Conference at Purdue ,July 16-19,*. 12.

[59] Li, Y.W., Wang, R.Z., Wu, J.Y. & Xu, Y.X. 2007a. Experimental performance analysis on a direct-expansion solar-assisted heat pump water heater. *Applied Thermal Engineering*. 27(2007):2858–2868.

[60] Li, Y.W., Wang, R.Z., Wu, J.Y. & Xu, Y.X. 2007b. Experimental performance analysis and optimization of a direct expansion solar-assisted heat pump water heater. *Energy*. 32(2007):1361–1374.

[61] Liu, H., Zhang, S., Jiang, Y. & Yao, Y. 2015. Simulation analysis of a solar-assisted heat pump system for space heating in severe cold areas. *Building Services Engineering Research & Technology*. 36(4):500–518.

[62] Malali, P.D., Chaturvedi, S.K. & Abdel-salam, T.M. 2016. An approximate method for prediction of thermal performance of direct expansion-solar assisted heat pump (DX-SAHP) systems for water heating applications. *Energy Conversion and Management*. 127:416–423.

[63] Martin-dominguez, I.R. 2014. Correlations for some saturated thermodynamic and transport properties of refrigerant R 22. *ASHRAE Transactions:Research*. (May):344–347.

[64] Matuska, T. & Zmrhal, V. 2009. Kolektor 2.2.

[65] Miguel, H., Bastos, C., Jesús, P., Torres, G. & Castilla, C.E. 2018. Numerical simulation and experimental validation of a solar-assisted heat pump system for heating residential water Simulation numérique et validation expérimentale d ' un système de pompe à chaleur solaire pour le chauffage de l ' eau á usage domestique. *International Journal of Refrigeration*. 86:28–39.

[66] Mohamed, E., Riffat, S. & Omer, S. 2017a. Low-temperature solar-plates-assisted heat pump : A developed design for domestic applications in cold climate . Solar energy and wasted heat in buildings are capable of supplying enough energy to answer the. *International Journal of Refrigeration*.

[67] Mohamed, E., Riffat, S. & Omer, S. 2017b. Low-temperature solar-plate-assisted heat pump : A developed design for domestic applications in cold climate Pompes à chaleur assistées par panneaux solaires à basse température : conception d ' un modèle pour des applications domestiques dans les climat. *International Journal of Refrigeration*. 81:134–150.

[68] Mohanraj, M., Belyayev, Y., Jayaraj, S. & Kaltayev, A. 2018a. Research and developments on solar assisted compression heat pump systems – A comprehensive review (Part A : Modeling

and modi fi cations). *Renewable and Sustainable Energy Reviews*. 83(February):90–123.

[69] Mohanraj, M., Belyayev, Y., Jayaraj, S. & Kaltayev, A. 2018b. Research and developments on solar assisted compression heat pump systems – A comprehensive review (Part-B : Applications). *Renewable and Sustainable Energy Reviews*. 83(2018):124–155.

[70] Mohd, Z. & Hawlader, M.N.A. 2013. A review on solar assisted heat pump systems in Singapore. *Renewable and Sustainable Energy Reviews*. 26(2013):286–293.

[71] Mohd, Z. & Hawlader, M.N.A. 2015. Analysis of solar desalination system using heat pump. *Renewable Energy*. 74:116–123.

[72] Nel, P.J.C., Booysen, M.J. & Merwe, B. Van Der. 2016. Energy perceptions in South Africa : An analysis of behaviour and understanding of electric water heaters. *Energy for Sustainable Development*. 32:62–70.

[73] Omojaro, P. & Breitkopf, C. 2013. Direct expansion solar assisted heat pumps : A review of applications and recent research. *Renewable and Sustainable Energy Reviews*. 22:33–45.

[74] Pegels, A. 2010. Renewable energy in South Africa : Potentials , barriers and options for support. *Energy Policy*. 38(9):4945–4954.

[75] Pollet, B.G., Staffell, I. & Adamson, K. 2015. ScienceDirect Current energy landscape in the Republic of South Africa. *International Journal of Hydrogen Energy*. 40(46):16685–16701.

[76] Popoola, O.M. 2014. Solar water heater contribution to energy savings in higher education institutions : Impact analysis. *Journal of Energy in Southern Africa*. 25(1):51–58.

[77] Poppi, S., Sommerfeldt, N., Bales, C., Madani, H. & Lundqvist, P. 2018. Techno-economic review of solar heat pump systems for residential heating applications. *Renewable and Sustainable Energy Reviews*. 81(March 2017):22–32.

[78] Qiao, H. & Radermacher, R. 2010. A Review for Numerical Simulation of Vapor Compression Systems. In Vol. 2315 *International Refrigeration and Air Conditioning Conference at Purdue ,July 16-19,*. 1–9.

[79] Reyes, E.T. & Ez, M.P.N.U.N. 1998. EXERGY ANALYSIS AND OPTIMIZATION OF A SOLAR-. *Energy*. 23(4):337–344.

[80] S. K. CHATURVEDI, D.T.C. and A.K. 1998. THERMAL PERFORMANCE OF A VARIABLE CAPACITY DIRECT EXPANSION SOLAR-ASSISTED HEAT PUMP S. *Energy Conversation and Management*. 39(3):181–191.

[81] SAMJ. 2019. ‘ Getting out of the dark ’: Implications of load shedding on healthcare in South Africa and strategies to enhance preparedness Cold storage. 109(12):899–901.

[82] SANS. 2011. *SANS 204-1 : 2007 SOUTH AFRICAN NATIONAL STANDARD Energy efficiency in buildings Part 1 : General provisions*.

[83] Sartori, E. 2006. Convection coefficient equations for forced air flow over flat surfaces. *Solar Energy*. 80(9):1063–1071.

[84] SAURAN. 2019. *index @ sauran.ac.za*. [Online], Available: https://sauran.ac.za/ [2015, October 20].

[85] Scalabrin, G. & Marchi, P. 2006. A Reference Multiparameter Viscosity Equation for R134a with an Optimized Functional Form. *J. Phys. Chem. Ref. Data,*. 35(2):841–867.

[86] Shi, G., Aye, L., Li, D. & Du, X. 2019. Recent advances in direct expansion solar assisted heat pump systems : A review. *Renewable and Sustainable Energy Reviews*. 109(January 2018):349–366.

[87] Shitzer, A. 2014. Wind-chill-equivalent temperatures : regarding the impact due to the variability of the environmental convective heat transfer coefficient. (April 2006).

[88] Soldo, V. & Balen, I. 2004. Thermal Performance of a Direct Expansion Solar Assisted Heat Pump. In *International Refrigeration and Air Conditioning Conference at Purdue, July 12-15, 2004*. 1–8.

[89] Sterling, S.J. & Collins, M.R. 2012. Feasibility analysis of an indirect heat pump assisted solar domestic hot water system. *Applied Energy*. 93(2012):11–17.

[90] Sun, X., Dai, Y., Novakovic, V., Wu, J. & Wang, R. 2015. Performance comparison of direct expansion solar-assisted heat pump and conventional air source heat pump for domestic hot water. 70:394–401.

[91] Tagliafico, L.A., Scarpa, F. & Valsuani, F. 2014. Direct expansion solar assisted heat pumps e A clean steady state approach for overall performance analysis. 66:216–226.

[92] Tagliafico, L.A., Scarpa, F. & De Rosa, M. 2014. Dynamic thermal models and CFD analysis for flat-plate thermal solar collectors - A review. *Renewable and Sustainable Energy Reviews*. 30:526–537.

[93] Tzivanidis, C., Bellos, E., Mitsopoulos, G., Antonopoulos, K.A. & Delis, A. 2016. Energetic and financial evaluation of a solar assisted heat pump heating system with other usual heating

systems in Athens Coefficient of Performance. *Applied Thermal Engineering*. 106:87–97.

[94] USAID. 2014. *Greenhouse Gas Emissions in South Africa*. [Online], Available: [12/12/2017 14:15] Frederic Hans: %0Ahttps://www.environment.gov.za/sites/default/files/docs/greenhousegas_invetorysouthafrica.pdf %0A %0A.

[95] Vindenes, E. 2018. Development and Comparison of Compressor Models for Heat Pump Applications in TRNSYS Master Thesis in Energy Thermal Machines. University of Bergen.

[96] Wang, Y., Li, M. & Qiu, Y. 2019. Performance analysis of a secondary heat recovery solar-assisted heat pump drying system for mango. *Energy Exploration & Exploitation*. 0(0):1–11.

[97] Wang, Z., Guo, P., Zhang, H., Yang, W. & Mei, S. 2017. Comprehensive review on the development of SAHP for domestic hot water. *Renewable and Sustainable Energy Reviews*. 72(March 2016):871–881.

[98] Xu, G., Zhang, X. & Deng, S. 2006. A simulation study on the operating performance of a solar-air source heat pump water heater. *Applied Thermal Engineering*. 26(11–12):1257–1265.

[99] Yamaguchi, S., Kato, D., Saito, K. & Kawai, S. 2011. International Journal of Heat and Mass Transfer Development and validation of static simulation model for CO 2 heat pump. *International Journal of Heat and Mass Transfer*. 54(9–10):1896–1906.

[100] Yang, W., Zhu, J., Shi, M. & Chen, Z. 2011. Procedia Environmental Sciences Numerical Simulation of the Performance of a Solar-Assisted Heat Pump Heating System. *Procedia Environmental Sciences*. 11(1):790–797.

[101] Yousefi, Masoud, Misagh, M. 2015. Thermodynamic analysis of a direct expansion solar assisted heat pump water heater. *Journal of Energy in Southern Africa*. 26(2):110–117.

[102] Zhang, D., Wu, Q.B., Li, J.P. & Kong, X.Q. 2014. Effects of refrigerant charge and structural parameters on the performance of a direct-expansion solar-assisted heat pump system. *Applied Thermal Engineering*. 73(2014):522–528.

[103] Zhou, J., Zhao, X., Ma, X., Qiu, Z., Ji, J., Du, Z. & Yu, M. 2016. Experimental investigation of a solar driven direct-expansion heat pump system employing the novel PV / micro-channels-evaporator modules. *Applied Energy*. 178:484–495.

Appendices

Appendix A : Matlab Code for DXSAHPWH

```
% Analytical Model of a Direct-Expansion Solar Thermal Heat pump
%Version 7.0 %This model is used for the hourly,monthly and annual simulation

clc;

%%%%%%%%%%%%%%%%%%%%%%%%%%%%%%%%%%%%%%%%%%%%%%%%%%%%%%%%%%%%%%%%%%%%%%%%%%%%
%Input Parameters

%Meteo Conditions

%
 I=0:1100;%input('Solar Radiation in W/m2 = ');
%
% %
% % Solar Radiation
%
 Ta=25;%input('Ambient temperature in C = ');
% %Ambient temperature
%
u=3;%input('wind speed in m/s =');
%  %wind speed
%
RH=50;%;
% %
% % u=WS_ms_S_WVT;
% % Ta=AirTC_Avg;
% % I=SunWM_Avg;

%%%%%%%%%%%%%%%%%%%%%%%%%%%%%%%%%%%%%%%%%%%%%%%%%%%%%%%%%%%%%%%%%%%%%%%%%%%%
%Water in Temperature Model ( Adjust depending on Daily or Hourly)

 x=1:8760;

 h_1=-1;

Tmin=15;

 Tmax=20;

Twin=20;%(Tmin-Tmax)/2-(((Tmax-Tmin)/2).*h_1.*cos(2.*pi().*((x-1)./8760)))+20;
%Annual Water in Temperature Model

Two0=55;
Two1=repmat(Two0,1,8760);
%Setpoint Water temperature


%%%%%%%%%%%%%%%%%%%%%%%%%%%%%%%%%%%%%%%%%%%%%%%%%%%%%%%%%%%%%%%%%%%%%%%%%%%%
%1. Solar Thermal Collector -Evaporator Input Parameters


A=4.2;
%Area of  Solar Thermal Collector
```

```
abs=0.9;
% Absorbtivity of Collector Plate

emis=0.1;
% Emissivity of Collector Plate

k=236;
%%thermal conductivity of Collector Plate(aluminium)

t=4E-3;
%Thickness of Absorber Plate

W=0.04;
%Pitch of Collector Tube

D=9.4E-3;
%Diameter of Collector Tube

Cb=15;
%Bond conductance

P2=1.66E6;
% Condensing Pressure

P1=0.808E6;
% Evaporating Pressure

PR=P1\P2;
% Pressure Ratio


%3 Storage Tank Input ParametersP2

V=0.15;
% Volume of Storage Tank

h=1.085;
% Height of Storage Tank

d=0.5;
% Diameter of Storage Tank

k_ins=0.055;
%thermal conductivity of the insultion

t_ins=0.038;
%thickness of the insultion
%%%%%%%%%%%%%%%%%%%%%%%%%%%%%%%%%%%%%%%%%%%%%%%%%%%%%%%%%%%%

Tp= Ta+5;
% Collector Plate Temperature
```

```
for k1=length(I)
if I(k1)< 0.25;
        Tdp=(237.7.*(17.27.*Ta)./((237.7+Ta)+log(RH./100))./(17.27-((17.27.*Ta).↙
(237.7+Ta))+log(RH./100)));
      emis1=0.741+0.0162.*(Tdp);%Night
   else
      Tdp=237.7.*(17.27.*Ta)./((237.7+Ta)+log(RH./100))./(17.27-(17.27.*Ta)./(237.↙
+Ta)+log(RH./100));
emis1=0.727+0.0016.*(Tdp); %Day
end
end

Tsky1=emis1.*(Ta+273.15).^0.25;

sigma= 5.670367E-8;
%Stefan Boltzman constant

hr=sigma*emis.*(((Tp+273).^4-(Tsky1+273).^4)./((Tp+273)-(Ta+273)));
%Radiation Heat Transfer Co-efficient

for k1=1:length(u)

if u(k1) <=5;

hw=5+3.8.*u(k1);

else

hw=6.74.*(u(k1)).^.78;

end
end
%Convection Heat Transfer  Co-efficient


UL=transpose(hw)+hr;
% Overall Collector Loss Co-efficient of Collector-Evaporator

 Te_opt=(Ta.^0.5).*((((abs.*I-0.1*77.24)./UL)+Ta)).^0.5-10;
%Evaporation Temperature of R22
Te=Te_opt;

lambda_R22_vapour=9.3837854793+6.40858703196E-2.*(Te)+9.6047166812E-5.*(Te).^2↙
4.47171748634E-6.*(Te).^3-5.67779208878E-8.*(Te).^4+1.8558049327E-9.*(Te).^5;
%thermal conductivity of R22 saturated vapour

hfi=4.36.*(lambda_R22_vapour./D);
%convective heat transfer coefficent of vapour R22

m=sqrt(UL./(k.*t));

F=tanh((m.*(W-D))./(2))./((m.*(W-D))./(2));
%Fin efficiency
```

```
F_prime =(1./UL)./(W./(UL.*(D+(W-D).*F)+W./Cb)+W./(hfi*pi()*D));
% Collector Factor Efficiency

T2=(Te_opt+273)*(((PR)^(0.1525)))-273;
%Compressor Discharge Temperature

Cp_R22=0.7231116101+4.32348766858E-3.*(Te)+3.83804797782E-5.*(Te).^2-3.73646207E-7↙
*(Te)-2.1617922739E-9.*(Te).^4+2.66288723405E-10.*(Te).^5;

T3= ((Ta.^2./4)+(lambda_R22_vapour./(Cp_R22.*Ta))).^0.5+(Ta./2)+Ta-10;
% %Condensing Temperature of R22 Vapour

%%%%%%%%%%%%%%%%%%%%%%%%%%%%%%%%%%%%%%%%%%%%%%%%%%%%%%%%%%%%%%%%%%%%%%%%%%%%5

   Qi=I.*A;
% Solar Radiation Incident on Collector

Qcoll=F_prime*A.*(I*abs-UL.*(Te_opt-Ta));
%Useful Heat gain in Collector -Evaporator

mr_com = (41.08571865 +1.516984.*Te-0.27540852.*T3+0.01482619.*Te.^2-0.007282845↙
*Te.*T3)./3600;


Wcom3= 272.07685 -1.68116.*Te+6.4135.*T3+0.0025426.*Te.^2+0.23186.*Te.*T3;
%Power consumption of the compressor

%%%%%%%%%%%%%%%%%%%%%%%%%%%%%%%%%%%%%%%%%%%%%%%%%%%%%%%%%%%%%%%%%%%%%%%%%%%%

% Storage Tank Model

T_film=((Two0+Ta)./2);
%Film temperature of air

rho_air=8.78552-7.54226E-2.*(T_film+273)+2.69671E-4.*(T_film+273).^2-3.42800E-7.↙
(T_film+273).^3;
%density of air

mu_air=3.2575E-5-7.56163E-7.*(T_film+273)+7.47235E-9.*(T_film+273).^2-2.86507E-11.↙
(T_film+273).^3+3.89067E-14.*(T_film+273).^4;
%absolute viscosity of air

nu_air=mu_air./rho_air;
%absolute viscosity of air

lambda_air=-3.0600E-4+9.89089E-5.*(T_film+273)-3.46571E-8.*(T_film+273).^2;
%thermal conductivity of air

Pr_air=0.80040 -0.00031*(T_film+273);
%Prandtl Number of air

Beta_air=1./(T_film+273);
```

```
%volumetric coefficent of  thermal expansion

Grashoff_air=(9.81.*Beta_air.*(Two0-Ta).*h^3)./(nu_air).^2;

Raleigh_air=Grashoff_air.*Pr_air;

Nusselt_air=((0.825+0.386.*(Raleigh_air).^0.1667/((1+(0.492./Pr_air).^0.5625)).^0↙
296296)).^2;

h_st=Nusselt_air*(lambda_air./h) ;
% Natural convective heat transfer coefficent

rho_w=1.0005776E+3+-7.062937E-2.*(Twin)-3.566433E-3.*(Twin).^2;
% Density of Water as a function of Temperature

Cp_w=(4.2152727E3-1.6342424E-3.*(Twin)+1.6515152E-5.*(Twin).^2);
% Specific Heat Capacity of Water as a function of Temperature

Qw=V.*rho_w.*Cp_w.*(Two0-Twin);
%Thermal energy required to heat water

Ast=1.845*(2+(h./d)).*V.^(2/3);
% Surface Area of Storage Tank

R_con_st=log((0.5+0.038)./0.5)./2*pi()*h*k_ins;
%Conductive Thermal Resistance of the tank

Q_conv_st=h_st.*Ast.*(Two0-Ta-5);
%Convection Heat Transfer Loss of the tank


Q_cond_st=(Two0-Ta)./R_con_st;
%Conductive Heat Transfer Loss of the tank

Q_rad_st=0.4*sigma*Ast*((Two0+273).^4-(Ta+273).^4);
%Radiation Heat Transfer Loss of the tank

Qst = Q_conv_st+Q_cond_st+Q_rad_st;
%Total Heat Transfer Loss to the tank

Qcon=Wcom3+Qcoll;
% Condenser Heat gain

%%%%%%%%%%%%%%%%%%%%%%%%%%%%%%%%%%%%%%%%%%%%%%%%%%%%%%%%%%%%%%%%%%%%%%%

%Performance Analysis

COP=(Qcon)./(Wcom3);
%Coefficient of Performance

coll_eff=(Qcoll./Qi)*100;

Sol_Frac=((Qcoll./((Qcon))))*100;
```

```
% Solar Fraction

%%%%%%%%%%%%%%%%%%%%%%%%%%%%%%%%%%%%%%%%%%%%%%%

% %%%%%%%%%%%%%%%%%%%%%%%%%%%%%%%%%%%
coll_eff(isinf(coll_eff)|isnan(coll_eff))=0;
 indicies=find((coll_eff)>150);
 coll_eff(indicies)=0;
 % Collector efficiency Data Clean-up


Time_2=((transpose((Qw))./(Qcon))/60);   %360%
%  indicies1=find((Time_2)<0);
 indicies3=find((Time_2)>600);
%  Time_2(indicies1)=0;
  Time_2(indicies3)=0;
%  Heating Time Data Clean-up
%
% % Plot
%
% subplot(2,2,1)
% x=linspace(0,6125,6125);
%
% plot(x,COP);
% xlabel('Time(Hours)')
% ylabel('COP')
%
% subplot(2,2,2)
%
% plot(x,coll_eff,'red')
% xlabel('Time(Hours)')
% ylabel('Collector Efficiency (%)')
%
%
% subplot(2,2,3)
%
%
% plot(x,Sol_Frac,'green');
% xlabel('Time(Hours)')
% ylabel('Solar Fraction (%)')
%
%
% subplot(2,2,4)
%
% plot(x,Time_2,'yellow')
% xlabel('Time(Hours)')
% ylabel('Heating Time (Minutes)')


% subplot(2,2,4)
%
% index=265:300;
% plot(x(index),Wcom2(index));
```

```
% xlabel('Time(Hours)')
% ylabel('Heating Time(Mintutes)')
%
% plot(x,I);

%%% Choose specific days
%%Spring Season
% plot(COP(5832:8016,1));
% plot(coll_eff(5832:8016,1))
% plot(Time_2(5832:8016,1));
% plot(Sol_Frac(5832:8016,1))

% Coll_eff_mean=mean(coll_eff(5832:8016,1))
% COP_mean=mean(COP(5832:8016,1))
% Solar_Fraction_mean=mean(Sol_Frac(5832:8016,1))
% Heating_Time_mean=mean(Time_2(5832:8016,1))
% rowname={'Spring'}
% varname={'COP_mean','Coll_eff_mean','Solar_Fraction_mean','Heating_Time_mean'}
% T1=table(COP_mean,Coll_eff_mean,Solar_Fraction_mean
Heating_Time_mean,'VariableNames',varname,'Rownames',rowname);
% disp(T1)
%
```

Appendix B : SAURAN SUN Station

SAURAN Station Details: SUN Stellenbosch University, Stellenbosch, Western Cape Province, South Africa

The SAURAN SUN station is located at Stellenbosch University, in Stellenbosch, South Africa. The instruments are positioned on the roof of an Engineering building with very good solar exposure. The horizons are partially obscured by surrounding mountains. The station was installed on 24 May 2010.

SAURAN station code: SUN	**Stellenbosch University, Stellenbosch, Western Cape, South Africa**	**Latitude:** -33.9281° (E) **Longitude:** 18.8654° (S) **Elevation:** 119 m AMSL			
Database notation:	**Measurement:**	**Instrument:**	**Serial number:**	**Last calibration:**	**Sensitivity factor:**
GHI_CMP11	Global horizontal irradiance in [W/m²]	Kipp & Zonen CMP11 unshaded	114667	31 August 2016	
DNI_CHP1	Direct normal irradiance in [W/m²]	Kipp & Zonen CHP1 on a SOLYS tracker	100235	06 September 2016	
DHI_CMP11	Diffuse horizontal irradiance in [W/m²]	Kipp & Zonen CMP11 under a shading ball on a SOLYS tracker	114668	8 August 2016	
DHI_CMP11_ShadowBand	Diffuse horizontal irradiance in [W/m²]	Kipp & Zonen CMP11 under a shadowband		N/A	
UVA_Avg	UVA in [W/m²]	Kipp & Zonen UVS-AB-T	120113		
UVB_Avg	UVB in [W/m²]	Kipp & Zonen UVS-AB-T	120113		
Air_Temp	Air temperature in [°C]	Campbell Scientific CS215 sensor			
BP	Barometric pressure in [mbar]	Vaisala PTB110 sensor			
RH	Relative humidity in [%]	Campbell Scientific CS215 sensor			
WS	Wind speed in [m/s]	R.M.Young 03001 sensor			
WD	Wind direction in [°]	R.M.Young 03001 sensor			
WD_SD	Standard deviation of the wind direction in [°]	R.M.Young 03001 sensor			